

Fall 11-2016

A Computer Program for the Coupled Implementation of Meanline and Throughflow Methods to Simplify the Aerodynamic Design of Multistage Axial Compressors

Alexander V. Rozendaal
Embry-Riddle Aeronautical University

Follow this and additional works at: <https://commons.erau.edu/edt>



Part of the [Aerodynamics and Fluid Mechanics Commons](#)

Scholarly Commons Citation

Rozendaal, Alexander V., "A Computer Program for the Coupled Implementation of Meanline and Throughflow Methods to Simplify the Aerodynamic Design of Multistage Axial Compressors" (2016). *Doctoral Dissertations and Master's Theses*. 313.
<https://commons.erau.edu/edt/313>

This Thesis - Open Access is brought to you for free and open access by Scholarly Commons. It has been accepted for inclusion in Doctoral Dissertations and Master's Theses by an authorized administrator of Scholarly Commons. For more information, please contact commons@erau.edu.

A COMPUTER PROGRAM FOR THE COUPLED IMPLEMENTATION OF
MEANLINE AND THROUGHFLOW METHODS TO SIMPLIFY THE
AERODYNAMIC DESIGN OF MULTISTAGE AXIAL COMPRESSORS

A Thesis

Submitted to the Faculty

of

Embry-Riddle Aeronautical University

by

Alexander V. Rozendaal

In Partial Fulfillment of the

Requirements for the Degree

of

Master of Science in Aerospace Engineering

November 2016

Embry-Riddle Aeronautical University

Daytona Beach, Florida

A COMPUTER PROGRAM FOR THE COUPLED IMPLEMENTATION OF
MEANLINE AND THROUGHFLOW METHODS TO SIMPLIFY THE
AERODYNAMIC DESIGN OF MULTISTAGE AXIAL COMPRESSORS

by

Alexander V. Rozendaal

A Thesis prepared under the direction of the candidate's committee chairman, Dr. Magdy Attia, Department of Aerospace Engineering, and has been approved by the members of the thesis committee. It was submitted to the School of Graduate Studies and Research and was accepted in partial fulfillment of the requirements for the degree of Master of Science in Aerospace Engineering.

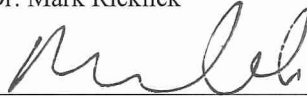
THESIS COMMITTEE



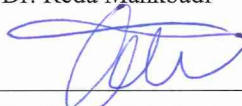
Chairman, Dr. Magdy Attia



Member, Dr. Mark Ricklick



Member, Dr. Reda Mankbadi



Member, Dr. Nafara Petralanda



Graduate Program Coordinator, Dr. Magdy Attia

11. 18. 2016

Date



Dean of College of Engineering, Dr. Maj Mirmirani

Date

11/18/2016



Vice Chancellor, Academic Support, Dr. Christopher Grant

Date

11/18/16

ACKNOWLEDGMENTS

First off, I would like to personally thank my advisor, Dr. Magdy Attia, for his ongoing guidance and assistance throughout the course of this Master's thesis.

I would like to extend my sincerest thanks to Mr. Darrell Stevens, Research Engineer with the Aerospace Engineering Department, not only for his assistance with technical matters, but also for providing a comfortable and enjoyable atmosphere for which to complete this project. Darrell's infinite bank of knowledge and experience provided an invaluable resource that helped me overcome many challenges. Darrell, thank you for your support, advice, and the many entertaining stories shared throughout the past two years.

I would also like to express my deepest appreciation to my fellow colleagues, Daniel Port, and especially Nicole Gagnon, for all of the great memories shared during the many sleepless nights in the Gas Turbine Lab. The countless coffee trips, midnight snack runs, and break time discussions always seemed to provide a much-needed level of comfort during stressful times. I have no doubt that there will be many more great memories in the years to come.

I cannot think of anyone else that I would like to thank more than my brother, Peter Rozendaal. My brother, without even the slightest hint of hesitation, welcomed me into his home for the duration of my Master's studies. His continuous encouragement throughout these past two years has helped me overcome one of the most stressful times in my career, and for this, I cannot thank him enough. Pete, this thesis would not have been possible without your support. Thank you.

TABLE OF CONTENTS

LIST OF FIGURES	ix
SYMBOLS.....	xvi
ABBREVIATIONS	xvii
ABSTRACT.....	xviii
1. Introduction	1
1.1. Overview of Introductory Theory	1
1.2. Review of Gas Turbine Theory	4
1.3. Review of Compressor Aerodynamics	6
1.3.1. Compressor Stage Definition.....	6
1.3.2. Velocity Triangles	7
1.3.3. Stage Energy Addition	8
1.4. Figures of Merit	10
1.4.1. Stage efficiency	10
1.4.2. Degree of Reaction	11
1.4.3. Diffusion Factor.....	12
1.4.4. Total Pressure Loss Parameter	13
1.4.5. Deviation Angle.....	15
2. Compressor Design Procedure	18
2.1. Overview of the Design Procedure	18
2.2. The Iterative Design Sequence	21
2.3. Current Work	22
2.4. Meanline Analysis	22
2.4.1. Radial Equilibrium	23
2.4.2. Vortex Design Strategies	25
2.5. Throughflow Analysis.....	27
2.5.1. Streamline Curvature.....	28
2.5.2. Throughflow limitations	29
3. Overview of C-STAAC.....	32
3.1. Objective	32
3.2. Programming	32
3.3. Meanline and Throughflow Integration	32
3.3.1. Meanline Application.....	33
3.3.2. Throughflow Application	33
3.4. Simplification of the Design Sequence	34
4. C-STAAC Functionality	36
4.1. Home Screen.....	36
4.2. Simulation Options.....	37
4.3. Selecting a Working Directory	37
4.4. Simulation Name	38

5.	C-STAAC Functionality: Meanline Application	39
5.1.	Meanline Interface.....	39
5.2.	Running a Meanline Simulation.....	39
5.3.	Minimum Input.....	40
5.4.	Navigation Tab	40
5.5.	Input Window	42
5.6.	General Input Tab.....	42
5.6.1.	Simulation Name	43
5.6.2.	Number of Spanlines.....	43
5.6.3.	Thermodynamic Properties.....	44
5.6.4.	Operating Conditions	44
5.6.5.	Flowpath Control.....	46
5.6.6.	Notifications.....	46
5.7.	Inlet Conditions Input Tab	47
5.7.1.	General Conditions at Rotor 1 Inlet	47
5.7.2.	Geometry Parameters at Rotor 1 Inlet.....	48
5.7.3.	Endwall Blockage at Rotor 1 Inlet	48
5.7.4.	Inlet Guide Vane Definition	49
5.8.	Blade Parameters Tab (Global Settings).....	52
5.8.1.	Global Parameters – All Blades.....	53
5.8.2.	Global Parameters – All Rotor Blades	56
5.8.3.	Global Parameters – All Stator Blades.....	56
5.9.	Blade Parameters Tab	57
5.9.1.	Station Details.....	59
5.9.2.	Blade Exit Swirl Definition	60
5.9.3.	Blade Aerodynamic Properties.....	61
5.9.4.	Blade Geometry Parameters	64
5.10.	Additional Input Window Commands.....	66
5.10.1.	Apply All Command.....	67
5.10.2.	Blade Navigation Pane.....	68
5.10.3.	Reset All.....	69
5.10.4.	Restore Last	70
5.10.5.	Export Data	70
5.11.	Post-Processing.....	71
5.11.1.	Blade Geometry Post-Processing Window.....	73
5.11.2.	Stage Plot Post-Processing Window	77
5.11.3.	Radial Data Post-Processing Window	79
5.12.	Meanline-to-Throughflow Window.....	80
6.	C-STAAC Functionality: Throughflow Application	83
6.1.	Throughflow Interface	83
6.2.	Running a Throughflow Simulation.....	84
6.3.	Minimum Input.....	84
6.4.	Navigation Tab	85
6.5.	Input Window	86
6.6.	General Input Tab.....	86

6.6.1.	Simulation Name	87
6.6.2.	Number of Streamlines	87
6.6.3.	Thermodynamic Properties.....	88
6.6.4.	Operating Conditions	89
6.6.5.	Inlet Conditions	89
6.6.6.	Radial Flow Fraction Distribution.....	91
6.6.7.	Loss Parameters	92
6.6.8.	Blade Surface Distance Fractions.....	94
6.7.	Design Input Tab (Flowpath Control).....	95
6.7.1.	Flowpath Coordinates	96
6.7.2.	Import Boundary	97
6.7.3.	Preview Coords.....	97
6.8.	Blade Navigation Pane.....	98
6.9.	Design Input Tab (Free Station Control)	99
6.9.1.	Station details.....	100
6.9.2.	Axial Location of Free Station	101
6.9.3.	Blockage Factors	102
6.9.4.	Mass Bleed Factor	102
6.10.	Design Input Tab (Blade Control).....	103
6.10.1.	Station Details.....	104
6.10.2.	Blade Design Options	104
6.10.3.	General Blade Properties	108
6.10.4.	Stacking Line Location	108
6.10.5.	Blockage Factors	109
6.10.6.	Mass Bleed Factors	109
6.10.7.	Aerodynamic Limit Criteria	110
6.10.8.	Profile Loss	112
6.10.9.	Blade Exit Profile	114
6.10.10.	Stage Energy Addition	116
6.10.11.	Stacking Line Tilt Angle.....	117
6.10.12.	Material Density	117
6.10.13.	Incidence Angle Treatment.....	118
6.10.14.	Deviation Angle Treatment	120
6.10.15.	Blade Element Shapes.....	121
6.10.16.	Blade Segment Transition Point.....	123
6.10.17.	Maximum Thickness Point.....	124
6.10.18.	Basic Radial Geometry Parameters.....	125
6.10.19.	Advanced Blade Definition Parameters.....	128
6.11.	Miscellaneous Input Tab.....	132
6.12.	Post Processing	134
6.12.1.	Blade Geometry Post-Processing Window.....	137
6.12.2.	Stage Plot Post-Processing Window	142
6.12.3.	Radial Data Post-Processing Window	143
7.	Conclusion.....	144
	REFERENCES	145

A.	Stage Variables Available for Plot - Meanline Application.....	148
B.	Radial Variables Available for Plot - Meanline Application	149
C.	Stage Variables Available for Plot - Throughflow Application.....	150
D.	Radial Variables Available for Plot - Throughflow Application	151

LIST OF TABLES

Table 2.1 Example vortex design strategies (Horlock, 1958).....	25
Table 4.1 Default file names and extensions	38
Table 5.1 Minimum input required to generate a Meanline solution.	40
Table 6.1 Minimum input required to generate a Throughflow solution.	85
Table 6.2 Default coefficients for variable specific heat model	89
Table A.1 Output variables solved by the program.	148
Table A.2 Input variables specified by the user.....	148
Table B.1 Variables for <i>Aerodynamic</i> plot type.	149
Table B.2 Variables for <i>Geometric</i> plot type.....	149
Table C.1 Mass averaged stage variables.	150
Table C.2 Cumulative sums of mass averaged stage variables.	150
Table D.1 Aerodynamic variables for <i>Free</i> stations.	151
Table D.2 Aerodynamic variables for <i>Rotor Inlet</i> stations.	151
Table D.3 Aerodynamic variables for <i>Rotor Outlet</i> stations.	152
Table D.4 Aerodynamic variables for <i>Stator Inlet</i> stations.	152
Table D.5 Aerodynamic variables for <i>Stator Outlet</i> stations.....	152
Table D.6 Geometric variables for <i>Rotor</i> and <i>Stator Inlet</i> stations.	152
Table D.7 Geometric variables for <i>Rotor</i> and <i>Stator Outlet</i> stations.....	152

LIST OF FIGURES

Figure 1.1 Example gas turbine configuration for aerospace applications (Pratt & Whitney).	1
Figure 1.2 Example gas turbine configuration for industrial applications (Siemens).	1
Figure 1.3 Typical gas generator configuration (Farokhi, 2014).	4
Figure 1.4 Enthalpy-Entropy characteristic for a typical gas generator (Farokhi, 2014). ..	4
Figure 1.5 A typical compressor stage consisting of a rotor and a stator in the meridional (side) view.	7
Figure 1.6 A typical compressor stage consisting of a rotor and a stator in the cascade (top-down) view.	7
Figure 1.7 Velocity vector representation of the flow through a single compressor stage.	8
Figure 1.8 Complete velocity triangle between a rotor and a stator.	8
Figure 1.9 Geometry of a rotor cascade with chord length (c) and spacing (s) shown for reference.	13
Figure 1.10 Variation of a measured loss parameter with Diffusion Factor (Hill & Peterson, 1992) – originally from NASA SP-36 (Lieblein et al., 1953).	13
Figure 1.11 Sketch of the exit flow conditions of a cascade exit with periodic wakes. (Farokhi, 2014).	14
Figure 1.12 Variation of m with chord (stagger) angle for both circular-arc and parabolic-arc airfoil cascades (Farokhi, 2014).	16
Figure 1.13 Common nomenclature for a compressor cascade (Farokhi, 2014).	17
Figure 2.1 Scheme of a typical compressor design process (Molinari & Dawes, 2006)..	18
Figure 2.2 Schematic representation of the streamline distribution employed by a typical Throughflow solver (Tiwari, Stein & Lin, 2013)	19
Figure 2.3 Scheme of the proposed iterative design process (Molinari & Dawes, 2006)	22
Figure 2.4 Coupled interaction considered by the current work.	22
Figure 2.5 Tangential motion of a small fluid particle (Hill & Peterson, 1992).	24
Figure 2.6 Velocity field of a rotor blade subjected to free-vortex design. (Farokhi, 2010)	24
Figure 2.7 Constant reaction design with $R = 0.6$ (Horlock, 1958).	26
Figure 2.8 Free vortex design with $R = 0.6$ at root (Horlock, 1958)	26
Figure 2.9 Free vortex design with $R = 0.6$ at mean (Horlock, 1958)	27
Figure 2.10 Exponential design with $R = 0.6$ at mean (Horlock, 1958)	27
Figure 2.11 Example streamline discretization of a 2-stage fan (Hirsch & Denton, 1981).	28

Figure 2.12 Comparison between the measured and predicted exit axial velocity profiles for a given rotor blade (Gallimore, 1999).	30
Figure 2.13 Comparison between the measured and predicted exit a flow angle profiles for a given rotor blade (Gallimore, 1999).	31
Figure 3.1 Schematic demonstrating the coupled abilities of C-STAAC.	35
Figure 4.1 C-STAAC home screen.	36
Figure 5.1 Meanline application interface.	39
Figure 5.2 Example warning messages.	41
Figure 5.3 Load/Save window.	41
Figure 5.4 General input tab.	42
Figure 5.5 Example radial profile using 11 spanlines.	43
Figure 5.6 Example radial profile using 5 spanlines.	43
Figure 5.7 Thermodynamic properties input field in the General input tab.	44
Figure 5.8 Default operating condition fields.	45
Figure 5.9 Pressure ratio convergence options.	45
Figure 5.10 Examples of comments produced by the Meanline code.	46
Figure 5.11 Inlet conditions input tab.	47
Figure 5.12 Default inlet conditions (at Rotor 1).	48
Figure 5.13 Default geometry conditions (at Rotor 1 inlet).	48
Figure 5.14 Blockage factor definition for Rotor 1 inlet.	49
Figure 5.15 Inlet guide vane definition.	49
Figure 5.16 IGV Swirl profile definition.	51
Figure 5.17 User-defined constant swirl profile at IGV exit (Rotor 1 Inlet)	52
Figure 5.18 Internally-calculated free-vortex swirl profile at IGV exit (Rotor 1 Inlet) ..	52
Figure 5.19 (Global) blade parameters tab.	53
Figure 5.20 Meridional geometry using the default gap spacing.	54
Figure 5.21 Meridional geometry using a custom gap spacing.	54
Figure 5.22 Constant spacing option.	55
Figure 5.23 Custom spacing option	55
Figure 5.24 Custom spacing input window.	56
Figure 5.25 Global rotor blade parameters.	56
Figure 5.26 Global stator blade parameters.	57
Figure 5.27 Blade row navigation pane.	58

Figure 5.28 Rotor blade parameters.....	59
Figure 5.29 Stator blade parameters.	59
Figure 5.30 Rotor exit swirl definition fields.....	60
Figure 5.31 Stator exit swirl definition fields.	60
Figure 5.32 Polytropic efficiency definition.	62
Figure 5.33 Warning message for efficiency specification change.	62
Figure 5.34 Blockage factor definition	63
Figure 5.35 Remaining aero input fields (rotors).....	63
Figure 5.36 Remaining aero input fields (stators).	63
Figure 5.37 Geometry input fields (rotors).....	64
Figure 5.38 Geometry input fields (stators).....	64
Figure 5.39 Stage 2 with tip and hub ramp angle limits of -6 and 6 degrees respectively.	66
Figure 5.40 Stage 2 with tip and hub ramp angle limits of -20 and 20 degrees respectively.	66
Figure 5.41 Complete user input window (Rotor blade parameter tab shown for reference).	67
Figure 5.42 Insert stage window.....	68
Figure 5.43 Export selection window.	71
Figure 5.44 Blade geometry post-processing window.....	72
Figure 5.45 Stage plot post-processing window.....	72
Figure 5.46 Radial plot post-processing window.	73
Figure 5.47 Stage view (stage 1 shown).	74
Figure 5.48 Single blade view (rotor 1 shown).....	74
Figure 5.49 Blades only view.	74
Figure 5.50 Boundary only view.	74
Figure 5.51 <i>Boundary only</i> view with aerodynamic stations (green) and staking lines (black) shown.....	75
Figure 5.52 Aerodynamic stations and stacking axes shown for stage 1 blades (with IGV).	75
Figure 5.53 Filled blade geometry.....	76
Figure 5.54 Blade outline view.....	76
Figure 5.55 Coordinates displayed at the trailing edge of stator 1.	76
Figure 5.56 Cumulative stage pressure ratios for the default 5 stage compressor.....	78
Figure 5.57 Equivalent raw stage pressure ratios for the default 5 stage compressor.	78

Figure 5.58 Cumulative stage adiabatic efficiencies for the default 5 stage compressor.	78
Figure 5.59 Cumulative stage polytropic efficiencies for the default 5 stage compressor.	78
Figure 5.60 Radial distributions of tangential velocity at the inlet and exit locations of rotor 2.....	80
Figure 5.61 Radial distribution (normalized to span) of tangential velocity at the inlet and exit locations of rotor 2.....	80
Figure 5.62 User input options to initialize the Throughflow simulation.....	81
Figure 5.63 Tangential velocity distribution at stator 2 exit.....	82
Figure 5.64 Tangential velocity distribution at stator 2 exit (scaled to 70%).....	82
Figure 6.1 Throughflow application interface.	83
Figure 6.2 General input tab.	86
Figure 6.3 Example axial velocity profile using 11 streamlines.....	87
Figure 6.4 Example axial velocity profile using 5 streamlines.....	87
Figure 6.5 Thermodynamic properties input field with constant C_p	88
Figure 6.6 Thermodynamic properties input field with variable C_p	88
Figure 6.7 Variable specific heat input window.	88
Figure 6.8 Operating conditions input fields.	89
Figure 6.9 Inlet conditions input fields.....	90
Figure 6.10 Inlet profile definition (swirl velocity shown).....	90
Figure 6.11 Streamline weight flow distribution options.	91
Figure 6.12 Streamline weight flow distribution definition (constant distribution shown).	92
Figure 6.13 Streamline weight flow distribution options.	92
Figure 6.14 Loss parameter input window.	93
Figure 6.15 Distance fraction definition window.	95
Figure 6.16 Flowpath control tab.....	96
Figure 6.17 Imported boundary *.csv file format.	97
Figure 6.18 Preview coords window.	98
Figure 6.19 Blade navigation pane.	99
Figure 6.20 Free station input tab.	100
Figure 6.21 Station details fields.	101
Figure 6.22 Free station axial location definition.	101
Figure 6.23 Example exit duct defined using slanted free stations.....	102

Figure 6.24 Blockage factor definition fields.	102
Figure 6.25 Mass bleed factor definition.	103
Figure 6.26 Rotor station input tab.	104
Figure 6.27 Stacked rotor 1 blade geometry.	105
Figure 6.28 Blade design/analysis options.	105
Figure 6.29 Meridional blade coordinate definition window.	106
Figure 6.30 Imported blade *.csv file format.	106
Figure 6.31 Blade meridional view for analysis mode.	107
Figure 6.32 General blade property fields.	108
Figure 6.33 Stacking axis coordinate definition.	108
Figure 6.34 Stacking axis definition of rotor 1.	109
Figure 6.35 Stacking axis re-defined for rotor 1.	109
Figure 6.36 Blade row blockage factor definition.	109
Figure 6.37 Blade row mass bleed factor definition.	110
Figure 6.38 Aerodynamic limits for rotor blades.	110
Figure 6.39 Aerodynamic limits for stator blades.	110
Figure 6.40 Rotor 1 profile with the default choke margin (i.e. none specified).	111
Figure 6.41 Rotor 1 profile with a choke margin of 0.2.	111
Figure 6.42 Profile loss definition (no loss sets specified).	112
Figure 6.43 Profile loss definition (when loss sets specified).	112
Figure 6.44 Constant total pressure profile at Rotor 1 exit.	112
Figure 6.45 Polynomial total pressure profile at Rotor 1 exit.	112
Figure 6.46 Exit total pressure profile definition.	113
Figure 6.47 Rotor exit profile definition.	114
Figure 6.48 Stator exit profile definition.	114
Figure 6.49 Exit total pressure profile definition for rotors (when using an internal loss correlation).	115
Figure 6.50 Exit swirl profile definition for stator blades.	116
Figure 6.51 Rotor energy addition definition.	116
Figure 6.52 Rotor tip total temperature definition.	116
Figure 6.53 Tip tilt angle definition.	117
Figure 6.54 Hub tilt angle definition.	117
Figure 6.55 Linearly tilted axis resulting from 20° tip angle definition.	117

Figure 6.56 Curved axis resulting from 20° hub angle definition.....	117
Figure 6.57 Rotor blade material density definition.	118
Figure 6.58 Incidence angle treatment options.	118
Figure 6.59 Rotor 1 LE geometry using 2D incidence treatment	119
Figure 6.60 Rotor 1 LE geometry using 3D incidence treatment	119
Figure 6.61 Manual incidence definition.....	120
Figure 6.62 Deviation angle treatment options.....	120
Figure 6.63 Rotor 1 TE geometry using Carter's rule.	121
Figure 6.64 Rotor 1 TE geometry using 3D treatment.	121
Figure 6.65 Airfoil reference and direction nomenclature (Crouse & Gorrell, 1981)...	122
Figure 6.66 Blade element shape definition.	122
Figure 6.67 Turning rate ratio definition.	123
Figure 6.68 Blade element transition point definition.	123
Figure 6.69 Transition point definition.....	124
Figure 6.70 Maximum thickness point definition.....	124
Figure 6.71 Max thickness point definition.....	125
Figure 6.72 Basic geometry definition options.....	126
Figure 6.73 LE/TE radius-to-chord definition.....	127
Figure 6.74 Max thickness-to-chord definition.	127
Figure 6.75 Axial chord-to-tip-chord ratio definition.....	128
Figure 6.76 Advanced geometry definition.....	129
Figure 6.77 Rotor 1 geometry with $a_{I, FWD} = 20$ and $a_{I, AFT} = -1$	130
Figure 6.78 Rotor 1 geometry with $a_{I, FWD} = 1$ and $a_{I, AFT} = -20$	130
Figure 6.79 Thickness distribution definition.....	131
Figure 6.80 Rotor 1 default (circular) LE geometry ($e = 0$)	132
Figure 6.81 Rotor 1 LE geometry with $B_{, FWD} = 2$ and $C_{, FWD} = 0.5$	132
Figure 6.82 Miscellaneous input tab.....	133
Figure 6.83 Rotor 1 stacking distribution (10 elements specified).....	134
Figure 6.84 Rotor 1 stacking distribution (24 elements specified).....	134
Figure 6.85 Blade geometry post-processing window (fabrication coords view).	135
Figure 6.86 Stage plot post-processing window.	136
Figure 6.87 Radial plot post-processing window.	136
Figure 6.88 Blade geometry post-processing window (meridional view).....	137

Figure 6.89 Blade geometry post-processing window (airfoil view).	138
Figure 6.90 Meridional view of rotor 1.	138
Figure 6.91 Airfoil view of rotor 1 (at 50% span).	138
Figure 6.92 Compressor geometry with stacking axes and free stations shown.	139
Figure 6.93 User-defined boundary with stacking axes and free stations shown for reference.	140
Figure 6.94 Smoothed boundary with stacking axes and free stations shown for reference.	140
Figure 6.95 3D (isometric) view of rotor 1.	141
Figure 6.96 <i>Top</i> view of rotor 1.	141
Figure 6.97 <i>Side</i> view of rotor 1.	141
Figure 6.98 <i>Front</i> view of rotor 1.	141
Figure 6.99 Mass averaged total pressure ratio across the compressor.	142
Figure 6.100 Cumulative sum of the mass averaged total pressure ratio across the compressor.	142

SYMBOLS

a	Ellipse semi-minor axis length
b	Ellipse semi-major axis length
c	Absolute velocity; Chord length
C_p	Ratio of specific heat at constant pressure
c_θ	Absolute tangential (swirl) velocity
D	Diffusion factor
e	Ellipse eccentricity
g/s	Axial gap spacing
h	Enthalpy
\dot{m}	Mass flow rate
N	Number of blades
P_0	Total pressure
R	Non-dimensional fraction of passage height
r	Radius
r_h	Hub radius
r_t	Tip radius
s	Entropy; Spacing
t/c	Thickness-to-chord ratio
T_0	Total temperature
U	Circumferential velocity
v_m	Meridional velocity
v_θ	Tangential (swirl) velocity
w	Relative velocity
z	Axial reference frame
α	Absolute flow angle
β	Relative flow angle
η_s	Adiabatic efficiency
θ	Tangential reference frame
θ^*	Trailing wake thickness
ϖ	Relative total loss coefficient
π_c	Overall compressor total pressure ratio
σ	Solidity
γ	Specific heat ratio
Ω	Angular rotation rate
ω	Shaft rotational speed
ω_p	Profile loss coefficient

ABBREVIATIONS

1D	One dimensional
2D	Two dimensional
3D	Three dimensional
C-STAAC	Coupled Spanline Throughflow Aerodynamic Axial Compressor design
CFD	Computational fluid dynamics
CG	Center of gravity
GUI	Graphical user interface
IGV	Inlet guide vane
NACA	National Advisory Committee for Aeronautics
NASA	National Aeronautics and Space Administration
ODE	Ordinary differential equation
RPM	Revolutions per minute

ABSTRACT

Name: Rozendaal, Alexander V.

Degree: Master of Science in Aerospace Engineering

Institution: Embry-Riddle Aeronautical University

Date: November 2016

Title: A Computer Program for the Coupled Implementation of Meanline and Throughflow Methods to Simplify the Aerodynamic Design of Multistage Axial Compressors.

A computer program capable of simplifying the preliminary aerodynamic design process of multistage axial compressors has been developed. This interactive design tool, named C-STAAC, combines the Meanline and Throughflow analysis capabilities of two independent compressor design codes to form one standalone system. The program greatly improves the efficiency of the Preliminary-to-Throughflow stages of compressor design by providing fully coupled interaction between the two platforms. The result enables the user to produce stacked airfoil geometry from only a handful of initial input parameters.

The program additionally offers a wide selection of pre- and post-processing capabilities that were not previously available with the independent design codes. This tool is accessed through an easy-to-use graphical user interface that allows for immediate visual feedback during design iterations, thus increasing user productivity and design turnaround time. An equivalent industry-standard process may take a substantial amount of time and effort. The unique “from scratch” design capabilities of C-STAAC are explained in complete detail, and the program’s abilities are demonstrated with illustrated examples.

1. Introduction

1.1. Overview of Introductory Theory

Gas turbine engines have continued to serve as the backbone for the aviation and power generation industries for many decades, and they will remain prominent in their roles until such time as their combined practicality and performance can be surpassed. Whether being applied as the primary source of propulsion for a commercial jet transport aircraft, or used to power an industrial generator supplying electricity to businesses and residential homes, the extremely high power-to-weight capabilities of a gas turbine engine underscore one of the many benefits associated with its design. Examples of both types of applications are illustrated in Figure 1.1 and Figure 1.2 below.

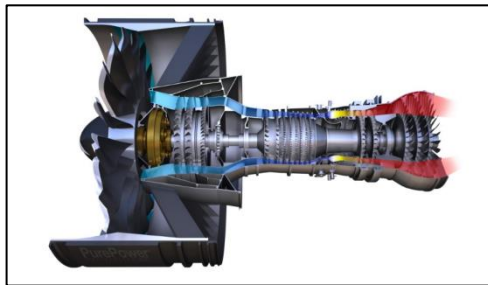


Figure 1.1 Example gas turbine configuration for aerospace applications (Pratt & Whitney).

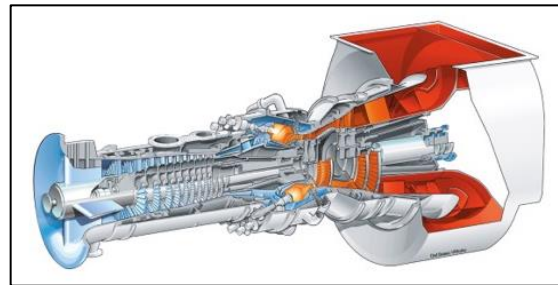


Figure 1.2 Example gas turbine configuration for industrial applications (Siemens).

As commercial air travel and industrial power requirements continue to rise, so does the cost of fuel required to operate these machines. The demand to lower the environmental impact of a gas turbine poses many challenges for engine manufacturers, and efforts to increase their operating efficiency are constantly being undertaken. Common areas of such research include higher-efficiency forms of combustion, alternative fuel development, and advancements in turbine blade cooling technology. Slightly lesser attention however is focused towards the optimization of turbomachinery,

specifically compressor blade geometry, within the engine itself. Considering that even a slight improvement in compressor efficiency can significantly benefit an engine's overall performance (Oyama, Liou, & Obayashi, 2004), the opposite is in fact also true. The effects of a poorly designed compressor can extend throughout the entire engine, even to the point of potential destruction. Factoring in as well the high level of risk and complexity involved in obtaining a reliable compressor design, blade re-design activities are often very costly, time consuming, and challenging to undertake. This sometimes leads manufacturers to focus their resources elsewhere in search of increasing an engine's operating efficiency.

Perhaps the most significant aspect contributing to delays stems from the efforts involved in predicting the complex flow structure that is synonymous with compressor aerodynamics. Simply put, the amount of time and effort required to iterate and refine an aerodynamic solution of a multistage compressor places a tremendous burden on computational resources, especially when a fully viscous three-dimensional (3D) representation of the flow is desired. The 3D techniques employed refer to the application of Computational Fluid Dynamics (CFD) principles, in which the Navier-Stokes equations are solved numerically in accordance with a set of boundary conditions specific to the compressor's operating environment. In cases where the flow is dominated by 3D effects, such as that experienced by a highly twisted fan blade, the use of CFD becomes the preferred design tool due to its ability to predict multi-dimensional flows with reasonable accuracy (Denton & Dawes, 1998). This numerical approach is not without its limitations, however, and often comes at a cost.

Denton (2010) provides a detailed discussion regarding the limitations of CFD for

turbomachinery applications, but perhaps the greatest cost associated with performing a CFD study is that it can be very computationally demanding. Achieving a high-fidelity CFD solution, especially with multistage simulations, often requires computational resources that are beyond the scope of that required to perform quick iterative studies. Instead, complete multistage simulations can take days or even weeks to converge depending on the complexity and unsteadiness of the flow structure, as well as the computing resources that are available. It is for this reason that extensive forms of analyses, such as conceptual design studies or parametric trend predictions, are commonly performed using simpler techniques.

Examples of such practices include Meanline (1D) and Throughflow (2D) methods, in which the aerodynamic representation of the flow is assumed in one and two dimensions respectively, as opposed to the full 3D representation exclusive to a CFD simulation. Although they are less effective in capturing the 3D effects described earlier, Meanline and Throughflow methods are regarded as being fundamental aspects of turbomachinery design (Denton & Dawes, 1998), and continue to remain as cost-effective alternatives to running 3D multistage CFD analysis (Petrovic, Dulikravich, & Martin, 2001). The coupled interaction between these two levels of analysis can be extremely valuable in performing quick iterative trend studies.

Quite often, solutions obtained from the higher-level CFD analyses are used for verification and validation purposes, but also for evaluating resulting pressure loss coefficients across blade rows (Oyama et al., 2004). The resulting coefficients are usually fed directly back into the preliminary calculations as part of a synergy loop, which allows for an increased margin of accuracy in the Meanline and Throughflow predictions.

1.2. Review of Gas Turbine Theory

At the core of every gas turbine engine, whether used for aircraft or industrial applications, is the gas generator. A conventional gas generator includes a compressor, combustion chamber, and a turbine section, and usually takes a form similar to the one shown in Figure 1.3. The combined operation of these three components forms a self-sustaining thermodynamic cycle known as the *Brayton cycle*, in which energy is harnessed from a controlled reaction of air and fuel before being transferred into useful mechanical work. An example of a typical Brayton cycle characteristic in the form of an enthalpy-entropy (h - s) diagram is illustrated in Figure 1.4.

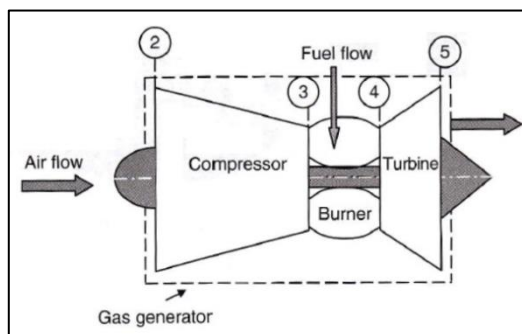


Figure 1.3 Typical gas generator configuration (Farokhi, 2014).

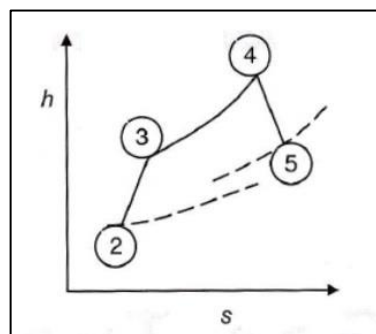


Figure 1.4 Enthalpy-Entropy characteristic for a typical gas generator (Farokhi, 2014).

The numbering convention shown in Figure 1.3 and Figure 1.4 refers to each relevant thermodynamic station of the Brayton cycle. Stations 2-3 for example define the compressor section of the gas generator, through which ambient air is gradually compressed through a series of rotating and stationary blade rows. The rotating components of the compressor are referred to as rotors, and are connected via a solid shaft to the turbine section where mechanical work is supplied. With a more detailed explanation of the compression process provided in a later section, the net result is a

significant increase in fluid pressure at station 3 as indicated by the sudden rise in enthalpy shown in Figure 1.4. Often when performing thermodynamic calculations for this process, it is common to assume the operation of the compressor as being isentropic, meaning that no heat is added or taken away from the system, and no dissipative flow phenomena occur (Anderson, 2003). This constant-entropy assumption is visually represented on the h - s diagram as a vertical line between stations 2 and 3. In reality however, irreversible losses are always present in the form of boundary layer formation, wake formation, and vortex shedding as a consequence of the fluid's viscous properties (Farokhi, 2014). The additional presence of relative supersonic shock formations add to this effect, and the combined result leads to an increase in entropy as illustrated by the horizontal shift in Figure 1.4. The magnitude of the shift on the h - s diagram is predominantly used as a measure of the compressor's operating efficiency, and the task to minimize this horizontal shift (i.e. maximize efficiency) becomes a subsequent challenge faced by every compressor designer.

Once a suitable level of compression is reached, the air is mixed with fuel and ignited within the engine's combustion chamber (station 3-4). The result leads to an even greater increase in enthalpy, most of which is then captured by another series of rotor and stator blades located in the turbine section (4-5). Much like a paddle wheel in a stream of flowing water, the high-energy flow exiting the combustor chamber causes the rotor blades of the turbine to spin, which allows mechanical energy to transfer back along a rotating shaft to power the compressor. In essence, the entire thermodynamic process, that is 2-3-4-5, is completely sustainable provided that a continuous supply of fuel is added to the system.

1.3. Review of Compressor Aerodynamics

The thermodynamic role of the compressor is fairly simple, in that it is tasked with increasing the pressure of the incoming fluid to a level where it can be efficiently mixed with fuel and ignited. The mechanics involved with achieving this task, however, are in fact quite complicated. Considering that a fluid tends to naturally flow in a direction defined by a pressure gradient, specifically from high to low pressures, intuition would therefore suggest that an increase in pressure in the direction of flow would cause certain complexities to arise. Like trying to force water to flow up a hill, a compressor must be designed to operate in this so-called *adverse* pressure gradient while still maintaining its thermodynamic goal as efficiently as possible. Any compromise to this effect, such as the formation of an unstable boundary layer leading to flow separation along an airfoil section, could result in a flow reversal phenomenon known as *surge*, and could be catastrophic to the overall health of the engine. This is one of the many challenges that compressor designers have to overcome. It is also one of the key factors that builds the challenging reputation of the compressor aerodynamics field.

1.3.1. Compressor Stage Definition

Inside every compressor lies a series of rotor and stator blade rows. With an exception of the very first stator blade, known as the Inlet Guide Vane (IGV), every successive rotor and stator pair forms what is referred to as a *stage*. Visual representations of a standard rotor-stator stage are shown in Figure 1.5 and Figure 1.6 with an IGV included for reference. Referring back to the previous discussion, the goal of each stage is to gradually increase the pressure of the fluid as efficiently as possible. However, the magnitude of pressure rise through each row becomes a limiting factor in

compressor design. Fundamentally, the internal channels that pass through each blade row take on the characteristic properties of a diffuser, and the viscous boundary layer that forms along the walls of these channels is naturally subject to a pressure increase, hence the adverse pressure gradient (Hill & Peterson, 1992). Due to their inherently low momentum, boundary layers cannot tolerate a significant rise in pressure, and so pressure ratios through a stage are generally limited to no more than about 2:1. (Farokhi, 2014). It is for this reason that compressors typically require a large number of stages to achieve their high overall pressure ratios, which gives rise to the term *multistage* compressor.

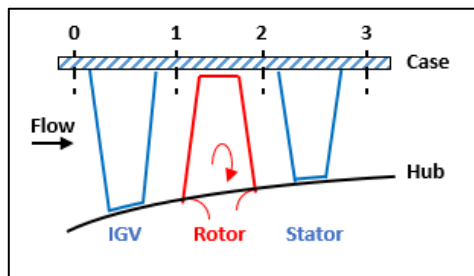


Figure 1.5 A typical compressor stage consisting of a rotor and a stator in the meridional (side) view.

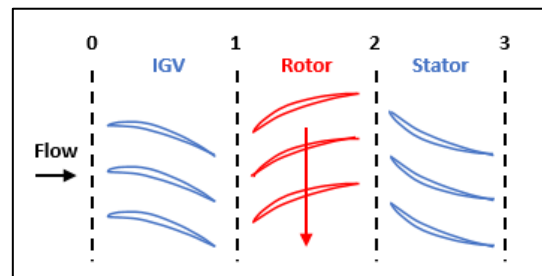


Figure 1.6 A typical compressor stage consisting of a rotor and a stator in the cascade (top-down) view.

1.3.2. Velocity Triangles

Considering that compressors encompass both rotating and stationary components, aerodynamic calculations are typically performed in two frames of reference. The stationary or *absolute* frame remains fixed to the outside frame of the compressor, while the *relative* frame corresponds to the rotating blades of the machine (Hill & Peterson, 1992). When considering the aerodynamic performance of a single stage, it is useful to represent the inlet and exit fluid velocity vectors between each blade row in both the absolute and relative frames of reference. The overlaid representation of

the two frames is what is referred to as a *velocity triangle*, and can be useful in providing a visual representation of the flow between each stage. This is illustrated in Figure 1.7. The absolute velocities ($c_{1,2,3}$) in Figure 1.7 are therefore represented as though the observer was to stand on the outside of the machine. All relative vectors on the other hand ($w_{1,2,3}$) are perceived as though the observer was to stand on a rotor blade as it spins. Figure 1.8 provides a complete breakdown of the velocity triangle which includes the absolute and relative flow angles (α , β) as well as axial and tangential (z , θ) velocity components between each blade row.

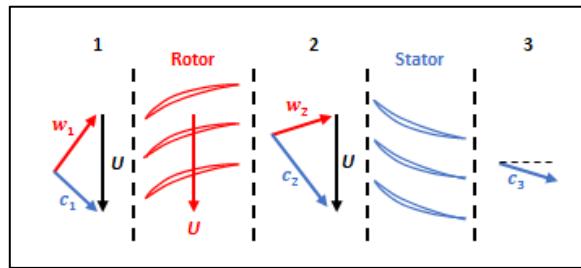


Figure 1.7 Velocity vector representation of the flow through a single compressor stage.

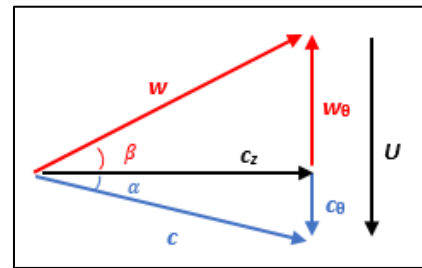


Figure 1.8 Complete velocity triangle between a rotor and a stator.

1.3.3. Stage Energy Addition

As air moves axially through a compressor cascade, the rotor imparts angular momentum onto the fluid by introducing a tangential component to the flow. This tangential component is also referred to as *swirl*, and could be described as total enthalpy that is added to the system through the rotation of the blade (Peng, 2008). The increase in total enthalpy consequently increases the kinetic energy and total pressure of the air exiting the rotor. The relative velocity is additionally reduced due to the channel's diffusive properties. The fluid then proceeds into the stator blade row where the swirl is removed, the kinetic energy is decreased, and the static enthalpy is recovered. A slight

reduction in total pressure occurs across the stator row due to various losses, however the benefit of doing so results in a significant increase in static pressure. This process is repeated through multiple stages of the compressor until the desired level of compression is achieved.

Through the process of accumulating kinetic energy, the fluid in fact becomes ‘torqued’ as it moves across each rotor blade row (Hill & Peterson, 1992). The amount of torque imposed on the fluid is dictated by the amount of swirl that is introduced, and is quantified by the following expression:

$$\tau = \dot{m}r(c_{\theta 2} - c_{\theta 1}) \quad (1.1)$$

In equation 1.1, \dot{m} is the mass flow rate of air passing through the rotor, r is the radius of the blade at which the calculation is being performed, and $(c_{\theta 2} - c_{\theta 1})$ is the difference between the swirl velocity magnitudes entering and exiting the rotor blade row. Considering that the power required to rotate a generic shaft is given as $P = \tau\Omega$, and Ω is the angular rotation rate defined as $\Omega = U/r$, the above expression is simplified to the following form:

$$P = -\dot{m}U(c_{\theta 2} - c_{\theta 1}) \quad (1.2)$$

The negative sign introduced in equation 1.2 derives from the thermodynamic convention that the power consumption is negative (Hill & Peterson, 1992). U is the circumferential velocity recalled from the velocity triangle notation discussed earlier. Given that the amount work done on a system is expressed simply as power per unit mass, or $w = -P/\dot{m}$, equation 1.2 is further simplified as follows:

$$w = U(c_{\theta 2} - c_{\theta 1}) \quad (1.3)$$

Alternatively, the work performed on the fluid can be represented as the change in total enthalpy as indicated by the following expression:

$$h_{02} - h_{01} = U(c_{\theta 2} - c_{\theta 1}) \quad (1.4)$$

Equation 1.4 is formerly referred to as the *Euler Turbomachinery Equation*, and is a widely recognized expression due to its unique ability to relate the aerodynamic and thermodynamic properties of a compressor blade row.

1.4. Figures of Merit

In addition to providing a quantitative representation of the amount of energy that is added to the system, the Euler equation provides a convenient way of relating the aerodynamic characteristics of a compressor stage to various figures of merit typically monitored throughout an iterative blade design cycle. These figures are predominantly used to evaluate the general health of the compressor, and to prevent adverse events such as flow-reversal.

1.4.1. Stage efficiency

Among the many performance characteristics monitored throughout the design cycle is the *Stage Adiabatic Efficiency* (η_s), or the ratio between the ideal to adiabatic work (Hill & Peterson, 1992). This parameter is defined as follows:

$$\eta_s \equiv \frac{h_{03s} - h_{01}}{h_{03} - h_{01}} = \frac{\Delta h_{0, isentropic}}{\Delta h_{0, actual}} \quad (1.5)$$

The subscripts in equation 1.5 refer to the inlet and exit locations of the stage as defined in Figure 1.7. An expected value for the stage efficiency is always less than one

for reasons relating to irreversibility effects. Such reasons include friction, and losses associated with supersonic shock formations. It is the goal of every designer to maximize the efficiency of a compressor stage. However, this sometimes becomes a compromising task giving way to additional design criteria such as the prevention of flow-reversal.

1.4.2. Degree of Reaction

Additional figures of merit used to monitor the health of a compressor include the *Degree of Reaction*, which is defined as the ratio of static enthalpy rise across the rotor to the total enthalpy rise across the entire stage. This relationship is written in terms of the Euler equation (equation 1.4) as follows:

$$R = \frac{h_2 - h_1}{h_{03} - h_{01}} = \frac{w_1^2 - w_2^2}{2U(c_{\theta 2} - c_{\theta 1})} \quad (1.6)$$

The degree of reaction is very useful as it provides a measure of the extent to which the rotor contributes to the static pressure rise across the stage (Saravanamuttoo, Rogers, & Cohen, 2001). Because the mechanism contributing to the pressure rise differs between rotors and stators (as explained earlier), it becomes important to ensure that the total contribution of stage pressure increase remains fairly equal between the two blades rows (i.e. $R = 0.5$). A value that strays significantly from this case would imply that the rotor ($R > 0.5$) or the stator ($R < 0.5$) contributes more than the other blade. In such cases, the possibility of flow-reversal could be expected for the higher loaded blade. Experimental results obtained over the years indicate that a boundary layer formed on a moving rotor blade is typically more stable than a corresponding boundary layer formed on a stator blade (Farokhi, 2014). For this reason, a slightly higher burden of stage pressure increase is usually allocated in favor of the rotor with $R \approx 0.6$.

1.4.3. Diffusion Factor

Another parameter used to address the health of a compressor, specifically the stability of its associated boundary layer, is the *Diffusion Factor*. This dimensionless parameter is defined as follows:

$$D = 1 - \frac{v_2}{v_1} + \frac{\Delta v_\theta}{2\sigma v_1} \quad (1.7)$$

All velocities in equation 1.7 are taken relative to their respective frames of reference in which they are applied. Hence $v_i = c_i$ for a stator, and $v_i = w_i$ for a rotor. The variable σ is further defined as the *solidity* of the blade as given by equation 1.8. The solidity of a blade is simply the ratio between its chord length (c) and spacing (s), both variables of which are illustrated in Figure 1.9.

$$\sigma(r) = \frac{c}{s} = \frac{N_b c}{2\pi r} \quad (1.8)$$

The application of the diffusion factor to determine boundary layer separation originated from the work carried out by Lieblein, Schwenk, & Broderick (1953). They characterized that there existed a quantifiable link between the deceleration of the flow on the suction surface of an airfoil, and the breakdown of the boundary layer that led to experimentally-observed flow separation. This phenomenon was quantified with the diffusion factor as a way of predicting when flow separation (and consequent flow reversal) would most likely occur. Recognizing that flow separation was more likely to occur in the presence of greater relative flow deceleration (Hill & Peterson, 1992), a better-suited parameter for the diffusion factor was later identified as follows:

$$D = \frac{w_{max} - w_2}{w_{max}} = 1 - \frac{w_2}{w_{max}} \quad (1.9)$$

Experiments have shown that the losses associated with flow separation grow rapidly for D values greater than about 0.4 (Johnson, & Bullock, 1965). For this reason, designers focus on limiting the Diffusion factor of a given blade to between 0.5-0.6 (Hill & Peterson, 1992). This trend is illustrated with respect to a measured profile loss parameter in Figure 1.10.

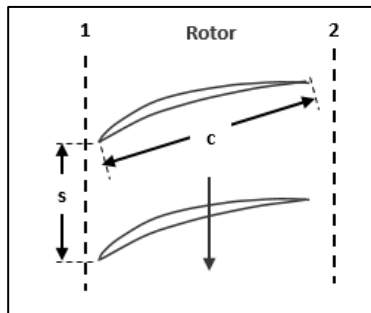


Figure 1.9 Geometry of a rotor cascade with chord length (c) and spacing (s) shown for reference.

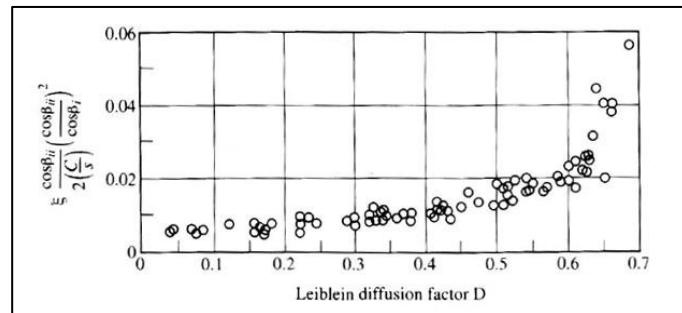


Figure 1.10 Variation of a measured loss parameter with Diffusion Factor (Hill & Peterson, 1992) – originally from NASA SP-36 (Lieblein et al., 1953).

1.4.4. Total Pressure Loss Parameter

Figures of merit such as the Degree of Reaction and Diffusion Factor provide guidelines to follow through the compressor design cycle, and a necessary baseline for preliminary aerodynamic calculations. These criteria however are usually applied at the lower levels of design (ex. Meanline), and so a higher level of detail is often desired to more accurately predict the losses through a compressor cascade. The introduction of a loss parameter came as a result of the initial work conducted by Lieblein et al., (1953) when they developed their Diffusion Factor correlations. As part of their work, they determined that it was necessary to consider the basic loss in total pressure relative to the blade in order to generalize the phenomenon involved with the blade-element flow. Their initial formulation, which they referred to as the *relative total-pressure loss coefficient*

(ϖ), considered only the relative total and static pressures at the inlet and exit of a blade row as follows:

$$\varpi = \frac{P_{01} - P_{02}}{P_{01} - P_1} \quad (1.10)$$

The subscript 0 in equation 1.10 refers to the total condition, and the subscripts 1 and 2 refer to the inlet and exit of the blade respectively. Further refinements to this function were made in the years that followed and considered other factors such as relative flow angles (β), blade solidity considerations (σ), and even trailing wake thicknesses (θ^*) as illustrated by Figure 1.11.

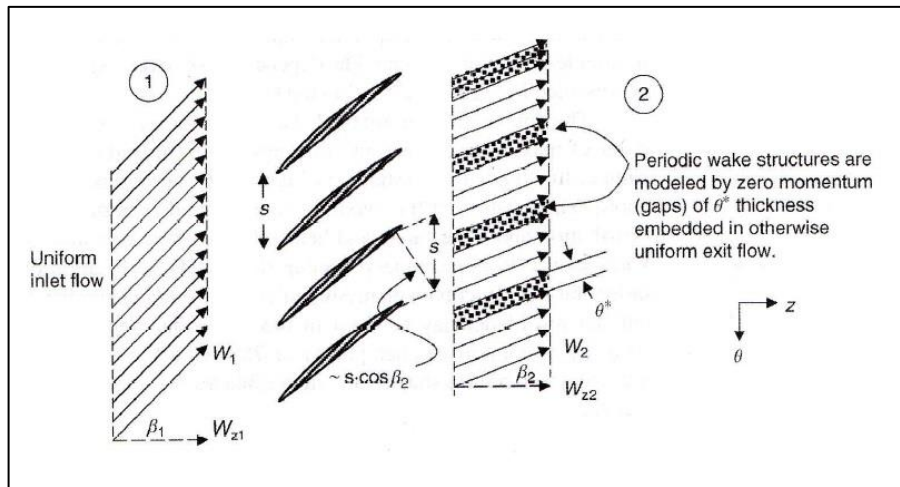


Figure 1.11 Sketch of the exit flow conditions of a cascade exit with periodic wakes. (Farokhi, 2014).

Factoring all such considerations defines a more accurate representation of the total pressure loss parameter as follows:

$$\varpi = \frac{P_{01} - \bar{P}_{02}}{\rho_1 w_1^2 / 2} = \left(\frac{\cos \beta_1}{\cos \beta_2} \right)^2 \frac{\sigma}{\cos \beta_2} \left(\frac{\theta^*}{c} \right) \quad (1.11)$$

The barred variable \bar{P}_{02} in equation 1.11 represents the area-average total pressure in the downstream wake region shown in Figure 1.11. The added benefit of applying the

total pressure loss function also includes the ability to now validate numerical predictions with experimental results. Provided that a manufacturer has the ability to perform cascade experiments and extract parameters such as those shown in Figure 1.11, the increased reliability would enable rapid iterative codes like Meanline and Throughflow solvers to be exploited as a principal design tools.

1.4.5. Deviation Angle

It is not common for air to exit the trailing edge of a blade at the exact angle defined by its geometry. The resulting nonconformity between the camber angle of the blade and the relative air angle is what is referred to as the *Deviation* angle, and occurs for two reasons. First, the diffusion process within the blade's channel implies that the fluid cannot flow in one single direction, but rather in multiple directions as it diverges through the blade row (Dixon & Hall, 2010). The phenomenon becomes exacerbated with increased blade spacing as fewer blades are present to guide the flow accordingly. Second, the level of deviation is further increased as a direct result of the growing boundary layer that forms along the suction surface of the blade. The magnitude of the deviation angle was quantified empirically for circular-arc airfoil cascades as follows (Carter, 1955):

$$\delta^* = \frac{m\varphi}{\sigma^n} \quad (1.12)$$

Equation 1.12 is formally referred to as *Carter's rule*, where φ is the camber angle of the blade, m is a function of chord angle and σ is the blade's solidity. The exponent, n , is an experimentally-determined constant given as 0.5 for a compressor blade and 1.0 for an inlet guide vane (Farokhi, 2014). Figure 1.12 provides a visual

representation of the chord function, m , for both circular and parabolic arc airfoils as referenced by Carter's rule.

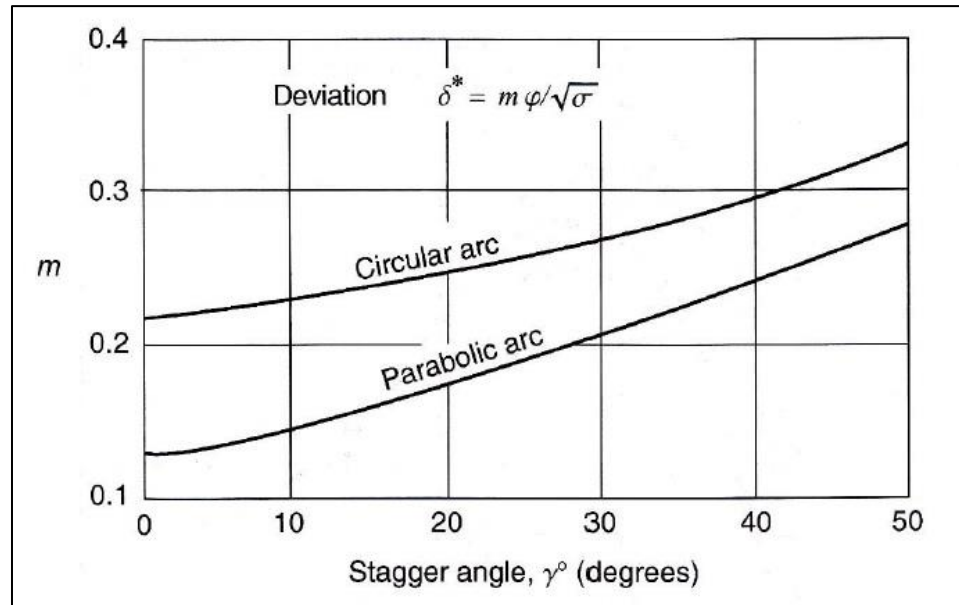


Figure 1.12 Variation of m with chord (stagger) angle for both circular-arc and parabolic-arc airfoil cascades (Farokhi, 2014).

The intensity of the trailing edge wake produced by the deviated flow can have a direct influence on the total pressure loss profile outlined in Figure 1.11, and hence the efficiency of the stage. Specifically, a higher deviation angle would effectively produce a greater trailing edge wake thickness (θ^*). The result, as expected, would lead to an increase in profile loss. A visual representation of the deviation angle with respect to its corresponding blade geometry is illustrated in Figure 1.13.

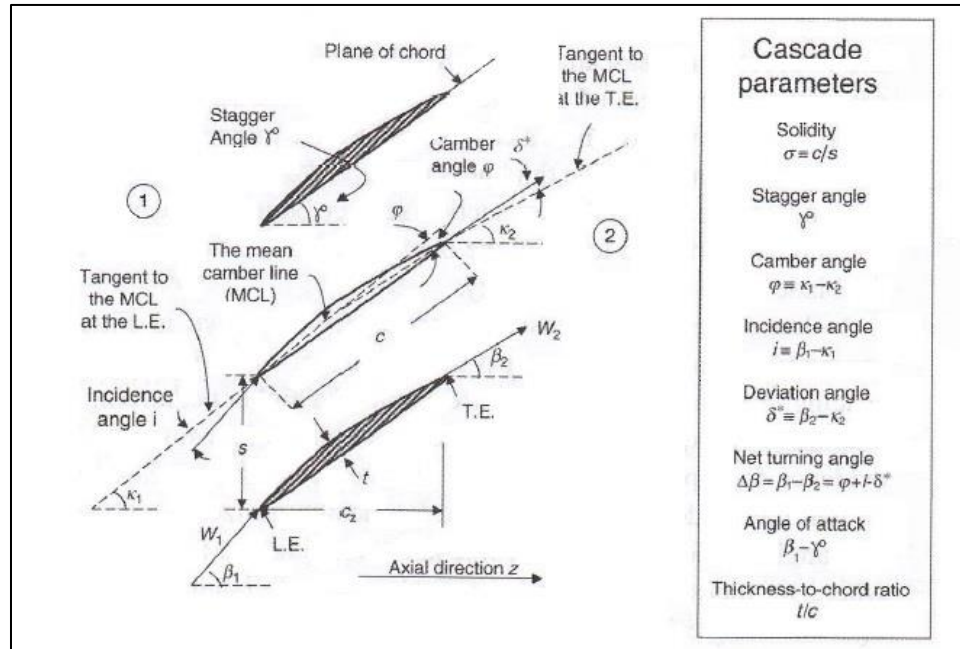


Figure 1.13 Common nomenclature for a compressor cascade (Farokhi, 2014).

2. Compressor Design Procedure

2.1. Overview of the Design Procedure

The process involved in designing an axial compressor is a long and demanding one, and often requires the combined efforts and strategies of countless experienced engineers across multiple disciplines (Gallimore, 1999). Full textbooks have been devoted to providing detailed explanations of the aerodynamic theories and practices involved with designing a compressor, two excellent examples of which include the works of Horlock (1958) and Cumpsty (1989). Gallimore (1999) summarizes the complete design procedure as a sequence of four major steps. The progression of this sequence is shown in Figure 2.1.

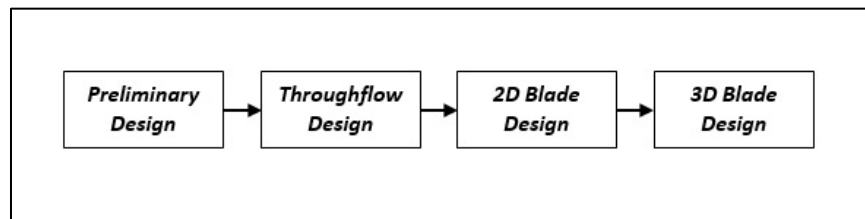


Figure 2.1 Scheme of a typical compressor design process (Molinari & Dawes, 2006)

The preliminary step outlined in Figure 2.1 focuses on determining basic thermodynamic properties in accordance with the overall requirements of the engine. Focal parameters including the compressor's total pressure ratio, mass flow rate, and energy/work addition are determined through a series of calculations consistent with the engine's thermodynamic (Brayton) cycle. Once an appropriate thermodynamic model has been established, the resulting variables are then carried over to the secondary portion of the preliminary step in which principle aerodynamic and geometric features of the compressor are defined. Referred to as *Meanline* analysis, this process applies one-

dimensional aero-thermal approximations to resolve the velocity triangles along the compressor's mean path. Theoretical correlations are then applied to extend the aerodynamic solution outwards along the span of each blade to determine the compressor's hub and tip annulus profile. Major design considerations are often defined at this level, thus leading the combined strategies of the cycle and Meanline analyses to take on dominant roles in the overall design sequence (Molinari & Dawes, 2006).

The next stage of the sequence defines the radial component of the aerodynamic solution through a process referred to as *Throughflow* design. In contrast to relying on theoretical correlations such as those employed by the Meanline methodology, Throughflow calculations incorporate numerical methods to refine the spanwise variation of flow angles and velocities at the inlet and exit of each blade row (Denton & Dawes, 1998). These calculations are usually performed along axisymmetric streamlines as shown in Figure 2.2.

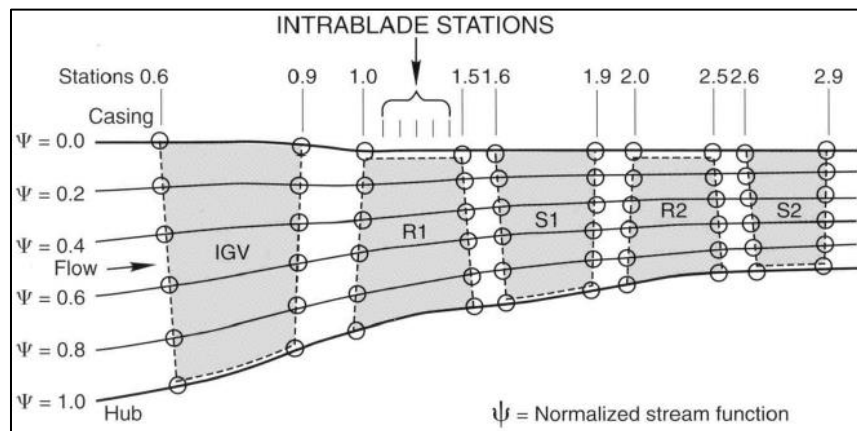


Figure 2.2 Schematic representation of the streamline distribution employed by a typical Throughflow solver (Tiwari, Stein & Lin, 2013)

The increased fidelity incorporated by the Throughflow approach greatly improves the accuracy of the aerodynamic predictions compared to its Meanline

counterpart. However, the calculations are still limited to only two spatial dimensions: axial and radial. For this reason, the reliability of Throughflow analysis is usually influenced by the level of empiricism employed to model the 3D effects contributing to deviation and profile loss. Nonetheless if careful considerations are taken, for example if experimental values for loss and deviation are input, or if a sophisticated method to predict these phenomena are utilized, the spanwise variations predicted by Throughflow calculations usually maintain a high degree of accuracy compared to experimental results (Denton & Dawes, 1998). It is for this reason together with their unmatched computational speeds that endorse Throughflow tools as being one of the most important resources for turbomachinery designers.

The remaining steps of the design sequence illustrated in Figure 2.1 refer to the application of Computational Fluid Dynamics techniques as briefly described earlier. Due to their ability to predict both viscous and 3D flow structures, the use of CFD tools, when applied correctly, can significantly improve the predicted accuracy of an aerodynamic solution. Also considering that computational resources, accuracy, and robustness of CFD simulations are constantly being improved, CFD methods are gradually becoming incorporated into principal roles of current turbomachinery design practices (Denton & Dawes, 1998).

These techniques however are not without their limitations as discussed in great detail by Denton (2010). Although a high level of fidelity could in fact be achieved, there commonly exists a false impression that a converged CFD solution is undoubtedly correct, when in fact the opposite may be true. Errors due to finite difference approximations, improper turbulence modeling, inadequate mesh application, and steady

flow assumptions are just a few of the many sources of errors that lead to significant inconsistencies in predicted results Denton (2010). Factoring in the tremendous burden on computational resources, the full exploitation of CFD is often limited to the refinement of an existing blade design rather than an iterative ‘from scratch’ design approach (Molinari & Dawes, 2006).

2.2. The Iterative Design Sequence

In a detailed review on the evolution of the compressor design process, Molinari & Dawes (2006) describe that the development of technology has reached an asymptote in turbomachinery design. They express that before further advancements in this field can be made, emphasis must first be placed on improving the methodologies and strategies of the design sequence rather than the perfection of the tools themselves.

In light of these considerations, a design system that could exploit the promptness of the preliminary phase with the fidelity of advanced methodologies would significantly increase the efficiency of the overall design procedure, as well as introduce a higher level of innovation in current blade design strategies. It is for this reason that a shift towards a more iterative design system is needed, in which refinements made by two and three-dimensional analyses are continuously fed back into the preliminary stage of design (Molinari & Dawes, 2006). Although it still relies on one-dimensional strategies, iterative refinements made at the preliminary level could have significant advantages to the overall design cycle including increased performance, reduced computational costs, and shorter design times. An example of such a design scheme is illustrated in Figure 2.3.

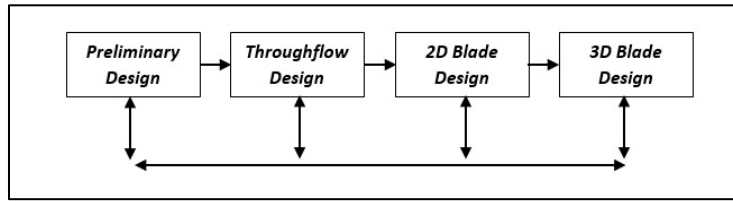


Figure 2.3 Scheme of the proposed iterative design process (Molinari & Dawes, 2006)

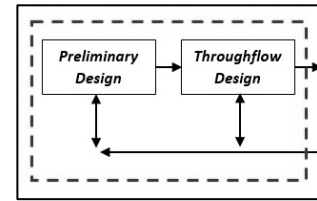


Figure 2.4 Coupled interaction considered by the current work.

2.3. Current Work

The work discussed herein is focused specifically on the coupled interaction between the preliminary (Meanline) and Throughflow steps of the proposed design system as highlighted in Figure 2.4. As part of this work, a computer program was developed to enhance the interaction between these two platforms in an effort to improve user productivity and design turnaround time. The remainder of this chapter is devoted to outlining the theory and methodology applied at the foundation of each stage of the sequence shown in Figure 2.4. The full functional capabilities of the code are discussed in detail in the following chapters.

2.4. Meanline Analysis

In the Meanline analysis portion of the preliminary design phase, basic aerodynamic and thermodynamic parameters are calculated at the mean radius of the compressor using simplified relationships. Under the assumption that the flow is steady, inviscid, and one-dimensional, key parameters including the number of stages, annulus profile geometry and overall compressor length are established through an iterative method in accordance with the thermodynamic requirements of the engine (Gallimore, 1999). Because of these assumptions, Meanline calculations are performed very quickly,

thereby allowing for an efficient screening of undesirable blade design possibilities. The Meanline phase remains the most significant step in the design sequence as it establishes the vast majority of the compressor's architecture. Consequently, an error made at this level would only propagate through the rest of the design cycle (Gallimore, 1999).

2.4.1. Radial Equilibrium

There are many considerations that go into the Meanline design process, the most significant of which is the concept of *Radial Equilibrium*. It is desired to maintain a relatively uniform distribution of work input along the radial length of each rotor blade (Hill & Peterson, 1992). In a rotating frame of reference however, this can only be achieved by balancing the forces resulting from the radial pressure gradient and the centripetal force caused by the fluid's outward acceleration. Under the assumption that the radial component of velocity is zero at the inlet and exit of a blade row ($c_r \approx 0$), the simple radial equilibrium condition is derived from the momentum equation as follows:

$$\frac{\partial p}{\partial r} = \rho \frac{c_\theta^2}{r} \quad (2.1)$$

Equation 2.1 is applied for a fluid element with an infinitesimal mass such as the one shown in Figure 2.5. The strategy of radial equilibrium relates back to equation 1.4 and the idea that the change in total enthalpy (i.e. work) across a blade row is influenced by the change in swirl at a specified radius. This relationship is demonstrated by the following expression:

$$\frac{\partial}{\partial r} (\Delta h_0) = \Omega \frac{\partial}{\partial r} (r \Delta c_\theta) \quad (2.2)$$

Consequently, a constant work distribution along the radial span of the blade is

achieved if the product $r\Delta c_\theta$ remains constant with radius (Hill & Peterson, 1992). This relationship is represented in the following form:

$$c_\theta = a/r \quad (2.3)$$

The variable a in equation 2.3 is a constant used to define the magnitude of the desired swirl velocity. This type of substitution is known as the *Free Vortex* design and produces what is referred to as a *constant-work* rotor (Farokhi, 2014). A visual representation of this approach is shown in Figure 2.6.

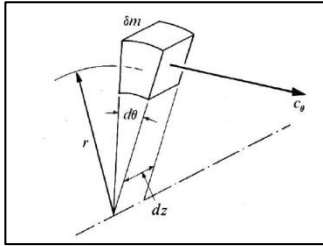


Figure 2.5 Tangential motion of a small fluid particle (Hill & Peterson, 1992)

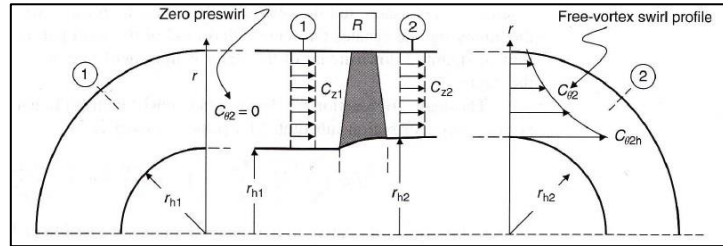


Figure 2.6 Velocity field of a rotor blade subjected to free-vortex design. (Farokhi, 2010)

Although the free vortex approach ensures that a uniform work distribution is satisfied, the physical geometry resulting from a free vortex design often requires the use of excessively high blade twist in order to maintain the desired exit swirl profile. Unless the ratio between the blade radius and diameter is limited to values near 1.0, this could in fact result in unreasonable flow characteristics at the blade's hub and tip locations (Hill & Peterson, 1992). Nonetheless, this assumption is simple and effective, and for this reason, it remains a popular starting point in compressor design.

2.4.2. Vortex Design Strategies

An alternative approach to satisfying the radial equilibrium condition while avoiding the limitations of the free-vortex distribution comes with the application of a more sophisticated swirl distribution at the trailing edge of the blade. In fact, the variation of angular momentum through a blade row is regarded as a design choice rather than a fixed requirement, and it is often defined based on experience, and knowledge of the flow requirements (Hill & Peterson, 1992). Vortex strategies commonly used to define the variation of work through a rotor are shown in Table 2.1.

Table 2.1 Example vortex design strategies (Horlock, 1958).

Vortex Design Strategy	Applied Swirl Distribution	Variation of Work with Radius	Radial Equilibrium Condition	Remarks
Free Vortex	$c_\theta = \frac{a}{r}$	Constant	Satisfied	Limited by high root deflection
Forced Vortex	$c_\theta = ar$	Increases with r^2	Satisfied	Rarely used
Exponential	$c_\theta = a \pm \frac{b}{r}$	Constant	Satisfied	A logical design method for low twist blades
Constant Reaction	$c_\theta = ar \pm \frac{b}{r}$	Constant	Satisfied	Logical design for highly twisted blades

The selection of a vortex design method is often influenced by a number of considerations. For example, a *Constant Reaction* strategy may be applied if a designer opts to maintain a constant degree of reaction ($R = 0.5$) spanning the entire radius of a compressor stage. This approach could be considered for blade rows that require high twist distributions such as first stage fan and compressor blades (Horlock, 1958). An example of this type of application is shown in Figure 2.7. In some cases, it could be advantageous to fix the reaction a highly loaded section (for example at the root) and

vary its distribution across the remaining span of the blade. When coupled with a free vortex assumption, this application produces flow angle distributions much like those illustrated in Figure 2.8.

Fixing the reaction at the mid-span of the blade is another common approach used by blade designers since the velocity triangles at this location are easily calculated through Meanline analysis. If coupled with the free vortex assumption however, this application could be inadequate for blades with low hub-to-tip ratios as the reaction can become unreasonably low at the root sections (Horlock, 1958). This effect is illustrated by referring to the low relative flow angles shown in Figure 2.9. The last example considers the application of the *Exponential* design method, in which the reaction at the mean radius may remain fixed and vary only slightly with radius. This strategy ensures that root blade loading is not compromised, and is usually applied for blades that require low twist distributions. This is visually demonstrated in Figure 2.10.

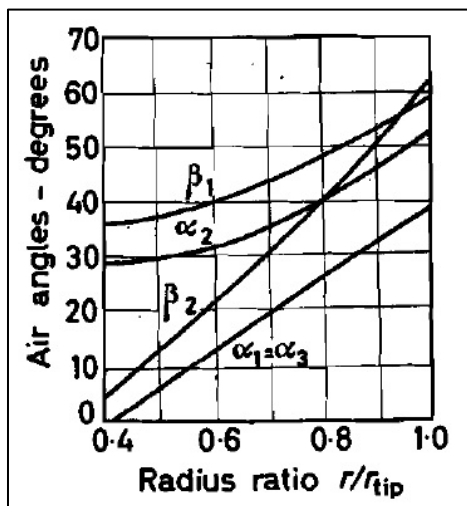


Figure 2.7 Constant reaction design with $R = 0.6$ (Horlock, 1958)

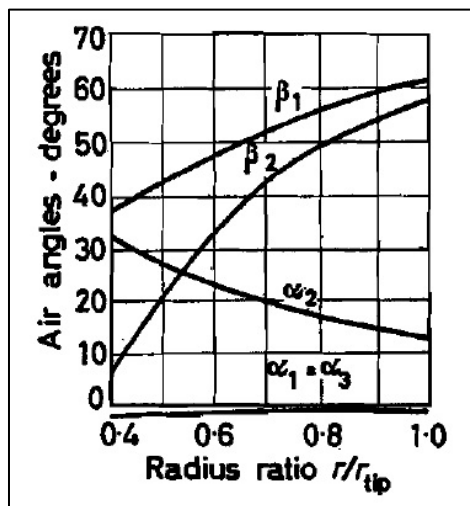


Figure 2.8 Free vortex design with $R = 0.6$ at root (Horlock, 1958)

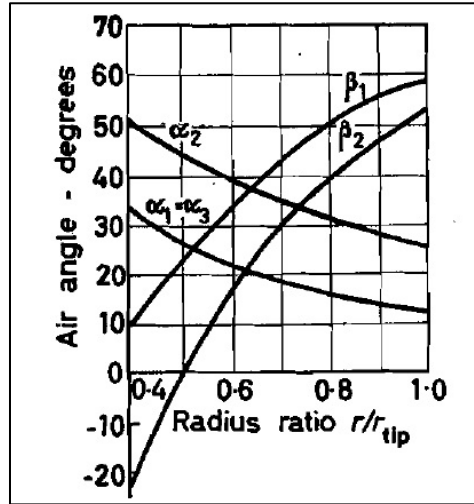


Figure 2.9 Free vortex design with $R = 0.6$ at mean (Horlock, 1958)

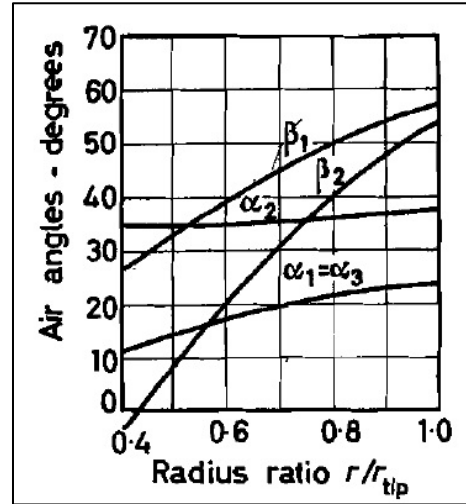


Figure 2.10 Exponential design with $R = 0.6$ at mean (Horlock, 1958)

2.5. Throughflow Analysis

Once an appropriate design strategy has been established, and a first-pass approximation of the compressor geometry is achieved, the design is then advanced to the Throughflow phase where further refinement is performed. This process is similar to the Meanline approach in the sense that the radial variation of blade work is defined. In this case, however, the resulting blade inlet and exit angles are predicted numerically as opposed to applying a vortex assumption (Denton & Dawes, 1998). This method is commonly referred to as the *inverse* approach for establishing stacked airfoil geometry. A second strategy can also be applied, in which the blade exit angles are specified (i.e. the geometry is fixed) and the inlet angles are predicted. This is known as the *direct* (or analysis) method, and is primarily used to predict the off-design performance of the compressor.

2.5.1. Streamline Curvature

In both design modes, the velocity distributions at the inlet and exit of each blade row are determined based on an axisymmetric treatment of circumferentially averaged flow (Wu, 1952). A common numerical scheme used to simulate this effect is the *Streamline Curvature* method, in which the flow through the compressor is determined by iteratively solving the radial equilibrium equation as applied to the flow along a streamline. The streamlines are not fixed in space, but rather shift with each successive iteration to a level of convergence defined by a specified set of boundary conditions (Hirsch & Denton, 1981). These conditions include a given mass flow rate, RPM, and inlet flow parameters (P_0 , T_0 , V_θ), as well as any additional physical laws used to treat viscous effects. An example of an iterative shift sequence is demonstrated in Figure 2.11.

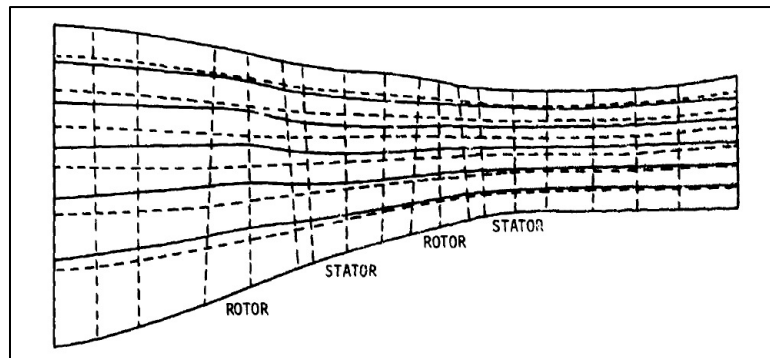


Figure 2.11 Example streamline discretization of a 2-stage fan (Hirsch & Denton, 1981).

The radial equilibrium equation solved by the streamline curvature method takes into account the relationship between the pressure forces and inertial forces acting on a fluid particle as briefly mentioned earlier (Tiwari, Stein & Lin, 2013). A general form of this relationship is given as follows:

$$v_m \frac{\partial v_m}{\partial s_2} = v_m^2 \left[\frac{\cos(\phi - \sigma)}{r_c} - \sin(\phi - \sigma) \frac{1}{v_m} \frac{\partial v_m}{\partial m} \right] + \frac{\partial H}{\partial s_2} - T_s \frac{\partial S}{\partial s_2} + f_q - \frac{1}{2r^2} \frac{\partial (rc_u)^2}{\partial s_2} \quad (2.4)$$

The full derivation of equation 2.4 is given by Smith (1966). With the assistance of a numerical solver, a solution for the spanwise variation in meridional velocity (v_m) at the inlet and exit of each blade row is obtained. This is achieved by first converting the above relationship into a first order ordinary differential equation (ODE), and then applying an iterative numerical scheme. Both the inverse and direct forms of the resulting ODE's are given as follows:

$$\text{Direct (Analysis):} \quad v_m \frac{\partial v_m}{\partial S_2} = A(S_2)v_m^2 + B(S_2)v_m + C(S_2) \quad (2.5)$$

$$\text{Inverse (Design):} \quad v_m \frac{\partial v_m}{\partial S_2} = P(S_2)v_m^2 + Q(S_2) \quad (2.6)$$

The coefficients $A(S_2)$, $B(S_2)$, $C(S_2)$, $P(S_2)$, and $Q(S_2)$ in equations 2.5 and 2.6 are *non-constant* quantities that are determined from the solution at previous iteration steps (Tiwari et al., 2013). The numerical procedure begins by first estimating a value for the meridional velocity where it is then integrated in the spanwise direction. This process is further coupled with the continuity equation such that the mass conservation condition is satisfied at each blade row station. A detailed review of the streamline curvature method including its complete derivations, limitations, and numerical schemes are given by Smith (1966), Hirsch & Denton (1981), and Novak (1967).

2.5.2. Throughflow limitations

Since Throughflow calculations consider the flow as axisymmetric and inviscid, additional treatment is required to model viscous effects such as deviation and loss. These effects can be artificially simulated by inputting known total pressure loss profiles (such estimates may be obtained through CFD analysis), or modeled with empirical correlations

(ex. Carter's rule). Additionally, the ability to incorporate so-called *spanwise mixing*, and interactions with the annulus walls, becomes important if accurate predictions of the radial total pressure and temperature distributions are to be achieved (Gallimore, 1999). This is often performed with the application of blockage factors to simulate the losses incurred from the development of the annulus boundary layer (Denton & Dawes, 1998). Neglecting real effects such as these could still produce viable first-pass estimates for the aerodynamic solution through the compressor. However, the reliability of the resulting Throughflow solution would more likely resemble that of a Meanline prediction. Otherwise, if viscous treatments were to be applied, the resulting calculations could correlate very well with experimental data. An example of the improvements that can be gained is shown in Figure 2.12 and Figure 2.13.

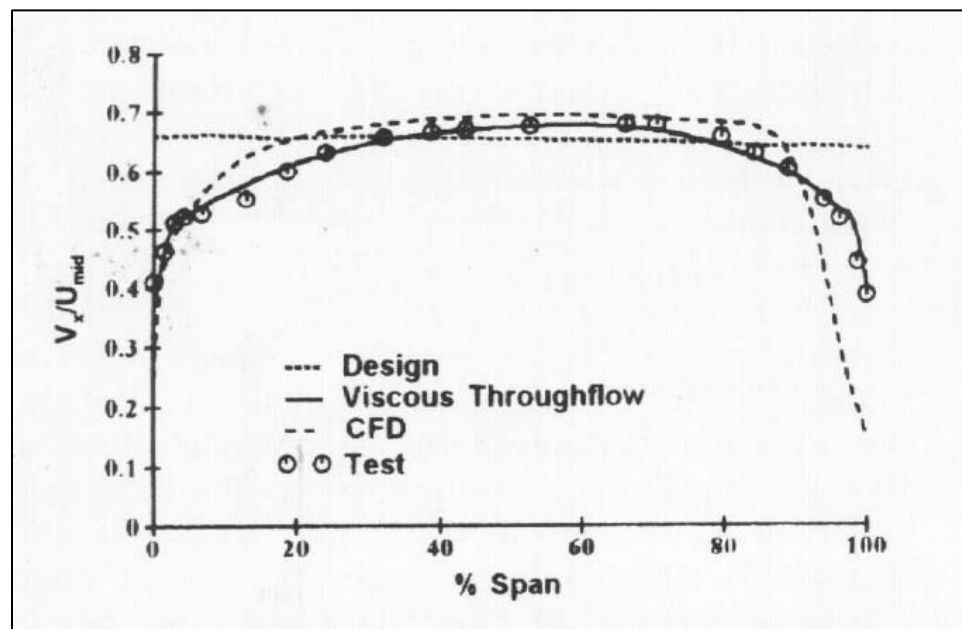


Figure 2.12 Comparison between the measured and predicted exit axial velocity profiles for a given rotor blade (Gallimore, 1999).

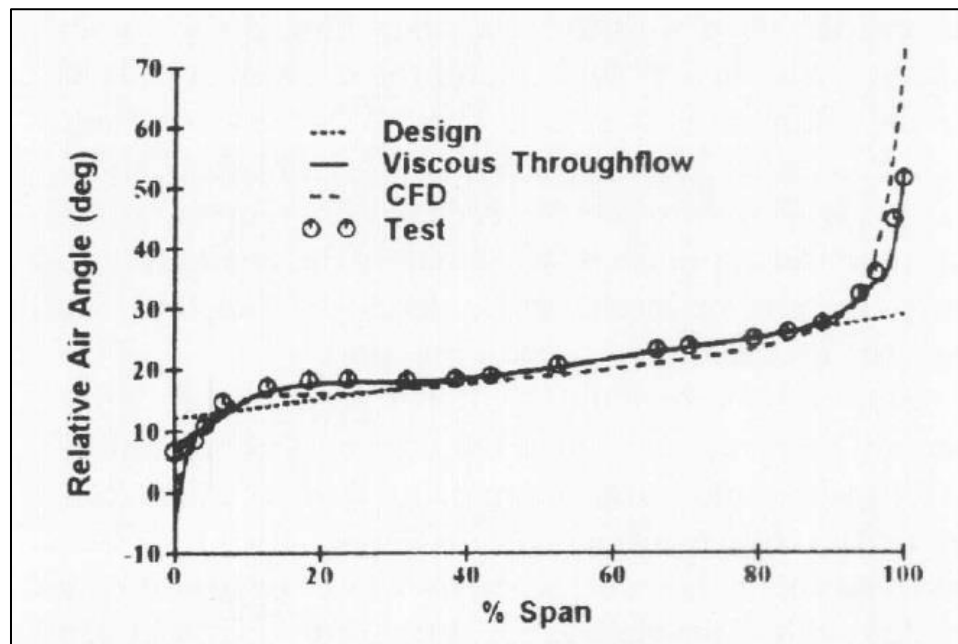


Figure 2.13 Comparison between the measured and predicted exit air flow angle profiles for a given rotor blade (Gallimore, 1999).

3. Overview of C-STAAC

3.1. Objective

The computer program developed for this Master's thesis focuses on improving the efficiency of the Preliminary-to-Throughflow design sequence outlined in Figure 2.4. This program, named C-STAAC (Coupled Spanline Throughflow Aerodynamic Axial Compressor design), combines the capabilities of two independent compressor design codes to form one standalone design platform. This program is accessed through an easy-to-use graphical user interface (GUI) and provides the fully coupled interaction of information between the Meanline and Throughflow phases of compressor design. As a result, the aerodynamic solution from each phase is obtained and post-processed quickly and efficiently, thereby increasing user productivity and design turnaround time.

3.2. Programming

All functions and scripts utilized by C-STAAC were written in the MATLAB[®] programming language (versions R2014b and R2015b). This language was selected because of its powerful graphical user interface, data storage, and matrix analysis capabilities. Additionally, this language is well known in the engineering community, which allows future work to be easily continued.

3.3. Meanline and Throughflow Integration

C-STAAC makes use of two independent compressor design codes in order to generate the Meanline and Throughflow solutions. Both codes were obtained with permission from the online software catalog at NASA Glenn Research Center in accordance with the *Technology Transfer Program*. These codes were not altered in any

way, and they are not imbedded into C-STAAC's source programming. Instead, they are called as standalone executables (*.exe) that produce solution data files from formatted input files.

3.3.1. Meanline Application

The Meanline application of the program, named CSPAN (Compressor SPanline Analysis) applies isentropic simple radial equilibrium assumptions to determine basic aerodynamic and geometric properties of an axial flow compressor. Based on the fundamental strategies of Meanline analysis, all internal calculations are performed at constant-span-fraction locations where energy addition is controlled through the specification of aerodynamic limits. This code requires only a handful of input parameters to run and allows for rapid conceptual design studies to be performed. A complete description of the code summarizing all underlying methodologies is given by Glassman & Lavelle (1995).

3.3.2. Throughflow Application

The Throughflow application, named ACD (Axial Compressor Design), computes the full meridional aerodynamic solution of an axial compressor (both subsonic and transonic) in addition to its stacked blade geometry. The code utilizes the streamline curvature method to calculate the velocity triangles at the leading and trailing edges of each blade row on selected stream cones. Blade inlet and exit angles are determined either from user-specified loss profiles, or from empirical incidence and deviation correlations. Rapid iterative studies can be conducted by applying quick corrective adjustments to a wide variety of parameters including but not limited to those that control

deviation and loss. The program can be executed in both direct and inverse modes, the latter of which defines 3D stacked airfoil geometry along each streamline. A detailed description of the code including all incorporated theories and design strategies is given by Crouse & Gorrell (1981).

3.4. Simplification of the Design Sequence

The Meanline and Throughflow codes were developed in early versions of the FORTRAN programming language, and so they require precisely formatted input files in order to be properly executed. The task of generating these input files from a standalone level is very complicated and requires the user to be familiar with the general structure of both codes. Additionally, the data files that are outputted by the programs are very dense and at times difficult to understand which makes post-processing very challenging. C-STAAC considerably simplifies this process by automating all of the requirements necessary to generate properly formatted input files, automating the input/output functions required to properly execute the codes, and by offering enhanced post-processing capabilities not previously available with the independent codes.

The addition of GUI interaction further allows the user to rapidly design and post-process the aerodynamic solution of a fully bladed compressor, whereas an equivalent process without the use of any aids could take a substantial amount of time and effort. The Meanline application of the standalone platform therefore gives the user the ability to continually iterate and refine the first-pass design of an axial flow compressor. The coupling features of the program further allow the Throughflow application to initialize using the converged parameters from the preliminary stage of analysis. A schematic demonstrating the iterative abilities of C-STAAC is shown in Figure 3.1.

C Coupled
S Spanline -
T Throughflow
A Aerodynamic
A Multistage Axial
C Compressor Design

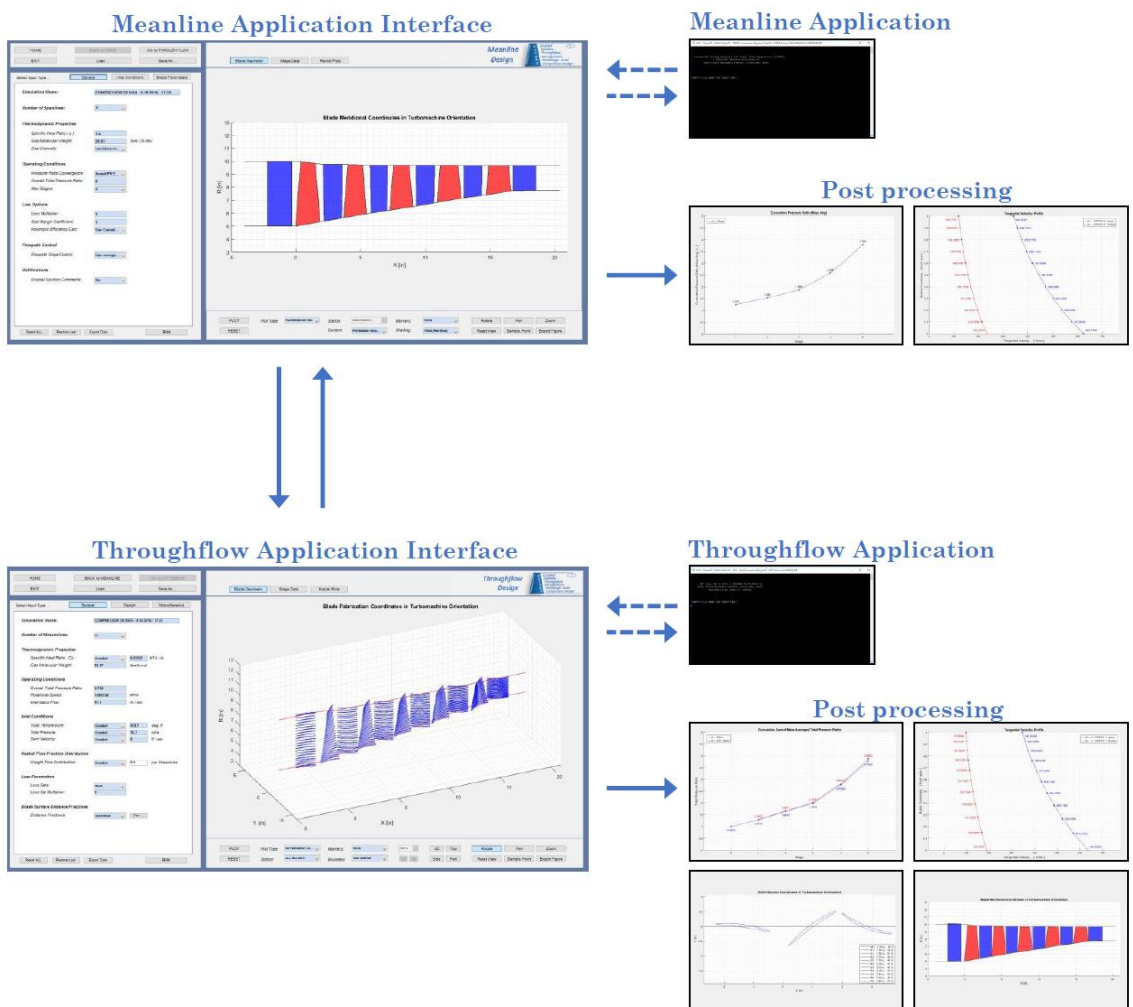


Figure 3.1 Schematic demonstrating the coupled abilities of C-STAAC.

4. C-STAAC Functionality

The following three chapters provide a complete overview of the functional capabilities of C-STAAC and its associated applications. These sections provide detailed descriptions of all input fields within the program, as well as any accompanying documentation relevant to their specific use. These chapters are included for the purpose of explaining the program in its entirety, but may substitute for a user manual if desired.

4.1. Home Screen

The first window that appears when running C-STAAC is the home screen. From here, the user has option to begin a new Meanline simulation, begin a new Throughflow simulation, load an existing Meanline solution, or load an existing Throughflow solution. Additionally, the user has the ability to select a working directory for which to save and export files, alter the file name, or alter the project title. The home screen is shown for reference in Figure 4.1.

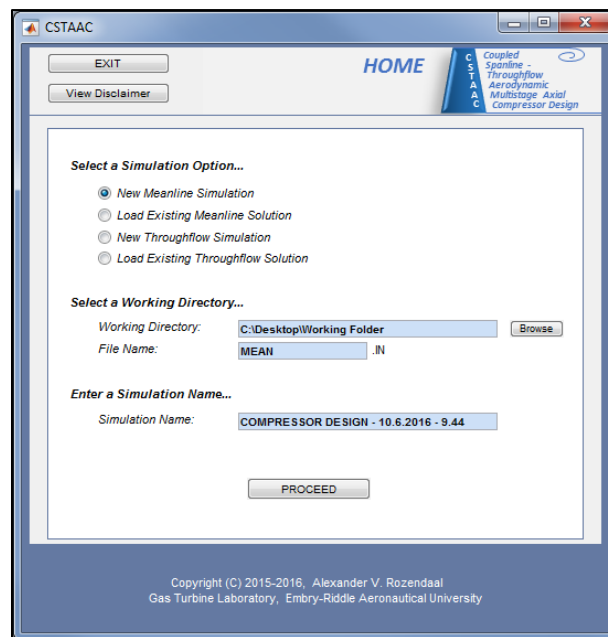


Figure 4.1 C-STAAC home screen.

4.2. Simulation Options

The user can select one of four options to run the program. The first option, *New Meanline Simulation*, automatically populates the fields shown in Figure 4.1 with their default settings. Clicking *PROCEED* with this option selected will begin a new Meanline simulation and automatically populate all fields with default parameters for a generic 5-stage axial compressor. The *New Throughflow Simulation* option performs a similar function, however, this process instead opens the Throughflow application. This option creates a blank Throughflow simulation with all fields left blank. If initialized input fields are desired, the user is instead encouraged to generate the default Meanline solution, and carry over all desired settings to the Throughflow application.

The two remaining options, *Load Existing Meanline Solution* and *Load Existing Throughflow Solution*, enable the user to load any previously saved solutions for further editing. When selected, all fields are reset and the user is instead prompted to open a desired application input file.

4.3. Selecting a Working Directory

The working directory refers to the location in which all input, output, and exported files will be saved. This location automatically defaults to the folder named *Working Folder*, which is located in the main directory along with the *Source Files* folder and the executable shortcut *C-STAAC*. If a working folder does not exist, the program will automatically create one. The location of the working directory can be changed at any time by clicking the *Browse* button shown in Figure 4.1. The working directory text field is un-editable, and is only intended to display the location of the current working directory. Any changes made to this field will revert back to the text originally displayed.

The name of the input and output files can be changed at any time in the box titled *File Name*. Only valid file names that do not include special characters ([.,"^*:? "<>|]) are accepted. Underscore characters can be used to separate words if desired. File extensions do not need to be entered as they are assigned automatically. All default file names extensions used by the program are shown in Table 4.1.

Table 4.1 Default file names and extensions

Application	Default File Name	Input File Extension	Output File Extension
Meanline	<i>MEAN</i>	<i>*.IN</i>	<i>*.OT</i>
Throughflow	<i>THRU</i>	<i>*.INP</i>	<i>*.OUT</i>

4.4. Simulation Name

The simulation name entered into this field is used to define the specific project. This string appears at the top of every raw input and output file, and is used as an additional means of distinguishing projects that may contain identical file names. By default, C-STAAC assigns a simulation name beginning with *COMPRESSOR DESIGN*, followed by the date and time at which the program was originally executed. For example, the simulation name shown in Figure 4.1 refers to a project that was initiated on October 6, 2016 (10.6.2016) at 9:44am (9.44).

5. C-STAAC Functionality: Meanline Application

5.1. Meanline Interface

This section provides a detailed overview of all functions associated with the Meanline application of the program. For consistency, the information presented herein refers to the Meanline solution for the default 5-stage axial compressor generated when a *new* simulation is initiated. The main interface of the Meanline application is shown in Figure 5.1.

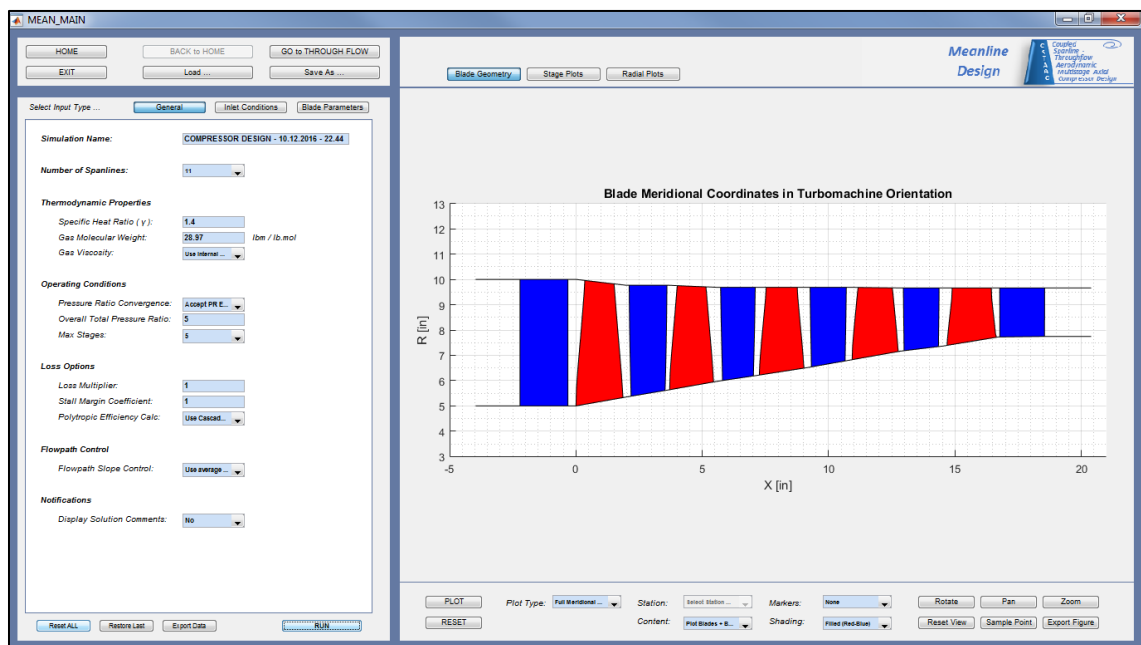


Figure 5.1 Meanline application interface.

5.2. Running a Meanline Simulation

A Meanline solution can be obtained at any time by clicking the *RUN* button located at the lower left corner of the screen. The time required to generate a solution depends on the complexity of the compressor as well as the computational resources that are available. Solutions however are typically obtained and post-processed in about one

or two seconds. For example, the solution for the default compressor shown in Figure 5.1 was obtained in less than 1.0 second. An equivalent solution for a 16-stage compressor on the other hand converged in about 1.7 seconds.

5.3. Minimum Input

The Meanline interface shown in Figure 5.1 provides the user with a wide variety of options to control the compressor's geometry and aerodynamic performance. Many of these parameters are modeled by empirical correlations, and so if desired, they can in fact be calculated by the program. Such parameters include but are not limited to free-vortex swirl profiles, blade solidities, and blade aspect ratios. These parameters may also be manually adjusted to match specific user requirements if desired. Because most variables are calculated automatically, the program only requires only a limited set of input parameters in order to run. The full list of minimum input is given in Table 5.1.

Table 5.1 Minimum input required to generate a Meanline solution.

Parameter	Assigned Variable	Units	Default Value
Overall Total Pressure Ratio	π_c	-	5
Max Number of Stages	-	-	5
Inlet Total Temperature	T_0	deg. R	518.7
Inlet Total Pressure	P_0	psi	14.7
Mass Flow Rate	\dot{m}	lb / sec	67.5
Shaft Rotational Speed	ω	RPM	12600
Rotor 1 Blade Tip Radius	r_{tip}	in.	10
Inlet Hub/Tip Radius Ratio	r_{hub}/r_{tip}	-	0.5

5.4. Navigation Tab

The navigation tab is located at the top left corner of the main window shown in

Figure 5.1. From here, the user has the option to: 1) Return to the home screen; 2) Exit the program; 3) Load an alternate Meanline simulation; 4) Save the existing Meanline simulation; or 5) Proceed to the Throughflow application. When selecting either of the first two options, the program will prompt the user with a warning message indicating that the Meanline application will close. Warning messages such as the ones shown in Figure 5.2 offer the user the option to cancel the request if desired. They commonly arise throughout the program where significant changes to the compressor's design could be implemented.

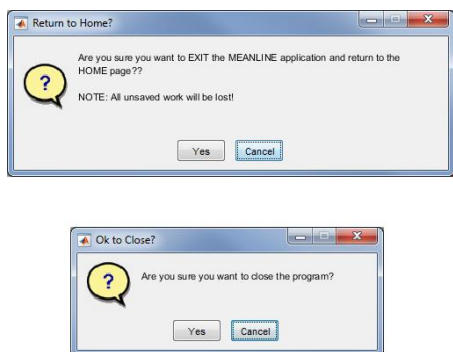


Figure 5.2 Example warning messages.

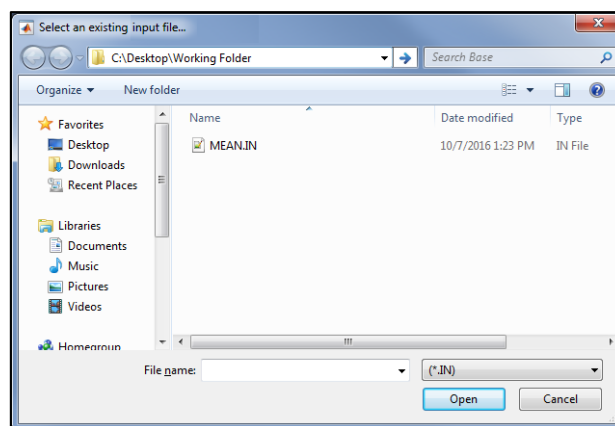


Figure 5.3 Load/Save window.

When loading or saving a simulation, a prompt window such as the one seen in Figure 5.3 is displayed. From here, the user can select a directory in which to load/save a simulation, as well as alter the name of the file being saved. The format and functionality of the load/save command window is consistent with the user's operating system.

The remaining navigation option closes the Meanline simulation and proceeds directly to the Throughflow application. All required Throughflow input variables are then initialized with their respective Meanline values. This function is explained in greater detail in section 5.12.

5.5. Input Window

With an exception of the file directory and post-processing commands, all input parameters required by the user can be defined in the window located directly below the navigation pane. There are three main input tabs where the user can enter data, each of which offers control over different aspects of the compressor's design. The user can switch between all three tabs using the toggle buttons located at the top of the input window. All three input modes are described in greater detail in the following sections.

5.6. General Input Tab

The *General* input tab gives the user control over basic parameters including fundamental thermodynamic properties, custom loss definition, and stage and pressure ratio specification. The general tab is shown in Figure 5.4 for reference.

Select Input Type ... **General** Inlet Conditions Blade Parameters

Simulation Name: COMPRESSOR DESIGN - 10.6.2016 - 9.48

Number of Spanlines: 11

Thermodynamic Properties

Specific Heat Ratio (γ): 1.4

Gas Molecular Weight: 28.97 lbm / lb.mol

Gas Viscosity: Use Internal ...

Operating Conditions

Pressure Ratio Convergence: Accept PR E ...

Overall Total Pressure Ratio: 5

Max Stages: 5

Loss Options

Loss Multiplier: 1

Stall Margin Coefficient: 1

Polytropic Efficiency Calc: Use Cascad ...

Flowpath Control

Flowpath Slope Control: Use average ...

Notifications

Display Solution Comments: No

Figure 5.4 General input tab.

5.6.1. Simulation Name

With a similar field located on the home screen, the user again has the ability to change the name of the project. This can be useful to distinguish simulations that contain identical file names. A default simulation name is assigned at the home screen when the program is first executed (refer to section 4.4 for more details). The user can specify any combination of characters to define the simulation name, however no more than 70 characters can be used. If more than 70 characters are entered, the program restores the previous simulation name and returns an error message.

5.6.2. Number of Spanlines

The user can control the number of spanlines at which radial calculations are performed throughout the compressor. A number in the range of 3-11 spanlines can be selected from a pre-defined dropdown list. By default, this field is set to its maximum value of 11 in order to maintain smooth curve fit correlations when carrying over radial profiles to the Throughflow application. Figure 5.5 and Figure 5.6 illustrate the difference between equivalent radial profile solutions using 11 and 5 spanlines respectively.

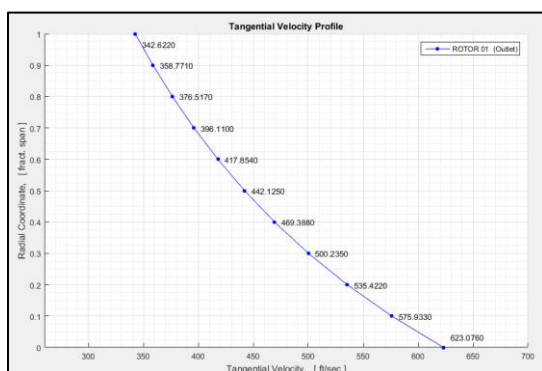


Figure 5.5 Example radial profile using 11 spanlines.

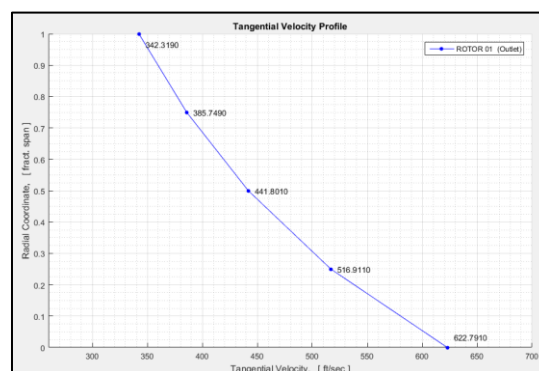


Figure 5.6 Example radial profile using 5 spanlines.

A lower number of spanlines may be specified in order to increase solution time,

however, the difference would be noticed to be negligible. For example, the difference in run time between the two solutions shown in Figure 5.5 and Figure 5.6 was approximately 0.1 seconds. The velocities at the hub, tip, and mean radius of the blade, however, differed slightly as a result.

5.6.3. Thermodynamic Properties

The next three input fields control the general thermodynamic properties of the compressor's working fluid. Specifically, the specific heat ratio (γ), gas molecular weight (in *lbm/lb.mol*), and gas viscosity can all be defined by the user. By default, the values for specific heat ratio and gas molecular weight are set to reflect the properties of air as shown in Figure 5.7. The gas viscosity on the other hand is calculated automatically using an internal computation. If desired, a custom value for gas viscosity may be specified by selecting the *Specify Value* option from the field dropdown menu. In doing so, a new input field becomes visible where a new value can be entered (in *lbm/sec.ft*). This is demonstrated in Figure 5.7.

Thermodynamic Properties	
Specific Heat Ratio (γ):	<input type="text" value="1.4"/>
Gas Molecular Weight:	<input type="text" value="28.97"/> <i>lbm / lb.mol</i>
Gas Viscosity:	<input type="text" value="0"/> <i>lbm / sec ft</i> Specify Value... <input type="button" value="Use Internal Computation"/> <input type="button" value="Specify Value ..."/>

Figure 5.7 Thermodynamic properties input field in the General input tab.

5.6.4. Operating Conditions

The three input fields located under the *Operating Conditions* heading provide the user with control over the compressor's overall total pressure ratio and maximum number of stages. These fields (with their default values) are shown for reference in Figure 5.8.

The overall mass-averaged total pressure ratio is specified by entering a numerical value in the associated input field. When non-numerical data is entered, the program produces an error message and resets the field to its original value. The maximum number of stages is selected from a drop-down menu. A minimum of one and a maximum of 20 stages (40 blade rows) may be selected. Depending on the overall characteristics of the compressor, the program may obtain a solution with fewer stages than that specified. The code however typically converges to (but never exceeds) the number of stages specified.

Figure 5.8 Default operating condition fields.

Figure 5.9 Pressure ratio convergence options.

The first input field shown in Figure 5.8 refers to the program's pressure ratio convergence switch. Here, one of two options may be selected from a dropdown menu as shown in Figure 5.9. The first option, *Converge to Specified PR*, fixes the maximum number of stages and attempts to achieve a solution for the specified pressure ratio. If the pressure ratio cannot be successfully achieved, the program may be forced to converge to a slightly lower value in order to produce a solution. At times, this too is unsuccessful and the program may in fact crash. The solved pressure ratio may be actively monitored in the post-processing window discussed in section 5.11.2.

The second option, *Accept PR Equal or Greater than that Specified*, again fixes the maximum allowed number of stages, but allows the program to achieve a solution with an overall pressure ratio equal to or greater than that specified. This 'floating' pressure ratio provides the Meanline code with greater flexibility when designing the compressor.

5.7. Inlet Conditions Input Tab

Selecting the *Inlet Conditions* button at the top of the input window displays the second user input tab as shown in Figure 5.11. Parameters regarding the compressor's general operating conditions can be specified in this window. All input fields within this window are discussed in detail below.

Select Input Type ... General **Inlet Conditions** Blade Parameters

General Conditions at Rotor 1 Inlet

Total Temperature: 518.7 deg. R
 Total Pressure: 14.7 psia
 Mass Flow: 67.5 lb / sec
 Rotational Speed: 12600 RPM

Geometry Parameters at Rotor 1 Inlet

Blade Tip Radius: 10 in.
 Hub / Tip Radius Ratio: 0.5

Endwall Blockage at Rotor 1 Inlet

Tip Blockage Factor: 0.0 Fraction of Annular Area
 Hub Blockage Factor: 0.0 Fraction of Annular Area

Inlet Guide Vane Definition

Include IGV: Yes
 IGV Exit Swirl Input Option: Calculate Fre...
 IGV Exit Swirl Profile: Constant 0 ft / sec
 IGV Total Pressure Loss: 0.005 Fraction of Total Pressure
 Absolute Flow Angle (Beta): 10 deg.

Figure 5.11 Inlet conditions input tab.

5.7.1. General Conditions at Rotor 1 Inlet

The input fields in this section make up the majority of the minimum input variables outlined in Table 5.1. In other words, values for the Inlet Total Temperature, Inlet Total Pressure, Mass Flow Rate, and Shaft Rotational Speed, are required in order to successfully run the program. Estimates for these parameters are generally obtained from thermodynamic cycle calculations in accordance with the Brayton cycle. It should be

noted that these parameters are specified at the inlet station of the first rotor blade, regardless of the presence of an inlet guide vane (IGV). Additional details regarding IGV definition are provided in section 5.7.4 of this report. The rotor 1 inlet input fields are shown for reference in Figure 5.12.

General Conditions at Rotor 1 Inlet		
Total Temperature:	518.7	deg. R
Total Pressure:	14.7	psia
Mass Flow:	67.5	lb / sec
Rotational Speed:	12600	RPM

Figure 5.12 Default inlet conditions (at Rotor 1).

5.7.2. Geometry Parameters at Rotor 1 Inlet

The remaining minimum input variables are entered in the two fields shown in Figure 5.13. These two variables, the Blade Tip Radius and the Hub/Tip Radius Ratio, are also required to successfully run the program. Similar to the general inlet conditions outlined in the previous section, both parameters are defined at the inlet of first rotor blade, regardless of the presence of an IGV. Specifying the blade hub and tip radius in this manner provides the program with a starting point in space for which to design the remainder of the compressor geometry.

Geometry Parameters at Rotor 1 Inlet		
Blade Tip Radius:	10	in.
Hub / Tip Radius Ratio:	0.5	

Figure 5.13 Default geometry conditions (at Rotor 1 inlet).

5.7.3. Endwall Blockage at Rotor 1 Inlet

In accordance with the theory presented earlier in this report, the boundary layer blockage effects at the hub and tip annulus endwalls may be simulated by specifying a

blockage factor value at these locations. Blockage areas are defined as the fraction of total annulus area at a particular blade inlet/exit station (e.g. $0.01 \approx 1\%$ of annulus area). By default, these values are calculated by the program for each blade row station using a 2D incompressible semi-empirical correlation based on the formulations of De Ruyck & Hirsch (1981). Manual control over these values may also be attained by selecting the appropriate option in the *Blade Parameters* tab. The blockage factor fields shown in Figure 5.14 apply to the hub and tip locations at the inlet of the first rotor blade only. Blockage factor controls for the remaining blades of the compressor are discussed in section 5.9.

Endwall Blockage at Rotor 1 Inlet		
Tip Blockage Factor:	<input type="text" value="0.01"/>	Fraction of Annular Area
Hub Blockage Factor:	<input type="text" value="0.01"/>	Fraction of Annular Area

Figure 5.14 Blockage factor definition for Rotor 1 inlet.

5.7.4. Inlet Guide Vane Definition

The Meanline application computes the aerodynamic and geometric solution for all blades within the compressor with an exception of the inlet guide vane. The flow through the IGV is instead manually defined by specifying an exit swirl distribution and a total pressure loss fraction through the blade row. The input fields used for specifying the IGV characteristics are shown in Figure 5.15.

Inlet Guide Vane Definition		
Include IGV:	<input type="button" value="Yes"/>	
IGV Exit Swirl Input Option:	<input type="button" value="Calculate Fre..."/>	
IGV Exit Swirl Profile:	<input type="button" value="Constant"/>	<input type="text" value="0"/> ft / sec
IGV Total Pressure Loss:	<input type="text" value="0.005"/>	Fraction of Total Pressure
Abs Angle (R1 Inlet Tip):	<input type="text" value="10"/>	deg.

Figure 5.15 Inlet guide vane definition.

The first field, *Include IGV*, gives the user the ability to include or neglect an IGV

from the compressor's overall configuration. Setting this function to *No* will disable all input fields shown in Figure 5.15, and neglect the influence of an IGV from the design. As a result, the flow upstream of rotor 1 will be uniform (un-swirled), and defined in accordance with the inlet conditions specified by the user (refer to Figure 5.12).

It is important to note that if an IGV is included, the program does not design its meridional geometry in the same way as it does the remaining compressor blades. Instead, the program manually inserts an IGV station upstream of the first rotor blade at an axial root spacing of $g/s = 0.25$. The spacing may be adjusted by the user in the *Blade Parameters* tab. Because the Meanline code does not perform calculations at the IGV station, the inserted IGV is assigned a uniform chord length distribution using the actual tip chord value of the first stator blade. IGV stations such as the one shown in Figure 5.1 are therefore displayed for visual reference only, and are intended to be placeholders when initializing the Throughflow geometry. Manual adjustments to this station including chord distribution and axial spacing may be made performed later in the Throughflow application.

Provided that an IGV is included in the compressor's design, the next input field shown in Figure 5.15, *IGV Exit Swirl Input Option*, controls the amount of information that is used to specify the exit swirl profile. The swirl distribution at the exit of the IGV, as well as all blade rows for that matter, is defined as a polynomial function with respect to radius (r) as follows:

$$v_{\theta} = \frac{B}{r} + C + Dr + Er^2 \quad (5.1)$$

All coefficients in equation 5.1 may be adjusted by the user by selecting the *Define Full Profile* option from the dropdown list. Alternatively, the free-vortex term

(coefficient B) may be calculated internally by the program by selecting the *Calculate Free-Vortex Term from Absolute Flow Angle* option. With this option, coefficient B is calculated internally using an absolute flow angle value specified by the user (discussed later). The result produces a free-vortex swirl distribution at the exit of the IGV. The remaining coefficients of equation 5.1 (C , D , E) may still be manually adjusted with this option if desired.

The next input field, *IGV Exit Swirl Profile*, provides the user with the ability to modify the swirl distribution at the exit of the IGV. By default, this option is set to *Constant*, and the corresponding edit box shown in Figure 5.15 defines the magnitude of coefficient C in equation 5.1. Alternatively, the complete swirl profile may be specified by selecting the *Polynomial* option. When selected, the input box shown in Figure 5.16 is displayed, and all coefficients in equation 5.1 may be modified according to the user's requirements.

IGV Exit Swirl Profile

Specify the coefficients for the polynomial equation to define the TANGENTIAL (Swirl) Velocity profile (in ft/sec) UPSTREAM of the FIRST Rotor blade.

$$V_{\text{Theta}} = B/R + C + DR + ER^2$$

B = C = D = E =

NOTE: R is the spanwise variation of the passage height (in inches).
NOTE: The coefficient "B" is internally computed using the inputted Absolute Exit Flow Angle

OK Cancel

Figure 5.16 IGV Swirl profile definition.

Note that if the option to calculate the free-vortex term is selected, the first input field in Figure 5.16 remains un-editable to the user. Otherwise, if the user opts to define the full profile, it becomes editable just like the remaining input fields. Examples of a constant user-defined swirl profile and an internally computed free-vortex distribution are shown in Figure 5.17 and Figure 5.18.

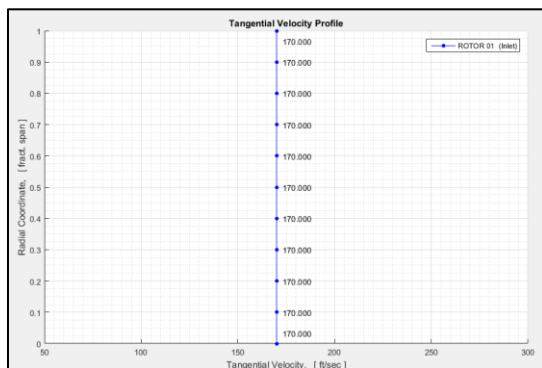


Figure 5.17 User-defined constant swirl profile at IGV exit (Rotor 1 Inlet)

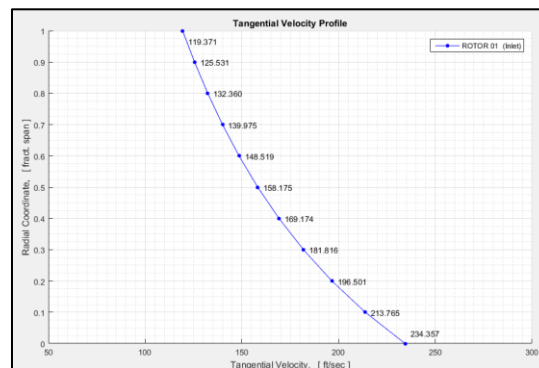


Figure 5.18 Internally-calculated free-vortex swirl profile at IGV exit (Rotor 1 Inlet)

The next input field, *IGV Total Pressure Loss*, defines the fraction of total pressure that is lost between the inlet and exit locations of the IGV station. Again, since the IGV station is not considered in the Meanline calculations, this parameter is used to simulate viscous losses for the flow entering the first rotor blade. By default, this value is set to 0.005 (0.5%) when the free-vortex term is calculated, and zero when the full exit swirl profile is defined.

The last input field in the IGV definition section, *Abs Angle (RI Inlet Tip)*, defines the magnitude of the absolute flow angle at the inlet tip location of the first rotor blade. This variable is used to calculate the resulting free-vortex swirl distribution at the exit of the IGV (Rotor 1 inlet). By default, this option is set to 10 degrees when the free-vortex option is selected. This field is disabled when the full swirl profile is defined by the user.

5.8. Blade Parameters Tab (Global Settings)

Selecting the *Blade Parameters* button at the top of the input window toggles the third user input tab. The blade parameter input pane is split into two sections. The first offers the user control over global design criteria applicable to all blades within the compressor. These fields are shown in Figure 5.19. The second section provides control

over design parameters that are unique to each individual blade. This is discussed in section 5.9.

Figure 5.19 (Global) blade parameters tab.

5.8.1. Global Parameters – All Blades

The first two input fields shown in Figure 5.19 refer to global design settings that are applicable to all rotor and stator blades within the compressor. The first field, *Endwall Blockage*, provides the user with the option either to calculate the endwall blockage factors internally, or to specify the blockage factors at each blade row manually. Selecting the *Calculate Hub/Tip Blockage* option disables all blockage-related input fields within the program. All values are instead calculated by the program using a semi-empirical correlation based on the formulation of De Ruyck & Hirsch (1981). The second option, *Specify Hub/Tip Blockage*, activates all blockage input fields so that the user may

specify these values manually. By default, when the second option is selected, rotor and stator blockage values are populated in the following sequence:

$$\text{Rotor Blockage } (R1 \dots Rn) = .01, .015, .02, .025, .03, .035, .04, .045, .05, \dots .05 \quad (5.2)$$

$$\text{Stator Blockage } (S1 \dots Sn) = .015, .02, .025, .03, .035, .04, .045, .05, \dots .05 \quad (5.3)$$

The next input field in this category, *Mid-Span Axial Spacing*, provides the user with control over the axial spacing parameter (g/s) at the mid-span location of each blade row. One of three options may be selected from a dropdown list. The first option, *Default*, does not apply any form of custom spacing to the meridional geometry. The resulting blade geometry that is displayed in the post-processing window represents the un-modified chord distributions that are calculated by the program. Due to the one-dimensional nature of the Meanline calculations, however, it will often be observed that the *Default* setting will produce blade spacing values smaller than what is normally expected in a compressor. This effect is demonstrated in Figure 5.20.

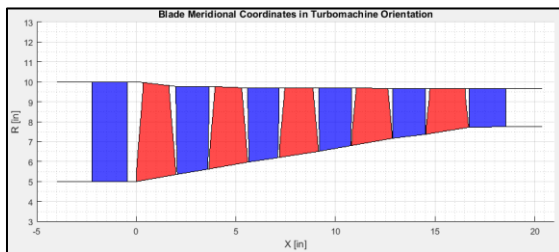


Figure 5.20 Meridional geometry using the default gap spacing.

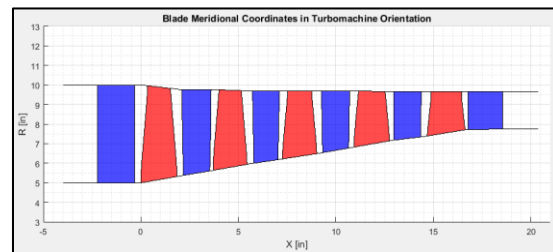


Figure 5.21 Meridional geometry using a custom gap spacing.

To counter this effect, the axial spacing parameter can be manually adjusted by the user to produce a more reasonable gap distribution like the one illustrated in Figure 5.21. It is important to note, however, that this feature only adjusts the coordinates that are displayed in the post-processing window, and not the locations at which the

aerodynamic calculations are performed. Correcting the spacing distribution in this manner prevents the occurrence of self-intersecting blade geometry, and provides more robustness when initializing the blade coordinates for the Throughflow simulation. All geometry produced by the Meanline simulation may be manually adjusted in the Throughflow application.

Either a constant, or a custom blade spacing distribution may be applied to the compressor geometry. Both options are available through the dropdown menu shown in Figure 5.19. When the *Constant* option is selected, a new input box appears next to the dropdown menu as shown in Figure 5.22. Here, a value may be entered to define a uniform axial spacing across the compressor. The spacing value is measured from the mid-span trailing edge of an upstream blade to the mid-span leading edge of a downstream blade. The default value for all blades is $g/s = 0.2$.

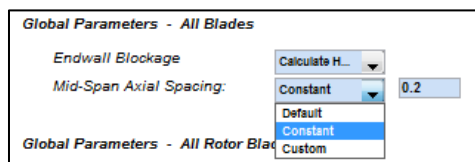


Figure 5.22 Constant spacing option.

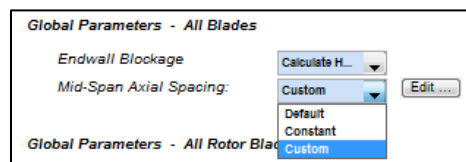


Figure 5.23 Custom spacing option

If the *Custom* option is selected, an *edit* pushbutton appears next to the dropdown list as shown in Figure 5.23. When selected, this feature produces a new window for which custom spacing values may be entered. The default distribution is linear, and is automatically constructed in accordance with the number of blades rows present in the compressor. The input window is shown for reference in Figure 5.24.

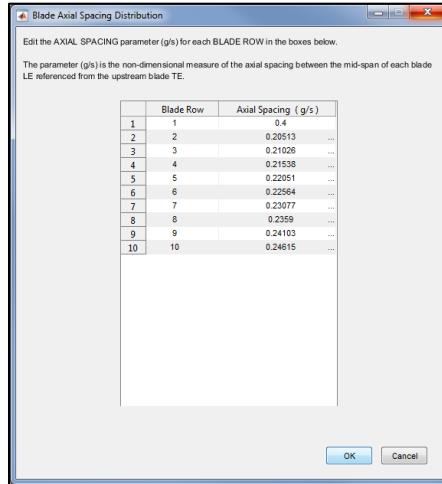


Figure 5.24 Custom spacing input window.

5.8.2. Global Parameters – All Rotor Blades

Global limits for the maximum thickness-to-chord and the tip-clearance to blade-height ratios can be applied for all rotor blades by specifying the corresponding values in the two input fields shown in Figure 5.25. The default values for these two parameters are 0.06 and 0.01 respectively.

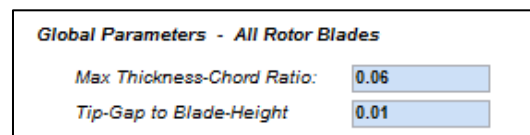


Figure 5.25 Global rotor blade parameters.

5.8.3. Global Parameters – All Stator Blades

Similar limit values for the thickness-to-chord and tip-gap height parameters can be applied for all stator blades in the subsequent input fields shown in Figure 5.26. The default value for the thickness ratio remains identical to that for rotor blades ($t/c = 0.06$). The tip-clearance to blade-height ratio on the other hand is set to zero by default.

Global Parameters - All Stator Blades	
Max Thickness-Chord Ratio:	0.06
Tip-Gap to Blade-Height	0
Exit Swirl Input Option:	Calculate Fr...
Middle Stage Tip Reaction:	0.6

Figure 5.26 Global stator blade parameters.

The global stator parameter section shown in Figure 5.26 further provides the user with the ability to edit the exit swirl profile condition for all stator blades within the compressor. Similar to the IGV definition section, the *Exit Swirl Input Option* field allows the user to select whether to calculate the free-vortex term internally using a specified middle-stage tip reaction, or to manually define the complete swirl profile at the exit of each stator blade row. When the first option is selected, all input fields associated with the free-vortex term (B/r) of equation 5.1 become un-editable throughout the program. The remaining coefficients of the swirl profile, however, may still be modified at each stator row if desired. Alternatively, if the latter option is selected, the tip reaction field in Figure 5.26 becomes un-editable, and all free-vortex controls throughout the program become active. Swirl definition fields are discussed in more detail in section 5.9.2.

5.9. Blade Parameters Tab

Selecting a specific blade row station in the navigation pane at the top of the *Blade Parameter* input window will display the remaining input fields for each individual blade. This can be done either by pressing the *NEXT* button, or by selecting a station from the dropdown list as shown in Figure 5.27.

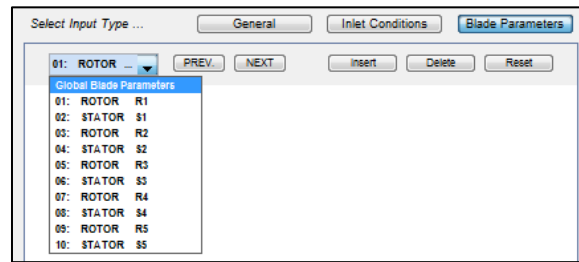


Figure 5.27 Blade row navigation pane.

At any point, the user may return to the *Global Blade Parameter* tab by selecting the first option from the dropdown menu, or by pressing the *PREV* button until the first page is reached. The navigation pane further provides the user with the option to toggle between specific blade row stations, insert/delete stages, and reset all input fields within a particular blade row station. These features are discussed in more detail in section 5.10.2. Depending on the type of station that is selected, the *Blade Parameter* window displays the input fields either for an individual rotor (as shown in Figure 5.28), or a given stator (such as Figure 5.29). Note that slight differences exist between the two input tabs depending on the type of station that is selected.

Select Input Type ... General Inlet Conditions **Blade Parameters**

01: ROTOR ... PREV. ... NEXT ... insert Delete Reset

Station Details

Global Index: 1
Blade Type: ROTOR
Blade ID: R1

Blade Exit Swirl Definition

Swirl Input Option: Calculate Fr...
Swirl Profile Definition: Constant 0 ft / sec

Blade Aerodynamic Parameters

Rotor Efficiency: Use Pressur...
Tip Blockage Factor: 0.0 Frac. Annular Area
Hub Blockage Factor: 0.0 Frac. Annular Area
Max Tip Diffusion Factor: 0.5
Exit / In Tip Mer. Vel Ratio: 1
Max Hub Turning Rate: 40
Max Inlet Hub Mach Number: 0.0

Blade Geometry Parameters

Rotor Tip Solidity: Use Default ...
Aspect Ratio (actual chord): Use Conven...
Exit / In Tip Radius Ratio: 1
Tip Ramp Angle Limit: -10 deg.
Hub Ramp Angle Limit: 10 deg.

Figure 5.28 Rotor blade parameters.

Select Input Type ... General Inlet Conditions **Blade Parameters**

02: STATOR ... PREV. ... NEXT ... insert Delete Reset

Station Details

Global Index: 2
Blade Type: STATOR
Blade ID: S1

Blade Exit Swirl Definition

Swirl Input Option: Calculate Fr...
Swirl Profile Definition: Constant 0 ft / sec

Blade Aerodynamic Parameters

Stage Efficiency: Use Pressur...
Tip Blockage Factor: 0.0 Frac. Annular Area
Hub Blockage Factor: 0.0 Frac. Annular Area
Max Hub Diffusion Factor: 0.6
Exit / In Tip Mer. Vel Ratio: 1
Max Hub Turning Rate: 0.0
Max Inlet Hub Mach Number: 0.85

Blade Geometry Parameters

Stator Hub Solidity: Use Default ...
Aspect Ratio (actual chord): Use Conven...
Exit / In Tip Radius Ratio: 1
Tip Ramp Angle Limit: -10 deg.
Hub Ramp Angle Limit: 10 deg.

Figure 5.29 Stator blade parameters.

5.9.1. Station Details

The first section of the blade input tab contains details regarding the specific blade row station that is selected by the user. The first field, *Global Index*, indicates the global position of the given blade within the compressor. For example, an index of 5 would correspond to the fifth blade in the compressor. The global index begins counting from the first rotor blade; it does not include the IGV. The next field, *Blade Type*, indicates the type of blade that is selected. Either *ROTOR* or *STATOR* is displayed. The remaining field, *Blade ID*, displays the blade type (*R* for rotor, or *S* for stator), as well as its global position relative to all similar blade types. For example, the next rotor and stator pair in the sequence following the ones shown in Figure 5.28 and Figure 5.29 would incorporate blade ID's of *R2* and *S2* respectively.

5.9.2. Blade Exit Swirl Definition

The next set of input fields provide the user with control over the exit swirl profiles for each individual blade row station. The swirl distributions for each blade row exit are defined in accordance with the polynomial function given in equation 5.1. Regardless of being applied to a rotor or a stator, the input fields are defaulted such that the free-vortex term (B/r) is internally calculated by the program. For rotor blades, the free-vortex term in equation 5.1 is calculated using a specified limit for the tip diffusion factor (described section 5.9.3). For stator blades, the free-vortex term is calculated using the middle-stage tip reaction value discussed in section 5.8.3. If desired, the remaining coefficients of equation 5.1 may be further modified either by editing the constant coefficient, C , as demonstrated in Figure 5.30, or by modifying the complete polynomial as shown in Figure 5.31. If the latter option is selected, the *Edit* pushbutton shown in Figure 5.31 enables the user to open an input window identical to the one shown in Figure 5.16. From there, all coefficients (with an exception of the free-vortex term) may be manually adjusted.

Figure 5.30 Rotor exit swirl definition fields.

Figure 5.31 Stator exit swirl definition fields.

Alternatively, a custom vortex distribution may be applied at each individual blade row station if desired. For rotor blades, this is done by selecting the *Define Full Profile* option from the *Swirl Input Option* dropdown list shown in Figure 5.30. By default, a uniform (constant) swirl profile is applied, the magnitude of which may be adjusted in the edit box next to the dropdown list. The complete swirl polynomial may

also be manipulated by selecting the *Polynomial* option from the dropdown list. All coefficients described by equation 5.1 may then be adjusted through an input window identical to the one shown in Figure 5.16. When this option is selected, the tip diffusion factor field becomes un-editable.

Stator blade swirl control is defined through the global control field as described in section 5.8.3. If the global setting is defined such that the free-vortex term is calculated by the program, the *Swirl Input Option* dropdown list becomes inactive as shown in Figure 5.31. If the global setting is set such that the complete polynomial may be edited by the user, the input dropdown list becomes active. Both the *Swirl Input Option* field and the *Swirl Profile Definition* field perform the same function as described for rotor blades.

5.9.3. Blade Aerodynamic Properties

This section provides the user with control over all aerodynamic characteristics associated with each blade row. Some input fields in this section may be inactive as they are only applicable to one of the two blade types (either rotors or stators). The differences can be seen in Figure 5.28 and Figure 5.29.

The first input field in this section controls the way in which efficiency is calculated. For rotors, this field is displayed as the *Rotor Efficiency*. In the stator tab, this field controls the efficiency of the stage (*Stage Efficiency*). One of three options may be selected from a dropdown list. With the first option, *Use Polytropic Efficiency Correlation*, the polytropic efficiency is calculated by the program using an internal correlation. The second (default) option, *Use Pressure-Loss Coefficient Correlation*, also applies an internal correlation, however, the corresponding calculation is based on an

associated pressure loss coefficient. Additional details regarding both internal formulations can be found in Glassman & Lavelle (1991). The last option, *Specify Polytropic Efficiency*, enables the user to apply a custom value for polytropic efficiency through an edit box as shown in Figure 5.32. If the program has already been executed, and the third option selected, the input box will automatically populate with a polytropic efficiency value that was previously solved by the program.

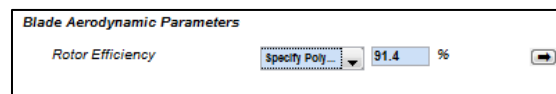


Figure 5.32 Polytropic efficiency definition.

It is important to note that the efficiency specification option must be consistent for all similar-type blade rows. For example, if an internal correlation is used for a given rotor blade, an identical correlation must be applied for all remaining rotor blades in the compressor. This is also true if a custom efficiency value is specified. When the efficiency specification option is modified, a warning message will appear to indicate that the change will be applied to all remaining blade rows. This gives the user the ability to cancel the request if desired. An example of the warning message is shown for reference in Figure 5.33.

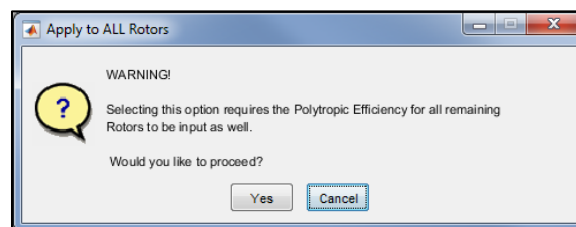


Figure 5.33 Warning message for efficiency specification change.

The next two input fields, shown in Figure 5.34, provide the user with control over the tip and hub blockage factors for a given blade row. By default, both fields,

regardless if for a rotor or a stator, are calculated by the program internally. For this reason, these input fields remain inactive. Custom blockage factors, however, may be applied by selecting the appropriate *Endwall Blockage* option in the *Global Blade Parameters* tab. Additional details regarding the endwall specification option may be found in section 5.8.1. Blockage areas are entered as a fraction of the annulus area at the particular blade station. For example, a blockage factor of 0.01 corresponds to a 1% blockage in annulus area. The application of custom blockage factors is demonstrated in Figure 5.34.

Tip Blockage Factor:	<input type="text" value="0.01"/>	Frac. Annular Area	<input type="button" value="→"/>
Hub Blockage Factor:	<input type="text" value="0.01"/>	Frac. Annular Area	<input type="button" value="→"/>

Figure 5.34 Blockage factor definition

The input field following the blockage factor entry section refers to the maximum allowable diffusion factor at the blade tip (for rotors) or at the blade hub (for stators). For rotors, this value is used to influence the free-vortex swirl calculation at the exit of the blade row (if applicable). The default diffusion factor limit is 0.5 for rotors, and 0.6 for stators. Both input fields are shown for reference in Figure 5.35 and Figure 5.36.

Max Tip Diffusion Factor	<input type="text" value="0.5"/>	<input type="button" value="→"/>
Exit / In Tip Mer. Vel Ratio:	<input type="text" value="1"/>	<input type="button" value="→"/>
Max Hub Turning Rate:	<input type="text" value="40"/> deg.	<input type="button" value="→"/>
Max Inlet Hub Mach Number:	<input type="text" value="0.0"/>	<input type="button" value="→"/>

Figure 5.35 Remaining aero input fields (rotors).

Max Hub Diffusion Factor	<input type="text" value="0.6"/>	<input type="button" value="→"/>
Exit / In Tip Mer. Vel Ratio:	<input type="text" value="1"/>	<input type="button" value="→"/>
Max Hub Turning Rate:	<input type="text" value="0.0"/> deg.	<input type="button" value="→"/>
Max Inlet Hub Mach Number:	<input type="text" value="0.85"/>	<input type="button" value="→"/>

Figure 5.36 Remaining aero input fields (stators).

The remaining aerodynamic input fields are shown in Figure 5.35 and Figure 5.36 as well. They include the exit-to-inlet tip meridional velocity ratio, the maximum hub-turning rate, and the maximum inlet hub Mach number. The turning rate is applicable to rotor blades only. This field is therefore disabled when a stator is selected. The

opposite effect is true for the stator hub Mach number limit. Default values for these fields are 40 degrees and 0.85 respectively.

5.9.4. Blade Geometry Parameters

The remaining input fields in the *Blade Parameter* tab provide the user with control over specific geometric properties. These fields are shown for reference in Figure 5.37 and Figure 5.38.

Figure 5.37 Geometry input fields (rotors).

Figure 5.38 Geometry input fields (stators).

This section remains nearly identical for both rotors and stators, with an exception of the first input field (solidity). For rotors, this field is used to control the solidity at the blade tip, while for stators this value is applied at the hub. In either case, the user can select one of two options from a dropdown list. When the first option is selected (*Use Default*), the local blade solidity is calculated by the program using one of the following internal correlations.

$$\sigma_{rotor (tip)} = 0.5 M_{rel (tip)} + 0.7 \quad (5.3)$$

$$\sigma_{stator (hub)} = 0.0206 \Delta\beta_{stator (hub)} + 0.794, \quad (\Delta\beta < 44 \text{ deg}) \quad (5.4)$$

$$\sigma_{stator (hub)} = 0.080 \Delta\beta_{stator (hub)} - 1.82, \quad (44 \text{ deg} < \Delta\beta < 60 \text{ deg}) \quad (5.5)$$

$$\sigma_{stator (hub)} = 3.0, \quad (\Delta\beta > 60 \text{ deg}) \quad (5.6)$$

More details regarding these correlations are provided by Glassman & Lavelle (1995). The second option, *Specify Value*, enables the user to enter a custom solidity

value in an edit box (shown in Figure 5.38). Similar to the efficiency specification option described in the beginning of section 5.9.3, the solidity option must remain consistent with all remaining blades of the same type. For example, if the default correlation is used for a given stator blade, the same correlation must be applied to all remaining stator in the compressor. The same is true if a custom solidity value is specified.

The next input field controls the aspect ratio of a given blade. One of three options may be selected from a dropdown list. If either of the first two options is selected, that is the *Conventional* option or the *Low Aspect Ratio* option, the program automatically calculates the aspect ratio for the given blade row in accordance with one of the following correlations:

$$AR_{Conventional} = 1.5 \frac{n-i}{n-1} + 1.0 \quad (5.7)$$

$$AR_{Low} = 0.5 \frac{n-i}{n-1} + 1.0 \quad (5.8)$$

The origin of these correlations is described in Glassman & Lavelle (1995). The remaining option in the dropdown list again enables the user to specify a custom value for the blade aspect ratio. It should be noted that this value is based on the actual chord length of the blade. Once again, the selected option must remain consistent with the remaining blades of similar type (ex. all rotors or all stators).

The remaining fields shown in Figure 5.37 and Figure 5.38 control the annulus geometry for a given blade row. The first field defines the exit-to-inlet radius ratio at the tip of a given blade row. The default value for both rotors and stators is 1.0 (i.e. constant inlet/exit radii). The remaining two input fields provide the user with the option to control the limit for the ramp angle of the annulus walls. The default values for the tip and hub

limits are -10 and 10 degrees respectively. In most cases, the program will consider these three values to be soft requirements. It may at times violate the limits that are entered by the user in order to achieve a converged design. If any of these limits are violated, the program will relay this information to the user in a notification window (refer to section 5.6.6 for more details). An example demonstrating the application of ramp angle limits is shown in Figure 5.39 and Figure 5.40.

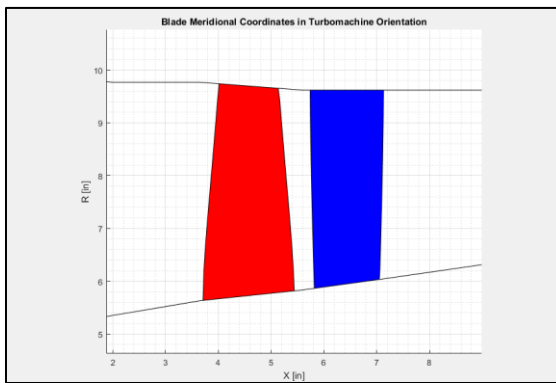


Figure 5.39 Stage 2 with tip and hub ramp angle limits of -6 and 6 degrees respectively.

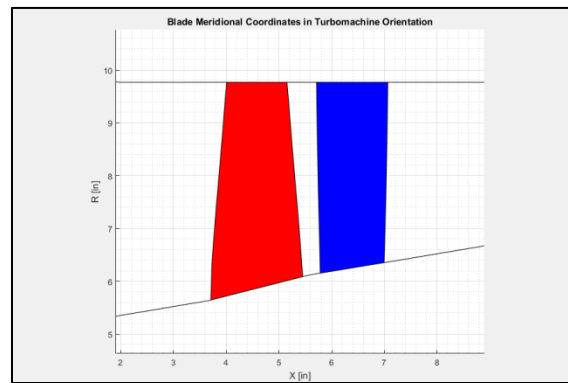


Figure 5.40 Stage 2 with tip and hub ramp angle limits of -20 and 20 degrees respectively.

5.10. Additional Input Window Commands

The following sections describe all remaining field commands that are available to the user when designing a given compressor. These functions are all located on the outer edge of the main input window as shown in Figure 5.41.

Select Input Type ... General Inlet Conditions **Blade Parameters**

01: ROTOR PREV. NEXT Insert Delete Reset

Station Details

Global Index: 1

Blade Type: ROTOR

Blade ID: R1

Blade Exit Swirl Definition

Swirl Input Option: Calculate Fr. Apply

Swirl Profile Definition: Constant 0 ft / sec Apply

Blade Aerodynamic Parameters

Rotor Efficiency: Use Pressur... Apply

Tip Blockage Factor: 0.0 Frac. Annular Area Apply

Hub Blockage Factor: 0.0 Frac. Annular Area Apply

Max Tip Diffusion Factor: 0.5 Apply

Exit / In Tip Mer. Vel Ratio: 1 Apply

Max Hub Turning Rate: 40 deg. Apply

Max Inlet Hub Mach Number: 0.0 Apply

Blade Geometry Parameters

Rotor Tip Solidity: Use Default... Apply

Aspect Ratio (actual chord): Use Conven... Apply

Exit / In Tip Radius Ratio: 1 Apply

Tip Ramp Angle Limit: -10 deg. Apply

Hub Ramp Angle Limit: 10 deg. Apply

Reset ALL Restore Last Export Data RUN

Figure 5.41 Complete user input window (Rotor blade parameter tab shown for reference).

5.10.1. **Apply All Command**

In referring to Figure 5.41, a small pushbutton labeled with an arrow may be observed to the right of most blade input fields. This feature may be used to apply a specified value to all remaining rotor or stator input fields in the compressor. This is beneficial if the user intends to apply one specific input value to all blades, and does not wish to change the value in each blade row individually. When selected, the program prompts the user with a warning message indicating that the given value will be applied to all remaining blades of similar blade type. This additional feature is meant to provide the user with the ability to cancel the request if it is selected by mistake.

5.10.2. Blade Navigation Pane

The navigation pane located at the top of Figure 5.41 (below the input selection buttons) enables the user to toggle between all blade row input tabs. The dropdown list at the left side of the pane provides a complete list of all stations in the compressor. Selecting a station from this list will display the blade parameter input window for the given blade row. The first option in this list opens the *Global Blade Parameters* tab that was discussed in section 5.8. An expanded view of this list can be seen in Figure 5.27.

The next two buttons, labeled *Prev* and *Next*, allow the user to cycle between blade rows one station at a time. When the last station is reached, the *Next* button becomes inactive. Similarly, when the global parameters input tab is reached (first option in the list), the *Back* button becomes disabled. Switching between blade row stations in this manner automatically updates the dropdown list with the station being viewed.

The remaining three buttons in the navigation pane provide the user with the ability to add a new stage, delete a given stage, or reset all local input fields with their default values. When the *Insert* button is selected, the input window shown in Figure 5.42 is displayed.

The image shows a dialog box titled "Insert Stage". It contains three dropdown menus arranged in two rows. The first row has "Stage Position:" followed by a dropdown menu showing "Insert Befo..." and another dropdown menu showing "Stage 01: ...". The second row has "Populate Fields:" followed by a dropdown menu showing "New (Defa...". At the bottom right of the dialog box are two buttons: "Ok" and "Cancel".

Figure 5.42 Insert stage window.

The input window shown in Figure 5.42 gives the user control over the global index of the new stage, as well as authority over populating its associated input fields.

The location of the new stage may be adjusted with the two upper-most dropdown menus. The first menu enables the user to insert the new stage either before or after an existing stage. The menu to the right specifies the stage in which the first option is in reference to. The menu directly below these fields offers the user the option to either populate the new stage with its default settings, or duplicate the parameters from an existing blade row.

The *Delete* button located at the top of Figure 5.41 removes a given stage from the compressor's configuration. A blade row may be deleted by first navigating to the station of interest, and then selecting the *Delete* button. The program will display a warning message indicating that the stage will be removed.

It is important to note that the *Max Stages* option discussed in section 5.6.4 performs a similar function as described above. For example, when the number of stages is increased in the *General* input tab, the program inserts the resulting number of stages at the end of the compressor. All input fields are then populated with their default values. On the other hand, if the number of stages is reduced in the *General* input tab, the program deletes the resulting number of trailing stages from the compressor's configuration.

The remaining function in the navigation pane, *Reset*, allows the user to reset all input fields for the blade row that is displayed. When selected, the program displays a warning message indicating that all fields will be reset to their default values.

5.10.3. **Reset All**

The *Reset All* button located at the bottom left corner of Figure 5.41 carries out a similar function as the local reset feature. In this case, however, all input fields in the

Meanline application are reset to their default values. When selected, the program displays a warning message indicating that all fields will be reset.

5.10.4. **Restore Last**

If the user is having difficulty obtaining a converged solution, the *Restore Last* feature offers the ability to restore the last working Meanline simulation. Every time a converged solution is obtained, the program additionally saves the corresponding input file to a temporary file named *temp* (no file extension). This file is saved in the working directory, and is deleted upon exiting the program. When the *Restore* function is enabled, the program populates all fields in the application with the data stored to the temporary file. This enables the user to restore a working solution if he or she cannot recall the changes made that originally caused the simulation to crash. Note that a converged solution must first be obtained before this feature may be implemented.

5.10.5. **Export Data**

All data that is displayed in the post-processing window may be exported at any time as a formatted *.csv file. This is done by selecting the *Export Data* button located at the bottom of Figure 5.41. When pressed, the program displays an input window that allows the user to select the amount of data to be exported, as well as the directory in which to save the files. Parameters that are available to be exported include 2D meridional blade coordinates, 2D annulus coordinates, stage information, and radial plots. The export selection window is shown in Figure 5.43.

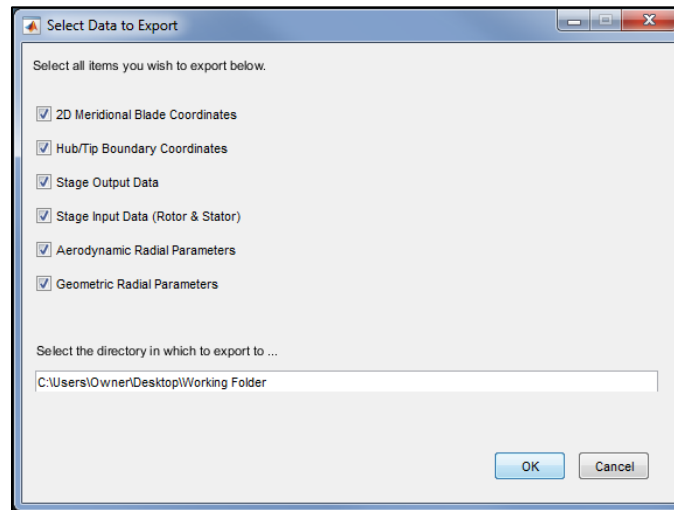


Figure 5.43 Export selection window.

5.11. Post-Processing

Once a converged Meanline solution is obtained, the outputted data is quickly post-processed and plotted in the window located to the right of the input pane. The three toggle buttons located at the top of the post-processing window enable the user to select one of three view modes: *Blade Geometry*, *Stage Plots*, and *Radial Plots*. Examples of all three are shown in Figure 5.44, Figure 5.45, and Figure 5.46. The post-processing capabilities offered by C-STAAC are the highlight of the program. They provide the user with immediate visual feedback during design iterations, and allow performance trends to be quickly recognized. The sections below give a general description of all post-processing functions.

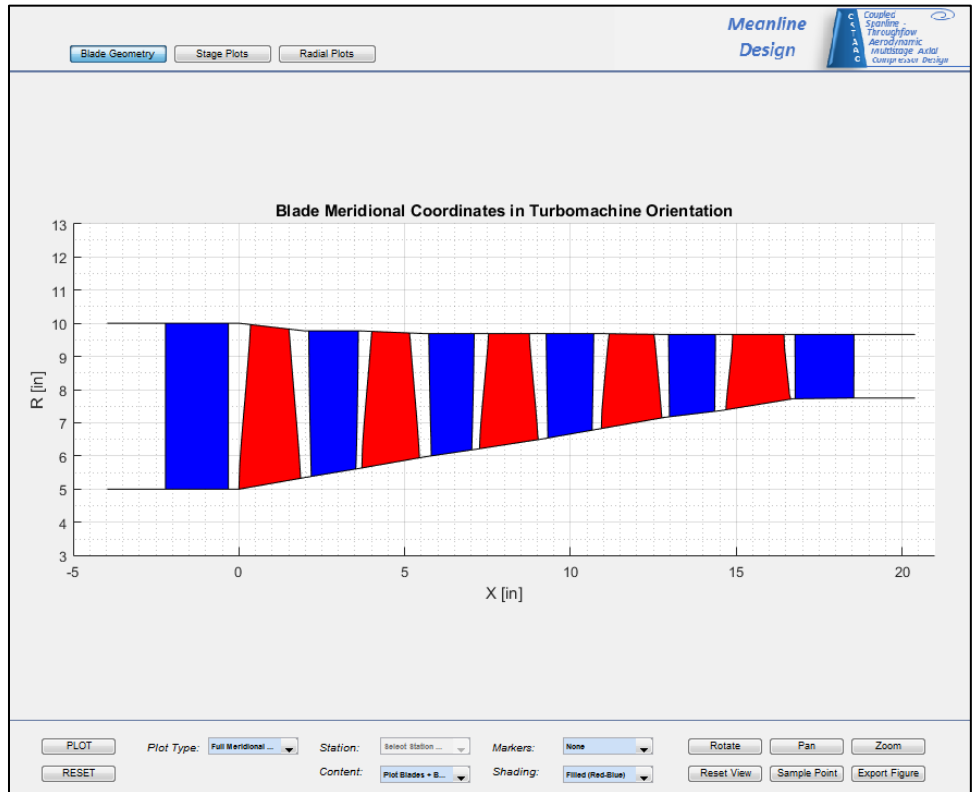


Figure 5.44 Blade geometry post-processing window.

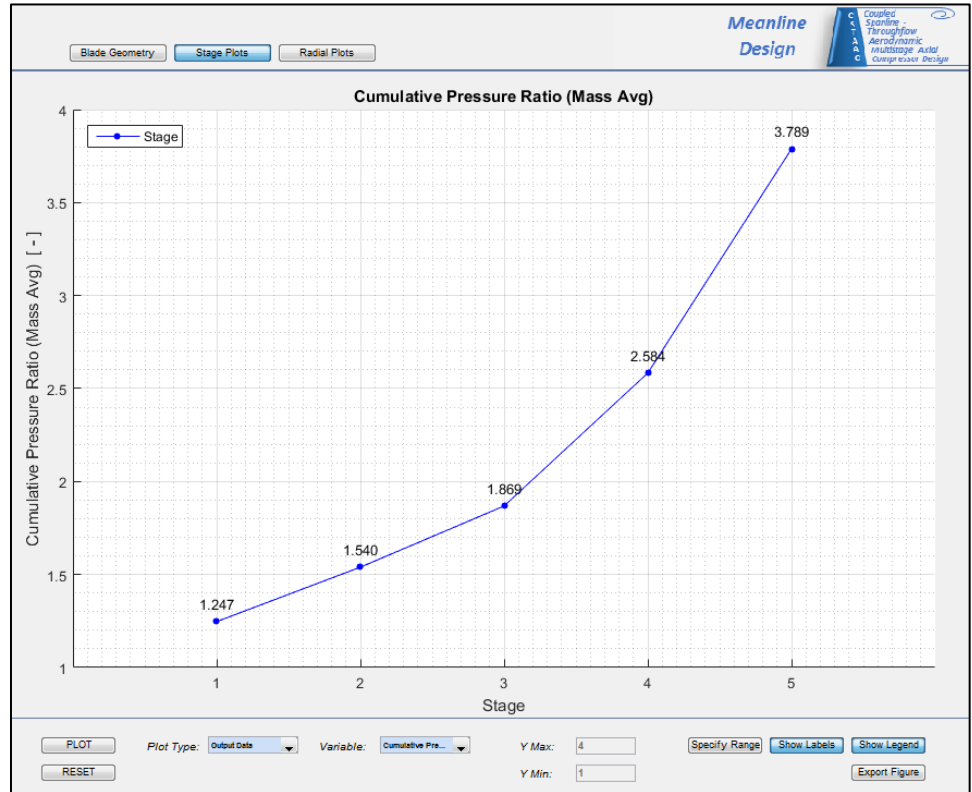


Figure 5.45 Stage plot post-processing window.

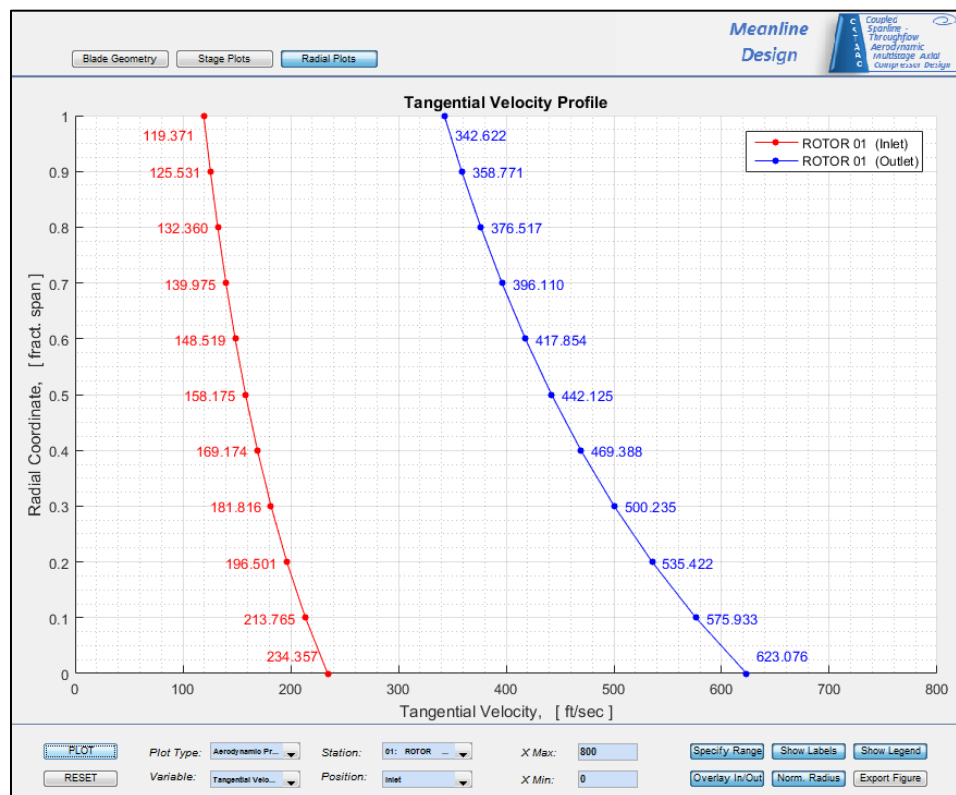


Figure 5.46 Radial plot post-processing window.

5.1.1.1. Blade Geometry Post-Processing Window

The input fields located at the bottom of the post-processing window provide the user with a wide variety of options to order to visualize the geometry of a newly designed compressor. In addition to the full meridional view displayed in Figure 5.44, the user may plot an enlarged view of a given stage or blade row by selecting the appropriate option from the *Plot Type* dropdown menu. Examples of these plot types are shown in Figure 5.47 and Figure 5.48. Enlarged views such as these may be beneficial to observe specific geometric changes made through successive iterations.

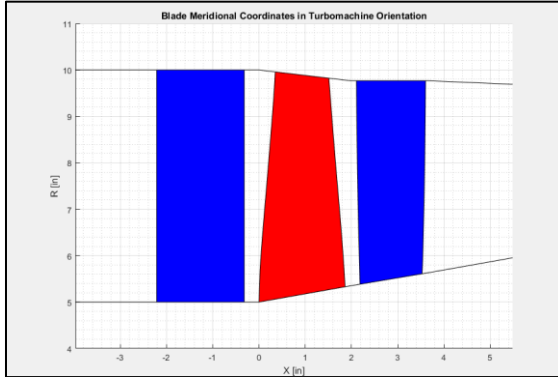


Figure 5.47 Stage view (stage 1 shown).

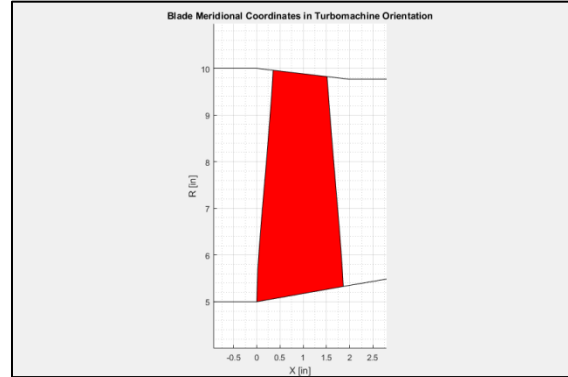


Figure 5.48 Single blade view (rotor 1 shown).

When either of the above plot types is selected, the dropdown menu, labeled *Station*, allows the user to plot the geometry of a given stage (if stage view selected) or blade row (if blade view selected). This field is disabled when the full meridional view is displayed.

The *Content* dropdown list controls the type of geometry that is displayed in the window. There are three options to choose. The first option, *Plot Blades + Boundary*, displays all compressor elements as shown in Figure 5.44. The remaining options, *Plot Blades Only*, and *Plot Boundary Only*, limit the displayed content to only blades, or only the annulus boundary as demonstrated in Figure 5.49 and Figure 5.50.

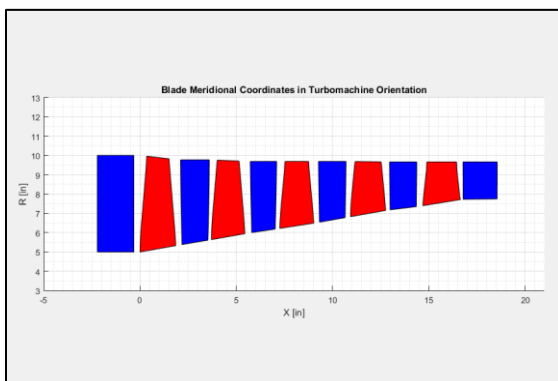


Figure 5.49 Blades only view.

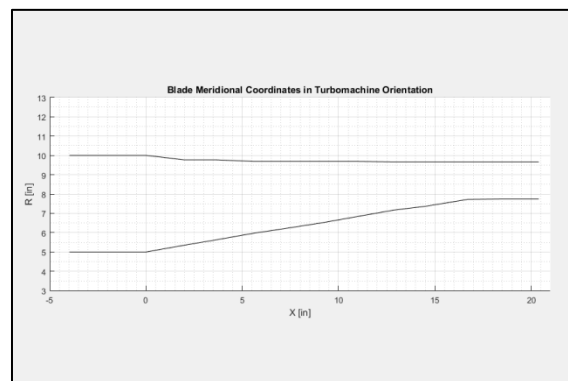


Figure 5.50 Boundary only view.

The next field, labeled *Markers*, provides an additional means of visualizing the blade row geometry. Three options may be selected. The first option, *Plot Stacking Lines*,

provides a visual representation of all blade stacking axes in the compressor. The stacking axis is defined at the mid chord location (distributed radially) of all blade elements. The next option, *Plot Aerodynamic Locations*, displays the axial locations of all aerodynamic stations where Meanline calculations are performed. They refer to the leading and trailing edges of each blade row in the compressor. The option to display both or none of these features is available to the user as well. The application of these options is demonstrated in Figure 5.51 and Figure 5.52.

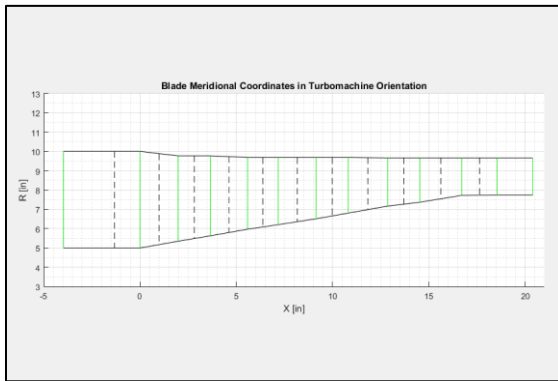


Figure 5.51 *Boundary only* view with aerodynamic stations (green) and staking lines (black) shown.

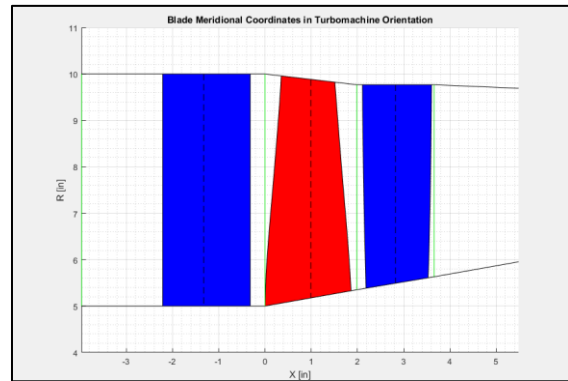


Figure 5.52 Aerodynamic stations and staking axes shown for stage 1 blades (with IGV).

The remaining dropdown list, *Shading*, provides the user with control over the color and shading of the blade geometry that is displayed. By default, rotor blades are colored red, and stator blades (including the IGV) are colored blue. All previous figures have represented the blade geometry in this manner. Alternatively, the user may plot all blades in one solid color (blue), or plot just the outlines of the blades themselves. These options are illustrated in Figure 5.53 and Figure 5.54.

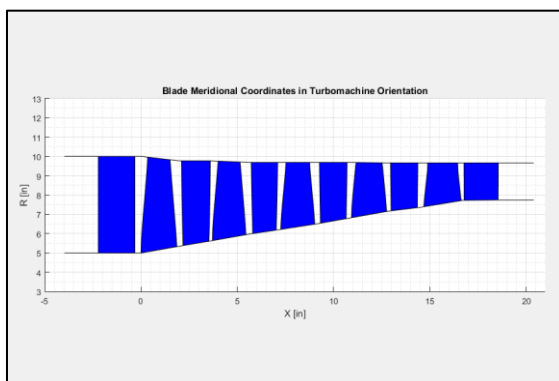


Figure 5.53 Filled blade geometry.

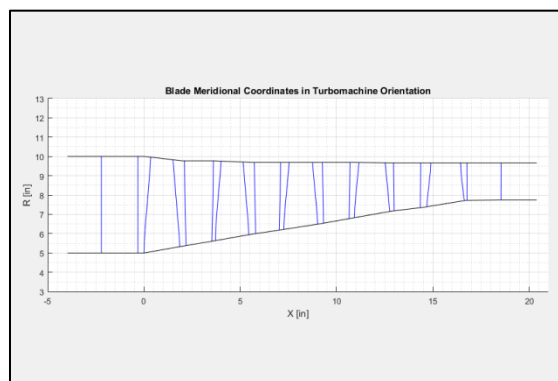


Figure 5.54 Blade outline view.

The button group located at the right of the user input window provides additional post-processing controls. The first three functions, *Rotate*, *Pan*, and *Zoom*, allow the user to navigate around the figure accordingly. These functions need no explanation. The next option, *Reset View*, resets the axis, rotation, and magnification settings of the figure to their original values. This option does not reset the content that is displayed, only the view that is projected.

By selecting the *Sample Point* option, the user may display the global coordinates of any point along the blade edges or annulus boundary. A specific point may be sampled with the cursor after the toggle button has been depressed. This feature is demonstrated in at the trailing edge of the stator in Figure 5.55.

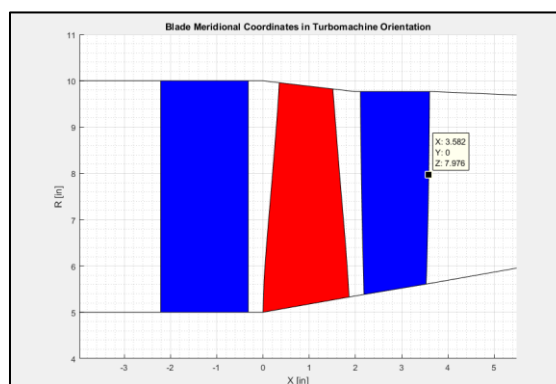


Figure 5.55 Coordinates displayed at the trailing edge of stator 1.

The last option, *Export Figure*, allows the user to export the figure that is

currently displayed in the post-processing window. When selected, the user is prompted with an input window to change the file name, as well as select the directory in which to save the image file. All figures exported from the window are saved in *.jpg* format.

The *RESET* command located to the left of the input pane provides a means of resetting all view settings and projected content. When selected, all input options are reset to their default values.

5.11.2. **Stage Plot Post-Processing Window**

In addition to its ability to post-process blade and annulus geometry, the program offers the user the option to plot and compare a wide variety of stage-specific aerodynamic and geometric variables. A complete list of stage output variables (variables solved by the program) is provided in Appendix A.

Any of the stage parameters displayed in Appendix A may be displayed by selecting the appropriate option from the *Variable* dropdown list. It is important to note that these variables are solved by the program, and slight discrepancies between input and output values may in fact be observed. This is because the majority of parameters that are input by the user are aerodynamic and geometric limits that the program utilizes in its design strategies. Some limits may be violated in order to achieve a converged solution for the remaining input requirements (discussed in section 5.9.4). Examples of output stage plots are shown in Figure 5.56, Figure 5.57, Figure 5.58, and Figure 5.59.

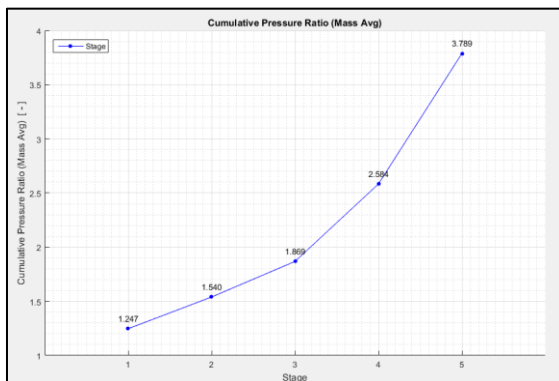


Figure 5.56 Cumulative stage pressure ratios for the default 5 stage compressor.

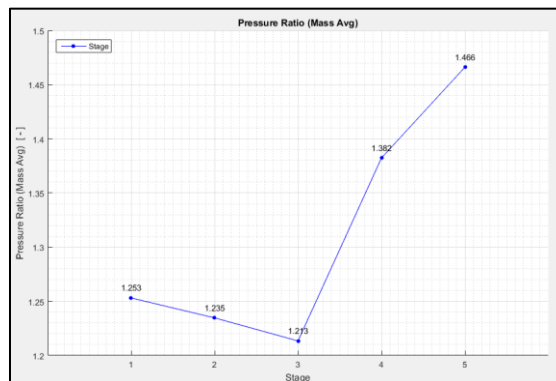


Figure 5.57 Equivalent raw stage pressure ratios for the default 5 stage compressor.

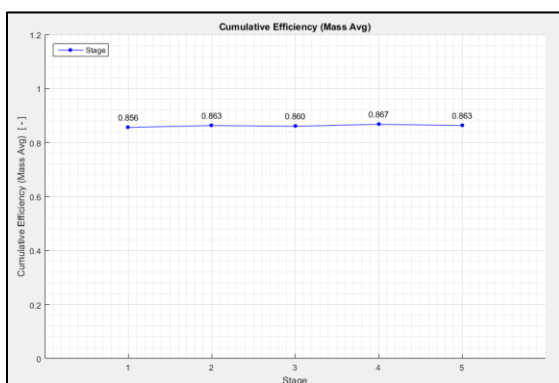


Figure 5.58 Cumulative stage adiabatic efficiencies for the default 5 stage compressor.

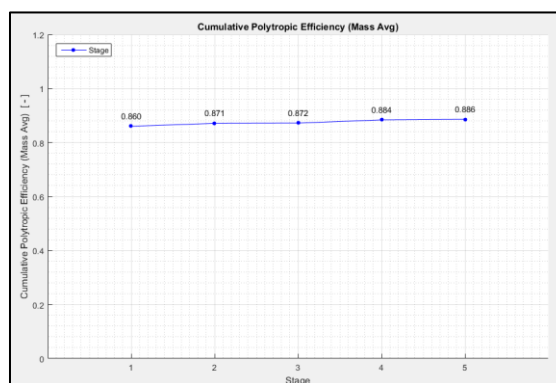


Figure 5.59 Cumulative stage polytropic efficiencies for the default 5 stage compressor.

The *Plot Type* dropdown menu shown in Figure 5.45 additionally provides the user with the option to monitor all stage variables that were manually input. This option provides an additional means of comparing the differences (if any) between the converged solution and the parameters that were initially specified by the user. A complete list of input stage variables available for plot is shown in Table A.2.

The two input fields, labeled *Y Max* and *Y Min*, specify the range of the y-axis of the figure. These values may be modified by selecting the *Specify Range* toggle button located in the local button group (right side of the input pane). When the button is depressed, the two input fields become active. Otherwise, the fields remain un-editable, and the y-axis in the displayed figure is set automatically.

In addition, the data labels and plot legend may be hidden from the view by selecting the respective *Show Labels* or *Show Legend* toggle buttons. The *Export Figure* function remains identical to the one discussed in the geometry post processing section (section 5.11.1).

5.11.3. **Radial Data Post-Processing Window**

The remaining post-processing tab, labeled *Radial Plots*, displays the radial variations of specific aerodynamic and geometric parameters. The axial locations of the radial plots correspond to the inlet and exit aerodynamic stations such as those illustrated in Figure 5.51 and Figure 5.52. The post-processing input options that are shown at the bottom of Figure 5.46 remain quite similar to those for the blade geometry and stage plot tabs. The *Plot Type* field provides the user with the option to display either aerodynamic or geometric data at the leading or trailing edge of a given blade. The parameters available for each plot type are shown in Appendix B, and may be selected from the *Variable* dropdown list shown in Figure 5.46.

The location at which the radial profiles are displayed may be selected through the *Station* and *Position* dropdown lists. The first field enables the user to select a specific blade row, while the latter field indicates whether the inlet (leading edge) or exit (trailing edge) profiles are displayed. For geometric plots, the *Position* field is disabled. The user may also modify the minimum and maximum limits of the x-axis by selecting the *Specify Range* toggle button, and then updating the values in their appropriate input fields. The *Show Labels*, *Show Legend*, and *Export Figure* options remain identical to the functions discussed in the stage plots tab (section 5.11.2).

The radial tab provides two additional features that can be accessed from the

toggle button group. The first, labeled *Overlay In/Out*, displays the radial distributions of the selected variable at both the inlet and exit locations of the blade row. Selecting this option overrides the option selected from the *Position* dropdown list. This feature is demonstrated in Figure 5.60. The remaining option, *Norm Radius*, provides the radial distribution normalized to leading or trailing edge span of the blade. Note that when this option is selected, the radius values are normalized to the span of the aerodynamic station in which they were initially calculated. Normalized profiles are shown in Figure 5.61.

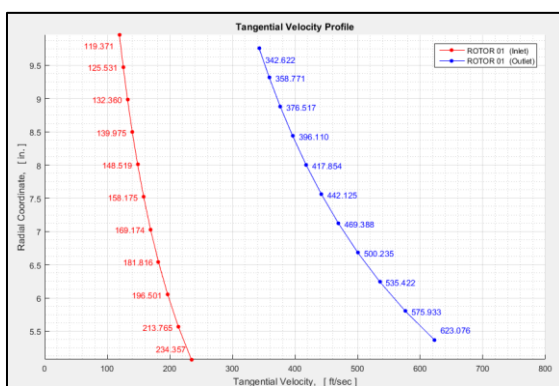


Figure 5.60 Radial distributions of tangential velocity at the inlet and exit locations of rotor 2.

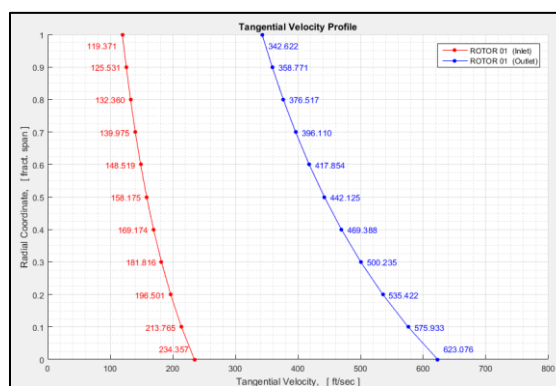


Figure 5.61 Radial distribution (normalized to span) of tangential velocity at the inlet and exit locations of rotor 2.

5.12. Meanline-to-Throughflow Window

The *Go to THROUGHFLOW* button located in the upper right corner of the navigation tab (described in section 5.4) enables the user to advance the Meanline solution to the Throughflow phase of design. In doing so, all minimum input variables required by the Throughflow simulation are automatically populated with the corresponding variables solved by the Meanline application. This feature highlights another major advantage of the program as it eliminates the time-consuming task of populating the Throughflow simulation.

In addition to populating the minimum input variables, the program offers the

user the ability to transfer additional data in order to better initialize the Throughflow solution. All such options are available through an input window displayed after the *Go to THROUGHFLOW* button is selected. The input window is shown in Figure 5.62.

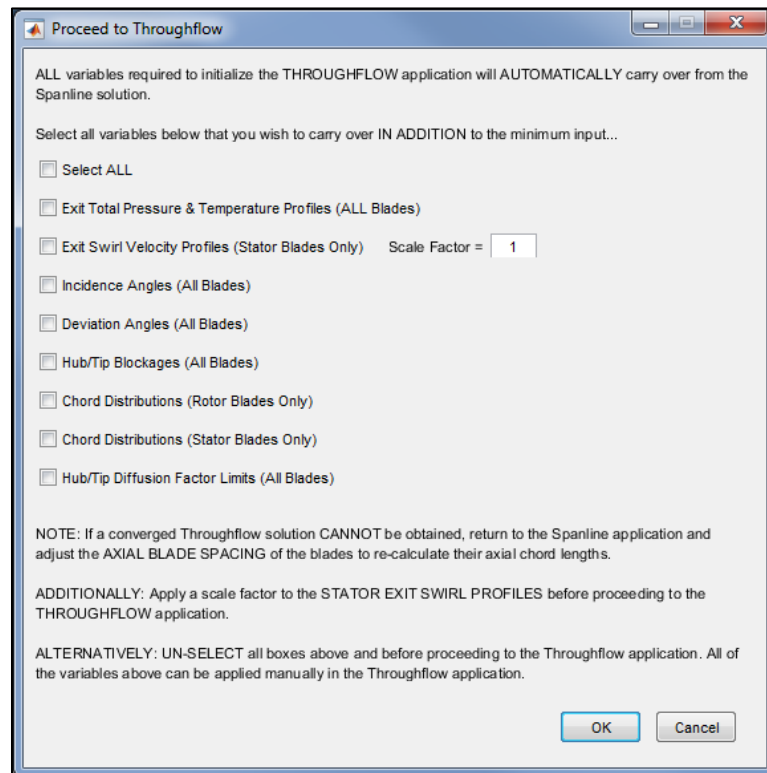


Figure 5.62 User input options to initialize the Throughflow simulation.

By default, only the minimum input variables are carried over to the Throughflow simulation (i.e. no options are selected). If desired, all advanced variables may be transferred by checking the *Select ALL* option. Alternatively, specific variables may be individually selected from the list. It is important to note that the *Select ALL* feature overrides any other selections. Therefore when carrying over individual parameters, the *Select ALL* feature must be disabled. Any of the advanced parameters shown in Figure 5.62 may be manually applied from within the Throughflow application.

If the trailing edge stator swirl profiles are selected to be transferred (second option in the list), the user is prompted with another input parameter named *Scale Factor*.

This feature applies a scaling factor to all stator exit swirl profiles in the compressor. By default, the Meanline code designs the compressor by applying free-vortex radial equilibrium assumptions. The free-vortex assumption, however, may sometimes produce unreasonably high velocity values near rotor and stator root locations that may in fact cause the Throughflow application to fail. Better robustness in the Throughflow phase may be achieved by scaling the stator swirl profiles to a more practical level (say 60–80%). This effect is demonstrated in Figure 5.63 and Figure 5.64.

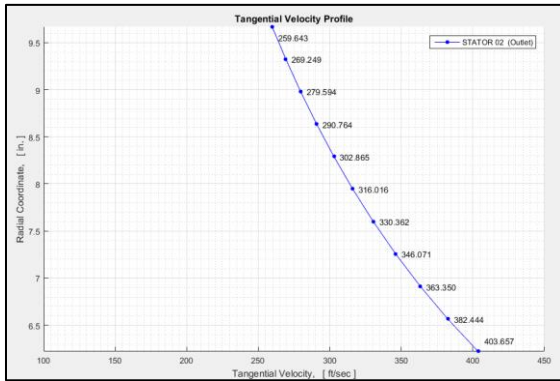


Figure 5.63 Tangential velocity distribution at stator 2 exit.

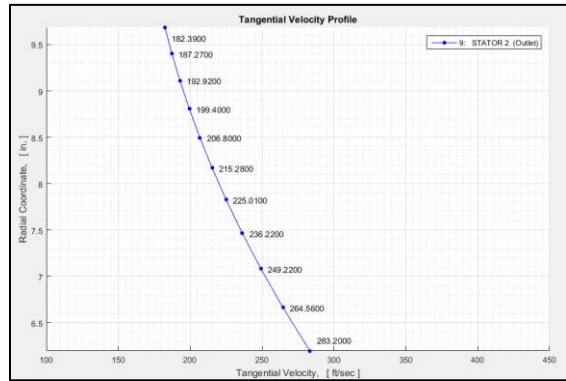


Figure 5.64 Tangential velocity distribution at stator 2 exit (scaled to 70%).

6. C-STAAC Functionality: Throughflow Application

6.1. Throughflow Interface

This section provides a detailed overview of all functions associated with the Throughflow application of C-STAAC. Because of its integration into a single platform, many of the features associated with the Throughflow application appear similar to those described in the Meanline section. Although some post-processing functions are in fact identical to their Meanline counterparts, the Throughflow application offers the user significantly more control over blade and annulus design parameters. For consistency, the details presented herein refer to the advancement of the solution for the default 5-stage compressor described in the previous chapter. The main interface of the Throughflow application is shown in Figure 6.1.

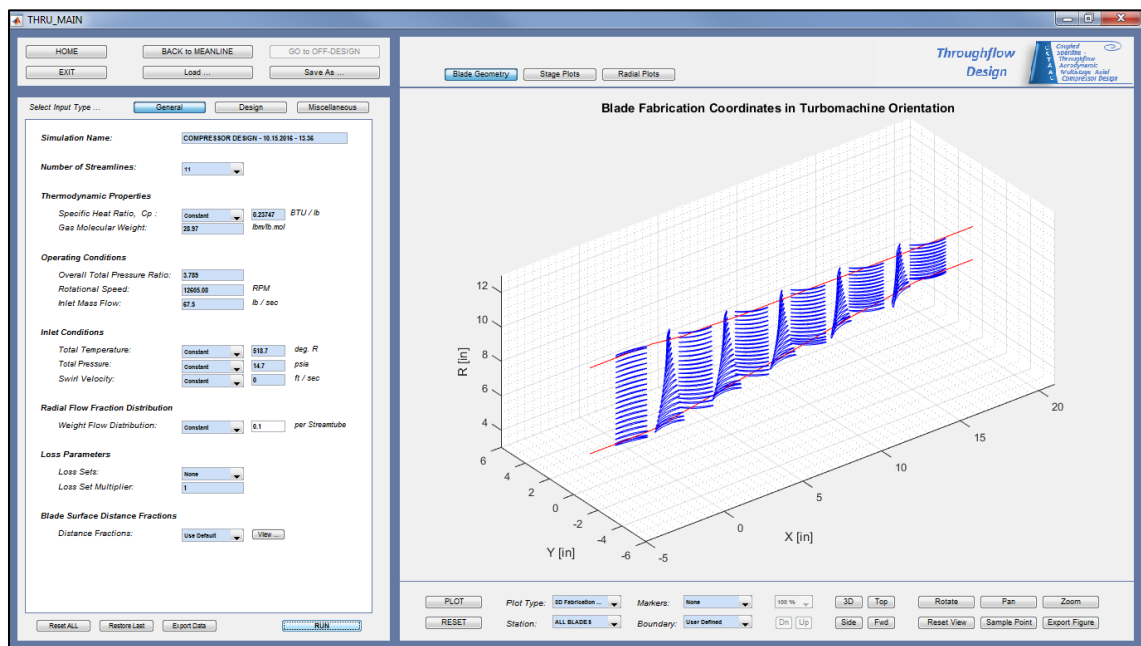


Figure 6.1 Throughflow application interface.

6.2. Running a Throughflow Simulation

Similar to the Meanline application, a Throughflow solution may be obtained by selecting the *RUN* command at the lower left corner of the screen. Due to its nature, a Throughflow simulation requires slightly more time to converge compared to its Meanline counterpart. The difference in computing time results from the implementation of numerical methods as opposed to analytical techniques in order to obtain the solution. The benefit of incorporating the Throughflow application, however, includes increased fidelity in the aerodynamic solution, as well as the generation of stacked airfoil geometry that resembles the 3D configuration of the compressor. The time required to generate and post-process a Throughflow solution depends on the complexity of the compressor, but can range between 1.0 and 4.0 seconds. The solution for the default 5-stage compressor shown in Figure 6.1 was obtained and post-processed in 1.4 seconds.

6.3. Minimum Input

When proceeding from the Meanline to the Throughflow application, all minimum input variables that are required to run the Throughflow code are automatically populated with values previously solved by the Meanline program. If the Throughflow application is executed from a standalone level, however, these variables must be input by the user manually. Table 6.1 lists all minimum input variables that are required to run the Throughflow program.

Table 6.1 Minimum input required to generate a Throughflow solution.

Parameter	Assigned Variable	Units
Overall Total Pressure Ratio	π_c	-
Shaft Rotational Speed	ω	RPM
Inlet Mass Flow Rate	\dot{m}	lb / sec
Inlet Total Pressure	P_0	psia
Inlet Total Temperature	T_0	deg.R
Inlet Swirl Velocity (if any)	V_θ	ft / sec
Annulus Hub and Tip Coordinates	-	in.
Stacking Line Coordinates (at each blade row)	-	in.
Number of Blades (at each blade row)	N	-
Tip Solidity (at each blade row)	σ	-

6.4. Navigation Tab

The navigation tab located in the upper left corner of Figure 6.1 provides the user with similar options as described for the Meanline application (refer to section 5.4). The main difference in this case is the supplemental option to revert to the Meanline solution. If a converged Throughflow solution cannot be obtained, this feature, labeled *BACK to MEANLINE*, allows the user to terminate the application and proceed back to the Meanline simulation for further refinement. This function may also be used if significant changes to the compressor's geometry are to be made and the minimum input variables listed in Table 6.1 need to be re-defined. This feature, together with the equivalent function described in section 5.12, rounds out the coupling capabilities of the program. The remaining option, labeled *GO to OFF-DESIGN*, is an inactive placeholder for future program development.

6.5. Input Window

All input to be specified by the user may be defined in the main input window located directly under the navigation pane shown in Figure 6.1. The window is split into three input tabs: *General*, *Design*, and *Miscellaneous*, each of which offers control over different aspects of the compressor's design. The user may toggle between all three tabs using the buttons located at the top of the input window. The input fields associated with all three tabs are described in the following sections.

6.6. General Input Tab

The *General* input tab provides the user with control over fundamental thermodynamic properties, inlet/operating conditions, loss parameters, and basic streamline definition options. The general tab is shown in Figure 6.2 for reference.

Select Input Type ... **General** Design Miscellaneous

Simulation Name: COMPRESSOR DESIGN - 10.15.2016 - 13.36

Number of Streamlines: 11

Thermodynamic Properties

Specific Heat Ratio, Cp : Constant 0.23747 BTU / lb

Gas Molecular Weight: 28.97 lbm/lb.mol

Operating Conditions

Overall Total Pressure Ratio: 3.789

Rotational Speed: 12600 RPM

Inlet Mass Flow: 67.5 lb / sec

Inlet Conditions

Total Temperature: Constant 518.7 deg. R

Total Pressure: Constant 14.7 psia

Swirl Velocity: Constant 0 ft / sec

Radial Flow Fraction Distribution

Weight Flow Distribution: Constant 0.1 per Streamtube

Loss Parameters

Loss Sets: None

Loss Set Multiplier: 1

Blade Surface Distance Fractions

Distance Fractions: Use Default View

Figure 6.2 General input tab.

6.6.1. Simulation Name

The *Simulation Name* field seen at the top of the input window in Figure 6.2 allows the user to change the name of the given project. If left unaltered, this field becomes populated with the name specified in the Meanline application (section 5.6.1) and the home screen (section 4.4). Any combination of characters may be used to specify custom project name for a given Throughflow simulation, however no more than 70 characters may be used. If more are entered, the program restores the previous simulation name and returns an error message.

6.6.2. Number of Streamlines

The user may control the number of streamlines at which radial streamline curvature calculations are performed. A minimum of 3 and a maximum of 11 streamlines may be selected from the *Number of Streamlines* dropdown list shown in Figure 6.2. By default, this field is set to its maximum value of 11 in order to obtain the highest solution fidelity, but a lower number can be selected to increase solution time (although the difference is almost negligible). The effect of altering the number of streamlines is demonstrated in Figure 6.3 and Figure 6.4.

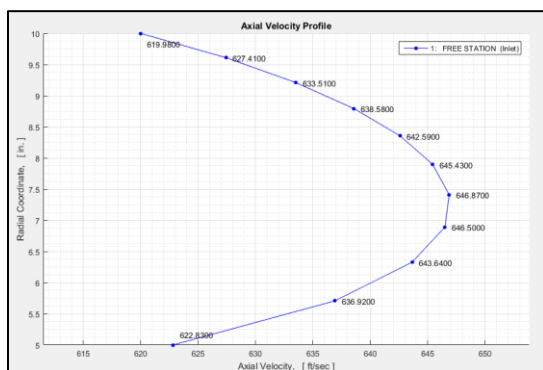


Figure 6.3 Example axial velocity profile using 11 streamlines.

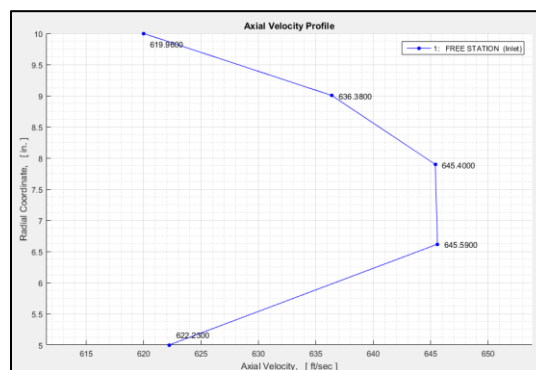


Figure 6.4 Example axial velocity profile using 5 streamlines.

6.6.3. Thermodynamic Properties

The next two input fields provide the user with control over the thermodynamic properties of the working fluid. Both the specific heat ratio (C_p) and the gas molecular weight (in *lbm/lb.mol*). By default, these values are set to reflect the properties of air as shown in Figure 6.5.

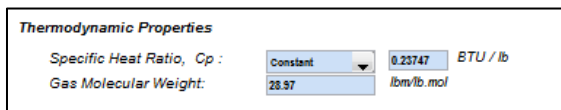


Figure 6.5 Thermodynamic properties input field with constant C_p

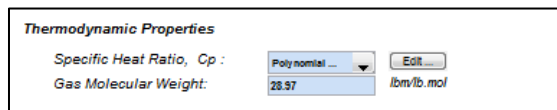


Figure 6.6 Thermodynamic properties input field with variable C_p

The program additionally offers the user the ability to apply a variable specific heat polynomial to account for the varying temperatures in the compressor. This can be done by selecting the *Polynomial* option from the corresponding dropdown list as shown in Figure 6.6. When selected, a new input window is displayed which allows the user to manually adjust the coefficients of the specified polynomial function. This window is shown in Figure 6.7 for reference. The default coefficients applied by the program are listed in Table 6.2.

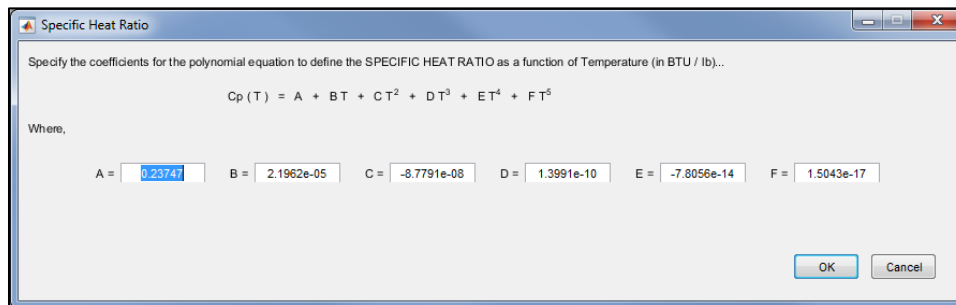


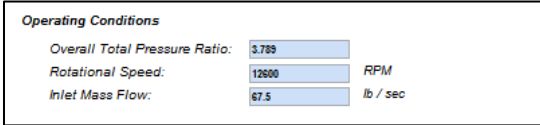
Figure 6.7 Variable specific heat input window.

Table 6.2 Default coefficients for variable specific heat model

Parameter	Default Value
Polynomial Function	$C_p(T) = A + BT + CT^2 + DT^3 + ET^4 + FT^5$
A	2.3747 E-01
B	2.1962 E-05
C	-8.7791 E-08
D	1.3991 E-10
E	-7.8056 E-14
F	1.5043 E-17

6.6.4. Operating Conditions

The next three input fields located under the *Operating Conditions* section provide the user with control over the compressor's overall total pressure ratio, shaft rotational speed (*RPM*), and inlet mass flow rate (*lb/sec*). If the simulation is initialized from the Meanline application, these variables are populated automatically. If the Throughflow simulation is executed from a standalone level, all three of these variables must be defined by the user as part of the minimum input requirements. These fields are shown in Figure 6.8 to be populated with the values extracted from the default Meanline solution.



The screenshot shows a window titled "Operating Conditions" with three input fields:

- Overall Total Pressure Ratio: 3.739
- Rotational Speed: 12600 RPM
- Inlet Mass Flow: 67.5 lb / sec

Figure 6.8 Operating conditions input fields.

6.6.5. Inlet Conditions

The following three input fields allow the user to specify the total temperature (degrees *Rankine*), total pressure (*psia*), and upstream swirl (*ft/sec*) at the inlet of the

compressor. Unlike the inlet specification requirements of the Meanline application, the inlet conditions specified in the fields shown in Figure 6.9 are referenced to the inlet of the compressor, regardless of the presence of an IGV.

Inlet Conditions		
Total Temperature:	Constant	518.7 deg. R
Total Pressure:	Constant	14.7 psia
Swirl Velocity:	Custom Distr...	Edit...

Figure 6.9 Inlet conditions input fields

By default, the parameters shown in Figure 6.9 are uniformly distributed at the inlet of the compressor. However, the user may apply any of these variables as a custom radial distribution if desired. To do so, the *Custom Distribution* option may be selected from any of the three dropdown lists shown in Figure 6.9. When selected, the corresponding edit box is replaced by an *Edit* pushbutton as demonstrated by the swirl velocity parameter. Selecting the button opens a new input window that allows the radial distribution to be manually edited. The radial profile input window is shown in Figure 6.10.

Edit the TANGENTIAL (Swirl) VELOCITY Distribution at the Compressor INLET in the boxes below.
Specify the velocity (in ft/sec) for each streamline, beginning with the tip and ending with the hub.

	Streamline	Swirl Velocity [ft/sec]
1	1 (Tip)	10
2	2	20
3	3	30
4	4	40
5	5	50
6	6	40
7	7	30
8	8	20
9	9	10
10	10	5
11	11 (Hub)	0

NOTE: Streamline 1 corresponds to the TIP location, and Streamline 11 corresponds to the hub location.

OK Cancel

Figure 6.10 Inlet profile definition (swirl velocity shown).

Note that a custom distribution can be specified by editing the values in the right

column shown in Figure 6.10. The first value (streamline 1) corresponds to the tip location, and the last value (streamline 11) corresponds to the hub location. The left column in the input window provides a visual representation of the streamline numbering sequence. This column appears to be editable, but any inputted values are disregarded by the program.

6.6.6. Radial Flow Fraction Distribution

The *Weight Flow Distribution* field, shown in Figure 6.11, enables the user to control the cumulative weight flow split between streamlines. By default, the streamtube areas between each streamline are evenly distributed. Hence, for 11 streamlines (10 streamtubes), this results in a 10 percent (0.1 fraction) weight flow distribution.

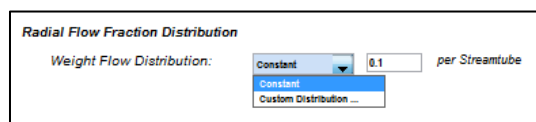


Figure 6.11 Streamline weight flow distribution options.

Similar to the inlet input fields, a custom weight flow distribution may be specified by the user by selecting the *Custom Distribution* option from the dropdown list. The result of doing so displays the input window shown in Figure 6.12. A custom weight flow distribution may be entered in the right-most column of the input window. Note that values must be entered as the cumulative fraction beginning at the tip streamtube. The first value must be greater than zero and the succeeding values must increase to 1.0 in order for the last value to account for the accumulation of flow for all streamtubes. The program will produce an error message for the user if this condition is not met.

Edit the Weight Flow distribution in the boxes below.

Specify the cumulative weight-flow split (as a percentage of total flow) between each streamline, beginning with the tip and ending with the hub.

	Streamtube	Weight Flow Fraction
1	1 (Tip)	0.1
2	2	0.2
3	3	0.3
4	4	0.4
5	5	0.5
6	6	0.6
7	7	0.7
8	8	0.8
9	9	0.9
10	10 (Hub)	1

NOTE: The first value must be greater than zero and succeeding values must increase to 1.0 in order for the last value to account for the accumulation of flow for all streamlines.

OK Cancel

Figure 6.12 Streamline weight flow distribution definition (constant distribution shown).

6.6.7. Loss Parameters

This section enables the user to define custom loss parameters for total pressure loss calculations. The desired number of specified loss sets may be selected from the *Loss Sets* dropdown list shown in Figure 6.13. Note that up to five loss parameter sets may be stored by the program.

Loss Parameters

Loss Sets: 4 Edit...

Loss Set Multiplier: 1

Figure 6.13 Streamline weight flow distribution options.

A loss set is defined as a table of diffusion factors (D) and corresponding loss parameters (ϖ). These variables are defined by the program as follows:

$$D = 1 - \frac{w_2}{w_1} + \frac{[(rV_\theta)_2 - (rV_\theta)_1]}{\sigma(r_1 + r_2)w_1} \quad (6.1)$$

$$\varpi = \frac{\omega_P \cos \beta_2}{2\sigma} \quad (6.2)$$

In equation 6.1, w_1 and w_2 refer to the relative velocity at the inlet and exit of a given rotor blade respectively. In addition, r is the radius from the axis of rotation, V_θ is the tangential flow velocity, and σ is the local blade solidity. In equation 6.2, β_2 is the exit flow angle relative to the meridional direction, and ω_p is the profile loss coefficient given by:

$$\omega_p = \frac{P_{02,i} - P_{02}}{P_{01} - P_1} \tag{6.3}$$

The correlation between the diffusion factor and loss parameter is generally obtained from experiments such as those described in sections 1.4.3 and 1.4.4. Therefore, if empirical data for a given compressor exists, values for diffusion factors and loss parameters may be entered into the program in order best represent the stage losses. This can be done by first selecting the number of loss sets from the dropdown menu, and then clicking the *Edit* pushbutton shown in Figure 6.13. This displays the input window shown Figure 6.14.

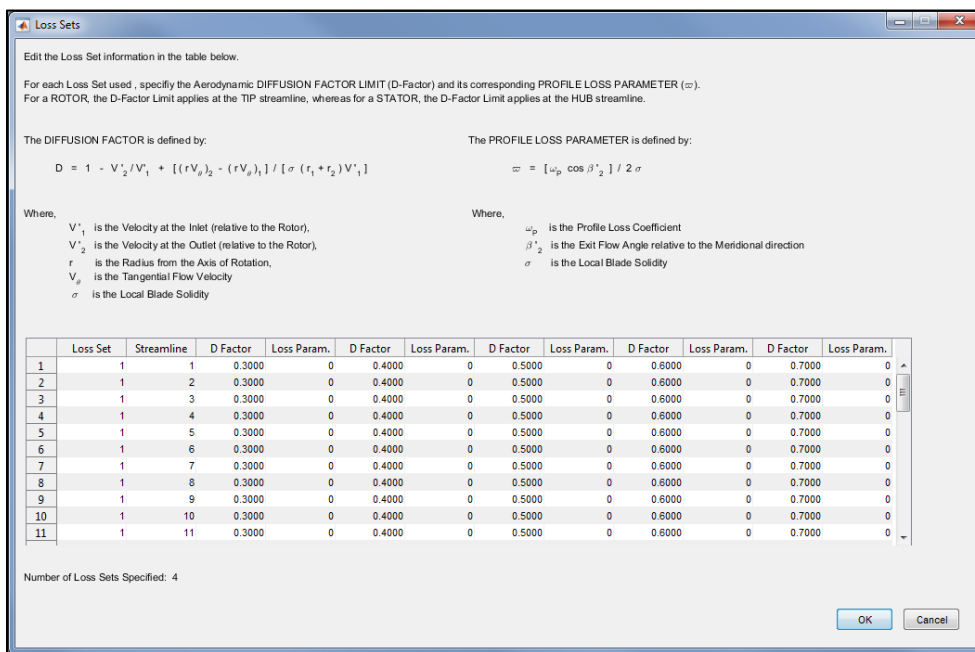


Figure 6.14 Loss parameter input window.

Each row seen in Figure 6.14 defines the loss parameter distribution for a given streamline. Up to five loss parameters may be specified per streamline. By default, the range of diffusion factors for each streamline is set between [0.3 - 0.7], but these values may be edited by the user. The corresponding loss parameters may be defined in the column to the right of the diffusion factor.

The number of rows that are displayed in the input window is defined by the number of loss sets that are specified by the user, as well as the number of streamlines that were originally selected for the simulation. For example, a simulation with 11 streamlines and 4 loss sets would produce 44 input rows in the window. The first two columns in the table display the index of a given loss set and streamline number. These fields are un-editable. The scroll wheel to the right of the input field allows the user to navigate through the full table. Note that if the user increases the number of loss sets in the original dropdown list, the program adds a new (blank) range of streamline rows for the new loss set at the end of the existing table. On the other hand, if the user decreases the number of loss sets, the excess rows are deleted from the table. A warning message appears for the latter case. The process of assigning a specific loss set to a blade row is discussed in a later section. By default, the *Loss Sets* dropdown list is set to *None*, and all losses are instead computed using internal correlations (discussed in a later section).

6.6.8. Blade Surface Distance Fractions

This field defines the blade-element surface distance fractions at which coordinates are obtained for blade-element definition. 21 values (between and including 0 and 1) are expected. The default distribution is shown in Figure 6.15, but may be manually edited by the user by selecting the *Specify Custom Fractions* option from the

dropdown list in the general input tab.

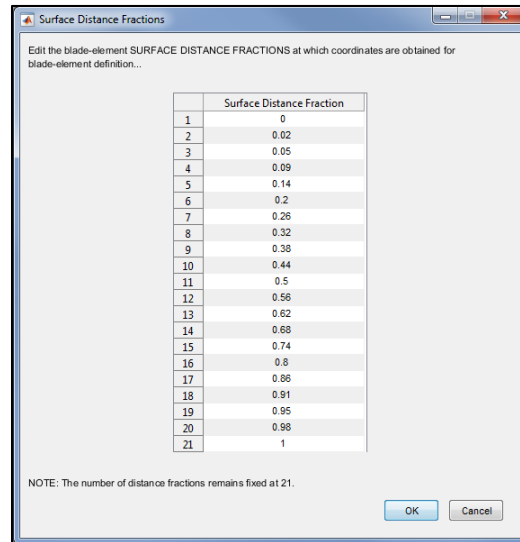


Figure 6.15 Distance fraction definition window.

6.7. Design Input Tab (Flowpath Control)

Selecting the *Design* button at the top of the input window toggles the second user input tab. This tab is split into two sections: The first enables the user to edit the geometry of the annulus boundary, and the second section offers the user control over a wide variety of blade design options. By default, the flowpath control tab is displayed when the *Design* togglebutton is selected. This tab is shown in Figure 6.16. The blade design section may be displayed using the navigation fields located at the top of the input window. These fields are discussed in section 6.10.

Select Input Type ... General **Design** Miscellaneous

Flowpath PREV. NEXT insert Delete Reset

Flowpath Boundary Coordinates

Specify the AXIAL and RADIAL coordinates (in Inches) of the flowpath TIP and HUB boundaries in the tables below. A MINIMUM of 4 and a MAXIMUM of 40 coordinate pairs can be specified per table.

TIP Boundary			HUB Boundary		
	Axial, X	Radial, R		Axial, X	Radial, R
1	-3.9684	10	1	-3.9684	5
2	0	10	2	0	5
3	1.9842	9.7676	3	1.9842	5.3499
4	3.6555	9.7676	4	3.6555	5.6303
5	5.5859	9.6875	5	5.5859	5.9707
6	7.1786	9.6875	6	7.1786	6.2068
7	9.1492	9.6875	7	9.1492	6.5122
8	10.8167	9.6875	8	10.8167	6.8062
9	12.8586	9.6611	9	12.8586	7.1663
10	14.5316	9.6611	10	14.5316	7.3662
11	16.7085	9.6611	11	16.7085	7.7232
12	18.5516	9.6611	12	18.5516	7.7460
13	20.3947	9.6611	13	20.3947	7.7460

Figure 6.16 Flowpath control tab.

6.7.1. Flowpath Coordinates

The two tables shown in Figure 6.16 enable the user to manually edit the coordinates (in inches) of the tip and hub annulus boundaries. If the simulation is initialized from the Meanline application, these tables are populated automatically using the solved boundary coordinates. If the Throughflow simulation is executed from a standalone level, these fields must be defined by the user as part of the minimum input requirements. A maximum of 40 axial and radial coordinate pairs may be used to define each boundary. Blank rows may be added to the end of each table using the *Insert* command shown in Figure 6.16. Trailing rows may also be deleted using the corresponding *Delete* button. The remaining function, *Clear*, resets all entries in the table.

6.7.2. Import Boundary

The functions discussed in section 6.7.1 provide the user with basic editing controls of the boundary axial and radial coordinates. Alternatively, the user may define the flowpath by importing a list of coordinates using the *Import Boundary* function located at the bottom of Figure 6.16. When selected, a system input window similar to the one shown in Figure 5.3 is displayed which allows the user to locate the file containing the coordinate list. Note that the list of coordinates may only be imported as *.csv file, and must adhere to the format shown in Figure 6.17.

	A	B	C	D
1	XTIP	RTIP	XHUB	RHUB
2	-3.9684	10	-3.9684	5
3	0	10	0	5
4	1.9842	9.7676	1.9842	5.3499
5	3.6555	9.7676	3.6555	5.6303
6	5.5859	9.6875	5.5859	5.9707
7	7.1786	9.6875	7.1786	6.2068
8	9.1492	9.6875	9.1492	6.5122
9	10.817	9.6875	10.817	6.8062
10	12.859	9.6611	12.859	7.1663
11	14.532	9.6611	14.532	7.3662
12	16.709	9.6611	16.709	7.7232
13	18.552	9.6611	18.552	7.746
14	20.395	9.6611	20.395	7.746
15				
16				

Figure 6.17 Imported boundary *.csv file format.

A header line must also be included at the top of the .csv file, but the exact text need not match the line shown in Figure 6.17. A maximum of 40 coordinate pairs may be specified per boundary (i.e. max 41 rows including the header line).

6.7.3. Preview Coords

The *Preview Coords* option located below the import button enables the user to plot the coordinates that are specified in the input tables. This feature provides a means of

previewing any changes made to the flowpath boundary before a solution is attempted. If a solution cannot be obtained, this feature additionally enables the user to troubleshoot the simulation by determining whether the flowpath coordinates are responsible for the problem. The preview window is shown in Figure 6.18 using the default 5-stage configuration from the Meanline simulation. The green lines represent the axial locations of the so-called *Free Stations* (discussed in section 6.9), and the black lines refer to the blade stacking axes (if any defined).

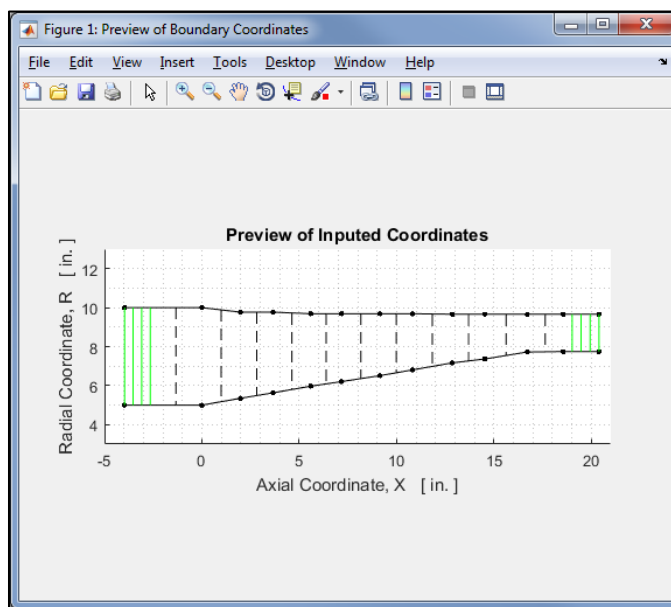


Figure 6.18 Preview coords window.

6.8. Blade Navigation Pane

The blade navigation pane enables the user to toggle between the flowpath control tab and the remaining blade row input tabs (described in section 6.10). The dropdown list at the left side of the pane provides a complete list of all stations in the compressor. Selecting a station from this list will display the blade parameter input window for the given blade row. The first option in this list opens the *Flowpath Control* tab that was

discussed in section 6.7. An expanded view of this list can be seen in Figure 6.19.

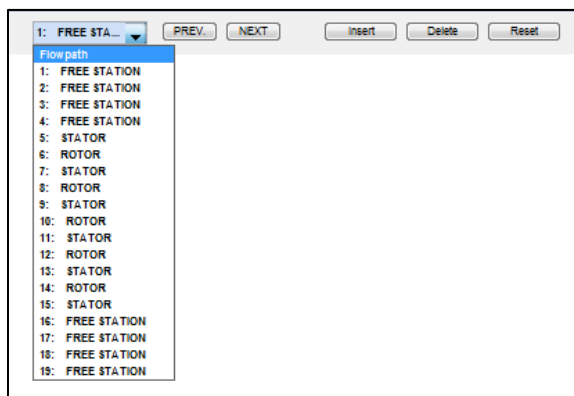


Figure 6.19 Blade navigation pane.

The remaining buttons in the navigation pane perform identical functions as those discussed in the Meanline application. Refer to section 5.10.2 for additional details.

6.9. Design Input Tab (Free Station Control)

In accordance with the streamline curvature discussion in section 2.5.1, the Throughflow solver produces the radial velocity distributions at axial stations located throughout the compressor. For blade rows, this corresponds with blade leading and trailing edge locations. However, the user has the ability to insert additional calculation stations, known as *Free Stations*, to further control the streamline flow parameters. Free stations act as empty placeholders in which certain flow features including blockage and mass bleed may be defined. They may be inserted in between each blade row if desired. In the very least, free stations must be placed at the inlet and exit of the compressor in order to fully define the inlet and exit flow conditions. This function is automatically performed if the solution is initialized from the Meanline application. It is recommended that at least four free stations be inserted at the inlet and exit locations of the compressor as illustrated by the green lines in Figure 6.18. This can be done using the *Insert* button

located in the blade navigation pane (refer to section 6.8).

All parameters corresponding to a given free station may be edited in the input fields shown in Figure 6.20. The input tab for a given free station may be selected using the controls in the blade navigation pane (located at the top of the input window). This may be done either by selecting the station from the dropdown list, or by toggling between stations with the *PREV* and *NEXT* buttons.

The screenshot shows a software interface for configuring a free station. The window title is "Select input Type ...". It has three tabs: "General", "Design" (which is active), and "Miscellaneous". At the top of the "Design" tab, there is a dropdown menu showing "1: FREE STA..." and buttons for "PREV.", "NEXT", "Insert", "Delete", and "Reset". The main content area is organized into four sections:

- Station Details:** Contains three input fields: "Global Index" with the value "1", "Station Type" with the value "Free Station", and "Station ID" with the value "F1".
- Axial Location of Free Station:** Contains two input fields: "Tip Coordinate" with the value "-3.9684" and unit "in.", and "Hub Coordinate" with the value "-3.9684" and unit "in."
- Blockage Factors:** Contains two input fields: "Tip Blockage" with the value "0" and a dropdown menu set to "Fraction of A...", and "Hub Blockage" with the value "0" and a dropdown menu set to "Fraction of A...".
- Mass Bleed Factor:** Contains one input field: "Mass Bleed" with the value "0" and a dropdown menu set to "Frac. Station Flow".

Figure 6.20 Free station input tab.

6.9.1. Station details

The first section of the free station input tab (and all input tabs for that matter) contains specific details regarding the station that is selected by the user. The first field, *Global Index*, indicates the global position of the station within the compressor. The global index begins counting from the first calculation station (whether a free station,

rotor, or stator). The next field, *Station Type*, indicates the type of station that is selected. Either *FREE STATION*, *ROTOR*, or *STATOR* is displayed. The remaining field, *Station ID*, displays the station type (*F* for free station, *R* for rotor, or *S* for stator), as well as its global position relative to all similar station types. For example, the third free station in the compressor would incorporate a station ID of *F3*, regardless of the presence of upstream rotor or stator blade stations. The three station details fields are shown for reference in Figure 6.21.

Station Details	
Global Index:	<input type="text" value="1"/>
Station Type:	<input type="text" value="Free Station"/>
Station ID:	<input type="text" value="F1"/>

Figure 6.21 Station details fields.

6.9.2. Axial Location of Free Station

The next set of input fields provide the user with control over the axial location of the selected free station. The first field shown in Figure 6.22 defines the axial coordinate at the tip of the free station. The second field defines the axial coordinate at the root of the free station. Both coordinates are specified in inches, and with respect to the global coordinate system of the compressor.

Axial Location of Free Station	
Tip Coordinate:	<input type="text" value="-3.9684"/> in.
Hub Coordinate:	<input type="text" value="-3.9684"/> in.

Figure 6.22 Free station axial location definition.

The split between the two values allows the user to define a slanted free station. In some cases, this may be required to define the flow field in a curved inlet or exit duct such as the one shown in Figure 6.23.

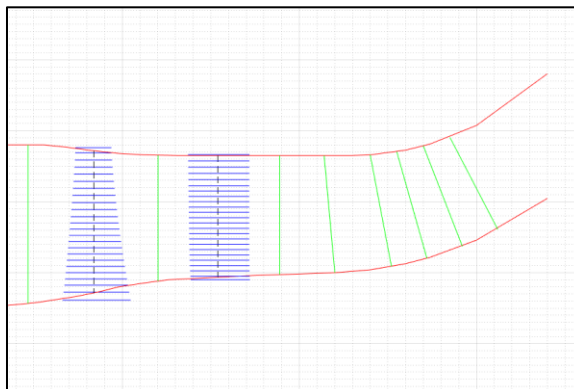


Figure 6.23 Example exit duct defined using slanted free stations.

6.9.3. Blockage Factors

Endwall blockage factors may be specified at tip and hub locations in the fields shown in Figure 6.24. By default, blockage areas are defined as the fraction of total annulus area at a particular calculation station (e.g. $0.01 \approx 1\%$ of annulus area). Alternatively, the blockage area may be specified in inches by selecting the appropriate option from the dropdown list. These input fields are automatically updated if blockage factors are selected to be carried over from the Meanline application (refer to section 5.12). They are not, however, required as part as the minimum input requirements.

Figure 6.24 Blockage factor definition fields.

6.9.4. Mass Bleed Factor

As part of the benefits of running a Throughflow simulation, a mass flow bleed factor may be applied to any given point in the compressor's flow path. This value is

specified as a fraction of the total mass flow passing through the given calculation station. A numerical value between 0 and 1.0 may be entered into the input field shown in Figure 6.25.

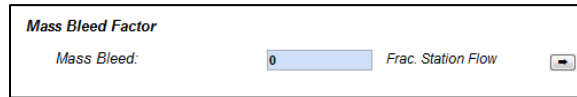
The image shows a software interface element titled "Mass Bleed Factor". It contains a label "Mass Bleed:" followed by a text input field containing the number "0". To the right of the input field is the text "Frac. Station Flow" and a small square button with a right-pointing arrow.

Figure 6.25 Mass bleed factor definition.

6.10. Design Input Tab (Blade Control)

Selecting a specific blade row station in the navigation pane will display the input fields for each individual blade row in the compressor. This can be done either by pressing the *NEXT* button, or by selecting a station from the dropdown list as shown in Figure 6.19. Depending on the type of station that is selected, the blade design input fields for an individual rotor or a stator will be displayed. Slight differences exist between the two input tabs depending on the type of station that is selected. The input tab for a rotor is shown for reference in Figure 6.26.

Figure 6.26 Rotor station input tab.

6.10.1. Station Details

The *Station Details* section located at the top of Figure 6.26 display the details of the blade row that is selected by the user. These fields are populated in the same way as described for Free Stations (refer to section 6.9.1 for additional details).

6.10.2. Blade Design Options

This section provides the user with the option to either design and stack the coordinates of each blade row (*3D Blade Design* option), or to compute the aerodynamic solution in the meridional plane only (*2D Analysis Only* option). In other words, the first option refers to the *inverse* (design) approach described in the theory section of this report (section 2.5), while the latter option corresponds to the *direct* (analysis) approach.

If the *3D Blade Design* option is selected, the program calculates the aerodynamic solution in the meridional plane of the compressor, and then produces stacked airfoil geometry using the radial solutions at the inlet and exit of each blade row. Blade parameters related to airfoil thickness, camber definition, and chord distributions, are defined by the user (refer to section 6.10.18). Blade metal angles, on the other hand, are calculated by the program at each streamline using internal correlations for incidence and deviation treatment. The net result produces stacked blade row geometry similar to that shown in Figure 6.27.

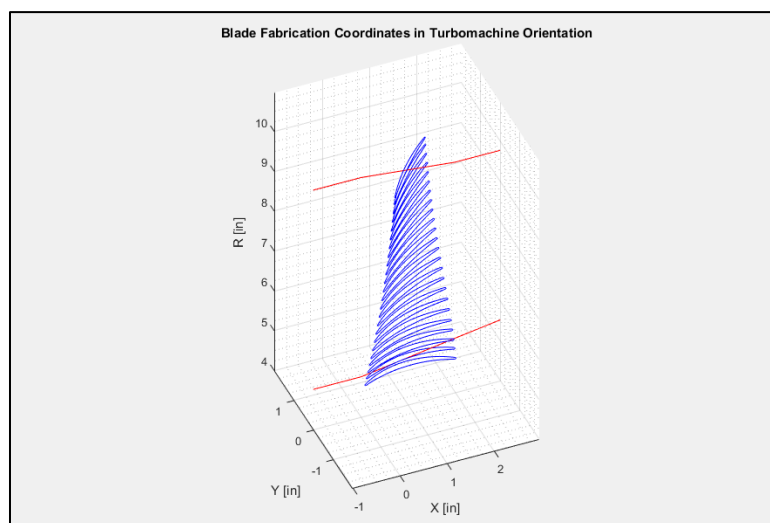


Figure 6.27 Stacked rotor 1 blade geometry.

The second option, *2D Analysis Only*, may be selected if the user wishes to neglect the blade design features of the program and only obtain the Throughflow solution of the compressor. This option is demonstrated in Figure 6.28.

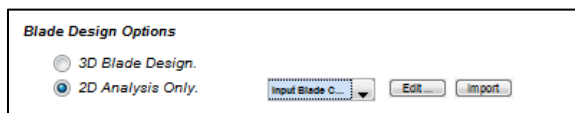


Figure 6.28 Blade design/analysis options.

Selecting the *2D Analysis* option de-activates all design-related fields in the

station input tab, and the program instead computes the aerodynamic solution based on fixed meridional blade coordinates. Blade coordinates may be specified in one of two ways. First, the user may edit the coordinates of the leading and trailing edges for each blade row manually by selecting the *Edit* option shown in Figure 6.28. This displays the input window shown in Figure 6.29. Note that five points must be used to specify the leading and trailing edge coordinates of each blade row.

	X LE	R LE	X TE	R TE
1	0.1927	5.0273	1.6949	9.7142
2	0.2481	6.3907	1.7386	8.7396
3	0.2914	7.4587	1.7934	7.5164
4	0.3455	8.7912	1.8371	6.5441
5	0.3896	9.8766	1.8914	5.3330

Figure 6.29 Meridional blade coordinate definition window.

Alternatively, the meridional blade coordinates may be imported as a **.csv* file using the *Import* button seen in Figure 6.28. When selected, a system input window is displayed which allows the user to locate the file containing the list of blade edge coordinates. The content of the **.csv* file must follow the format shown in Figure 6.30.

	A	B	C	D
1	X LE	R LE	X TE	R TE
2	0.19274	5.0273	1.6949	9.7142
3	0.24809	6.3907	1.7386	8.7396
4	0.29144	7.4587	1.7934	7.5164
5	0.34553	8.7912	1.8371	6.5441
6	0.38958	9.8766	1.8914	5.333
7				
8				

Figure 6.30 Imported blade **.csv* file format.

A header line must be included at the top of the *.csv* file, but the exact text need

not match the line shown in Figure 6.30. Note that only five coordinate pairs must be defined per blade edge. All coordinates must be specified in inches, and in the global reference frame of the compressor.

The program additionally offers the user option to calculate the blade edge locations automatically instead of inputting them manually. This option may be selected from the dropdown list shown in Figure 6.28. When selected, the program estimates the coordinates of the leading and trailing blade edges based on the location of the stacking axis. This feature may be used if specific leading and trailing edge coordinates are not known.

When the program is executed in the analysis mode, the stacked 3D blade coordinates shown in Figure 6.27 are not computed, and therefore are not displayed in the post-processing window. The compressor geometry may instead be viewed in the meridional view as shown in Figure 6.31.

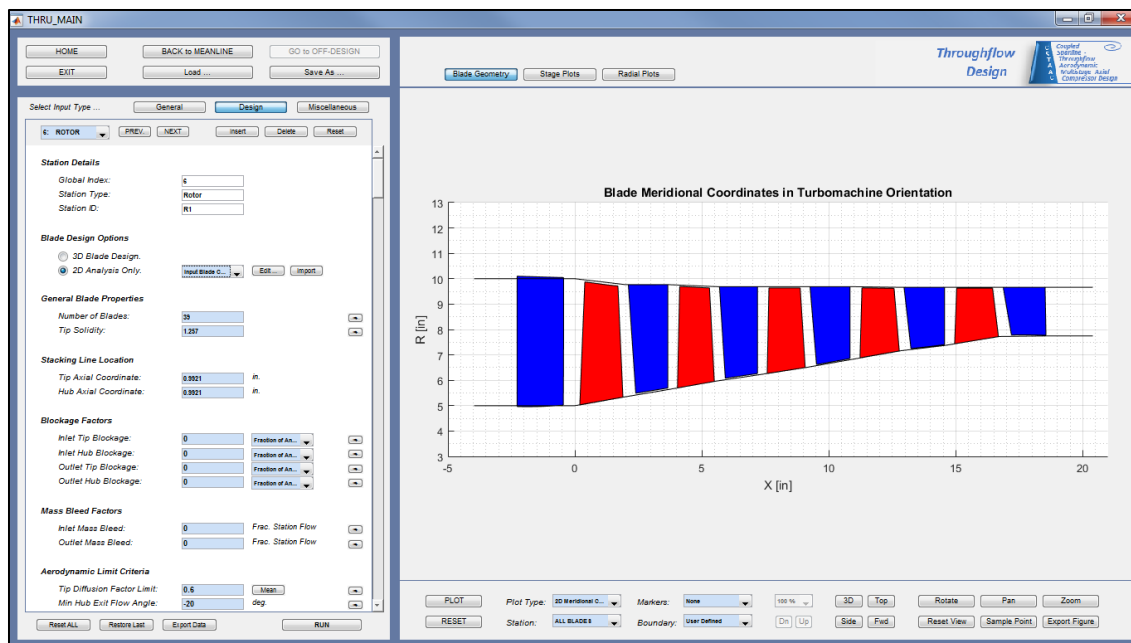


Figure 6.31 Blade meridional view for analysis mode.

It should be noted that the program might sometimes not be able to achieve a converged solution if all blade stations are set to the analysis mode. This problem may be avoided by leaving one blade (recommended IGV) in the design mode to ensure that a converged solution is obtained.

6.10.3. General Blade Properties

General properties including the number of blades and tip solidity must be specified for each blade row as part of the program's minimum input requirements. These values may be defined in the input fields shown in Figure 6.32. If the simulation is initialized from the Meanline application, these fields are populated automatically using the solved parameters. The solidity is defined at the tip location of each blade, regardless of being a rotor or a stator. The equation for solidity is given by equation 1.8.

General Blade Properties	
Number of Blades:	39
Tip Solidity:	1.257

Figure 6.32 General blade property fields.

6.10.4. Stacking Line Location

The next set of input fields provide the user with control over the axial coordinates of the blade stacking axis. The axis tip and hub location may be edited in the input fields shown in Figure 6.33. The effect of altering the stacking axis coordinates are demonstrated in Figure 6.34 and Figure 6.35.

Stacking Line Location	
Tip Axial Coordinate:	-1.3275 in.
Hub Axial Coordinate:	-1.3275 in.

Figure 6.33 Stacking axis coordinate definition.

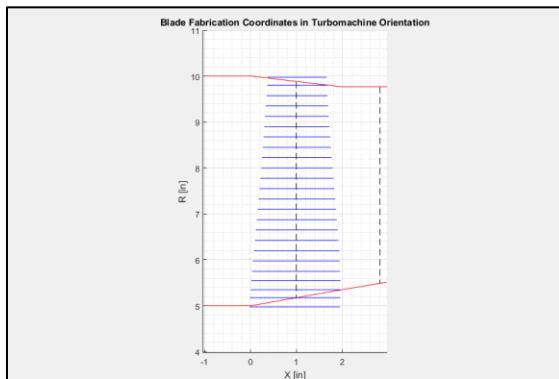


Figure 6.34 Stacking axis definition of rotor 1.

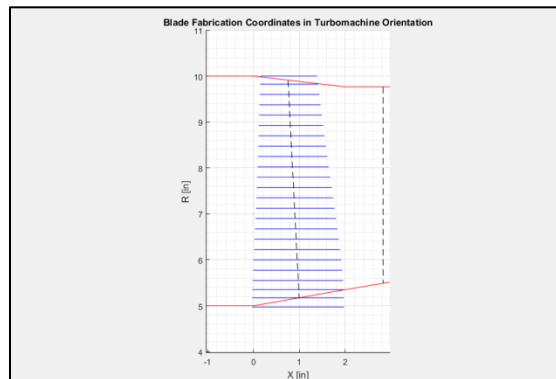


Figure 6.35 Stacking axis re-defined for rotor 1.

6.10.5. Blockage Factors

Endwall blockage factors at each blade row are defined in the same way as for free stations. The only difference in this case is that values may be specified at both the leading and trailing edge locations of the blade row. Additional details regarding blockage factor definition may be found in section 6.9.3. The blade row input fields are shown in Figure 6.36 for reference.

Blockage Factors			
Inlet Tip Blockage:	<input type="text" value="0"/>	Fraction of An...	<input type="button" value="▶"/>
Inlet Hub Blockage:	<input type="text" value="0"/>	Fraction of An...	<input type="button" value="▶"/>
Outlet Tip Blockage:	<input type="text" value="0"/>	Fraction of An...	<input type="button" value="▶"/>
Outlet Hub Blockage:	<input type="text" value="0"/>	Fraction of An...	<input type="button" value="▶"/>

Figure 6.36 Blade row blockage factor definition.

6.10.6. Mass Bleed Factors

Mass bleed factors are again specified in the same way as for free stations (refer to section 6.9.4 for additional details). Mass bleed air fractions may be defined at the leading and trailing edge location of each blade row if desired. By default, these fields are set to zero (no bleed air). The input fields for both rotor and stator blade rows are shown in Figure 6.37.

Figure 6.37 Blade row mass bleed factor definition.

6.10.7. Aerodynamic Limit Criteria

The input fields under the *Aerodynamic Limit Criteria* indirectly control the stage energy addition conditions for each blade row in the compressor. When executed in the design mode, the program will reduce the energy of a given stage in an attempt to satisfy these conditions. If aerodynamic limits have not been reached in other stages of the compressor, the program will attempt to recover the energy loss of the limiting stage, and apply it to a stage where the limits have not yet been achieved. If all stages have reached their specified aerodynamic limits, the program will reduce the overall pressure ratio until the criteria are satisfied.

The first input field defines the maximum diffusion factor for the blade. For rotors, this limit applies at the blade's tip location as shown in Figure 6.38. For stators, it is applied at the blade hub as demonstrated by Figure 6.39. By default, the diffusion factor limit is set to 0.6. The diffusion factor value that is solved by the Meanline program may also be applied if desired. If not previously transferred during the initialization phase (see section 5.12), it may be manually recalled using the *Mean* button located to the right of the input field.

Figure 6.38 Aerodynamic limits for rotor blades.

Figure 6.39 Aerodynamic limits for stator blades.

The input field below the diffusion factor defines one of two limit parameters at the blade's hub location. For rotors, the value specified by the user refers to the minimum allowable relative flow angle (in degrees) exiting the hub (as shown in Figure 6.38). For stators, it is the maximum allowable Mach number entering the blade at the hub (Figure 6.39). These parameters are defaulted to be -20 degrees and 0.85 respectively. It should be noted that these values are limits used by the program when computing the Throughflow solution. They do not describe the exact values to be expected at the corresponding blade locations.

The last input field refers to the minimum choke margin of a given blade row. Specifically, the value entered by the user defines the minimum desired value of $[(A/A^*) - 1.0]$, where A/A^* is the ratio of local streamtube area in the channel to the area required to choke the blade passage ($M_{rel} = 1.0$). If a value greater than zero is specified, the program increases the incidence angle of the blade up to a maximum of +2.0 degrees (with respect to the leading edge of the suction surface) in an attempt to apply the specified choke margin at the entrance of the channel. If the dropdown list is set to *None* (default), then no adjustments to this effect will be made by the program. The application of the choke margin is demonstrated in Figure 6.40 and Figure 6.41.

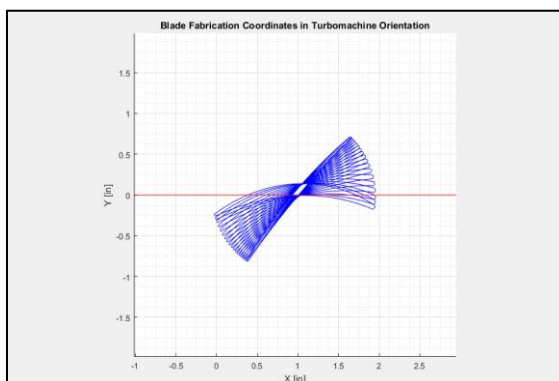


Figure 6.40 Rotor 1 profile with the default choke margin (i.e. none specified).

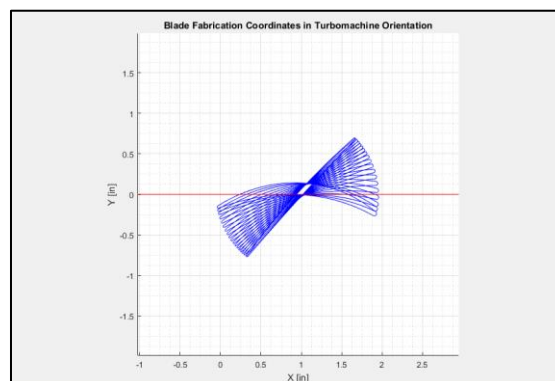


Figure 6.41 Rotor 1 profile with a choke margin of 0.2.

6.10.8. Profile Loss

This section defines the method in which the total pressure at the exit of each blade row is calculated. One of three options may be selected as shown in Figure 6.42 and Figure 6.43. If the first option is selected, *Use Internal Correlation*, the program calculates the magnitude of total pressure using empirical correlations based on the work of Johnsen & Bullock (1965). The shape of the profile at the blade exit, however, must be specified by the user (refer to section 6.10.9).

Figure 6.42 Profile loss definition (no loss sets specified).

Figure 6.43 Profile loss definition (when loss sets specified).

The next option, *Input Total Pressure*, enables the user to manually define the total pressure profile in its entirety. The profile may be defined either as a uniform distribution or as a fifth-order polynomial function. Both options are available from the dropdown list shown in Figure 6.42. If a uniform distribution is specified, the magnitude of total pressure is input by the user in the edit box located to the right of the dropdown list. This produces a profile like the one shown in Figure 6.44.

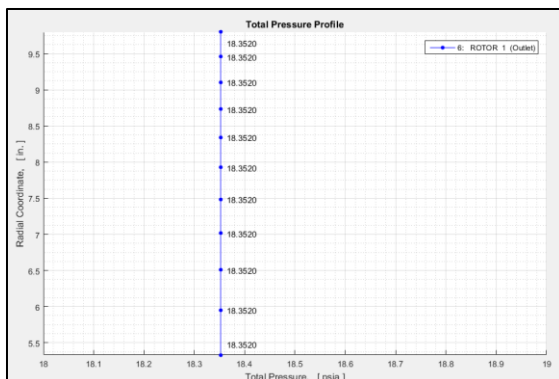


Figure 6.44 Constant total pressure profile at Rotor 1 exit

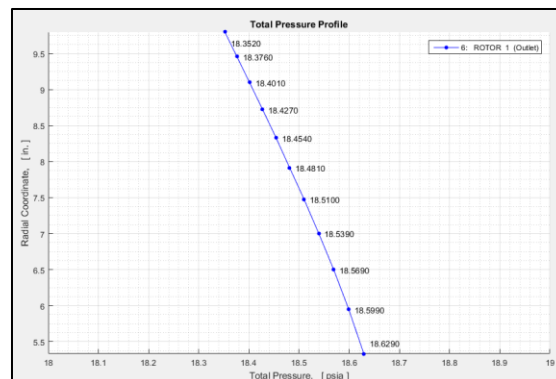


Figure 6.45 Polynomial total pressure profile at Rotor 1 exit

If the *Polynomial* option is selected from the dropdown list, a total pressure profile like the one shown in Figure 6.45 may be specified. All parameters required to define the function may be manually edited by selecting the *Edit* button that appears next to the dropdown list. Once pressed, the input window shown in Figure 6.46 is displayed. The polynomial function used to define the blade exit total pressure profile is shown at the top of the input window for reference. All corresponding coefficients refer to the profile illustrated in Figure 6.45.

Exit Total Pressure Profile

Specify the coefficients for the polynomial equation to define the TOTAL PRESSURE PROFILE (in psia) at the blade row EXIT.

$$P_{\alpha, \text{exit}}(R) = P_{\alpha, \text{tip}} [1.0 + A R + B R^2 + C R^3 + D R^4 + E R^5]$$

Where,

$P_{\alpha, \text{tip}} =$ [psia] is the TOTAL PRESSURE at the TIP of the blade row EXIT

And,

A = B = C = D = E =

$R = (r_1 - r) / (r_1 - r_h)$ is the fraction of passage height at the blade row EXIT.

OK Cancel

Figure 6.46 Exit total pressure profile definition.

A third option, *Use Meanline*, is also available from the dropdown list. This option enables the user to manually apply the total pressure profile that was previously solved by the Meanline application. Selecting this option automatically populates all input fields shown in Figure 6.46 with curve-fit coefficients obtained from the Meanline solution.

It is important to note that if the pressure profile is manually defined by the user, the corresponding total temperature profile must be specified as well (discussed in section 6.10.9).

The remaining profile loss option, *Use Loss Set*, becomes available only if the user has manually input a loss parameter table (refer to section 6.6.7). The desired loss set to be applied to the blade row may be selected from the dropdown list shown in Figure 6.43. With this option, the pressure magnitude at the exit of the blade row is computed using the loss parameter data from the tables. The profile shape, however, must again be defined by the user (refer to section 6.10.9 for additional details).

6.10.9. Blade Exit Profile

The input fields under the *Blade Exit Profile* section provide additional control over the exit profile behind each blade row. In most cases, this section is used in conjunction with the Profile Loss input described in section 6.10.8. The availability of options in this section relies on the type of blade that is selected by the user. For rotor blades, two out of the three options become available as shown in Figure 6.47. For stators, only the last option is shown (Figure 6.48).

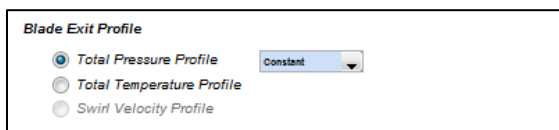


Figure 6.47 Rotor exit profile definition.



Figure 6.48 Stator exit profile definition.

When an internal correlation is used to compute the profile loss magnitude of a given rotor blade (refer to section 6.10.8), the two input fields shown in Figure 6.47 enable the user to define the corresponding profile shape at the exit of the blade row. Either the total pressure profile or the total temperature profile shape may be defined. By default, a uniform total pressure distribution similar to the one shown in Figure 6.44 is applied to all blade row exits. The profile may also be defined as fifth-order polynomial by selecting the *Polynomial* option from the dropdown list. When selected, the input

window shown in Figure 6.49 is displayed which allows the user to edit the coefficients of the polynomial function. Note that the coefficients specified in the window control only the shape of the profile. The magnitudes are calculated by the program using internal loss correlations. Selecting the *Total Temperature Profile* option performs a similar function, but the total temperature distribution is specified instead.

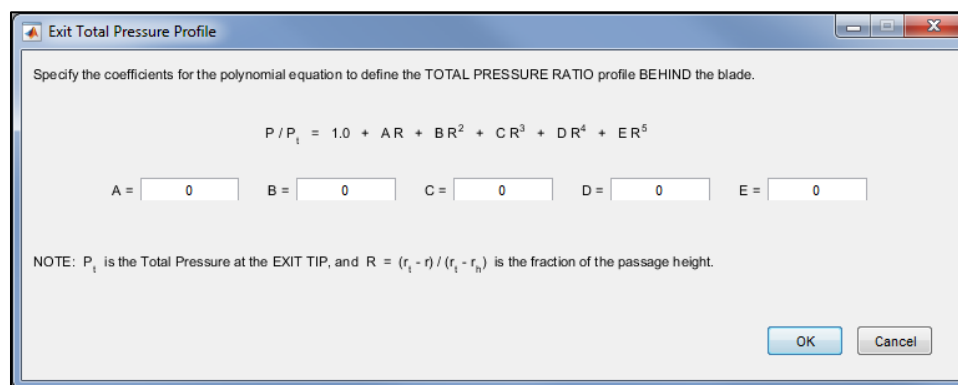


Figure 6.49 Exit total pressure profile definition for rotors (when using an internal loss correlation)

The third option, *Swirl Velocity Profile*, enables the user to define an exact swirl distribution (magnitude and profile shape) at the exit of a given blade row. This feature is only available for stator blades as shown in Figure 6.48. The corresponding options that are available from the dropdown list allow the user to neglect the swirl contribution, specify a uniform swirl distribution, or specify the swirl profile as a fifth-order polynomial. When the latter option is selected, the input window shown in Figure 6.50 is displayed. From here, the coefficients of the polynomial function (shown at the top of the figure) may be edited to produce a desired swirl velocity distribution.

A fourth option may also be selected from either of the dropdown lists shown in Figure 6.47 and Figure 6.48. This option, labeled *Use Meanline*, enables the user to manually apply the total pressure and temperature profiles (for rotors) or the swirl velocity profile (for stators) that solved by the Meanline application (if available).

Figure 6.50 Exit swirl profile definition for stator blades.

6.10.10. Stage Energy Addition

The input field shown in Figure 6.51 defines the fraction of the cumulative energy addition applied to a given rotor compared to the overall energy added to the compressor. This feature is only available when an internal correlation is used to compute the profile loss of a given rotor blade (refer to section 6.10.8). The energy fraction of the first rotor must be greater than zero, and progressively increase through successive stages. The last rotor blade in the compressor must be assigned an energy addition fraction of 1.0.

Figure 6.51 Rotor energy addition definition.

Figure 6.52 Rotor tip total temperature definition.

When a total temperature profile is used to define the blade exit profile (refer to section 6.10.8), the total temperature at the blade's trailing edge tip location is specified by the user instead of an energy fraction. When selected, the input field shown in Figure 6.52 is appropriately displayed. The inputted temperature value is converted to an energy fraction by the program during internal computations.

6.10.11. Stacking Line Tilt Angle

The tilt angle of the blade stacking axis may also be adjusted by the user. The tilt angle is referenced in the circumferential direction (r - θ plane), and is positive in the direction of rotation. A linear tilt angle may be applied by selecting the *Linear* option from the dropdown list, and specifying a value for the tip location as demonstrated by Figure 6.53 and Figure 6.55. Alternatively, a curved tilt distribution may be applied by selecting the *Polynomial* option from the dropdown list, and editing the hub angle as shown in Figure 6.54 and Figure 6.56. Any combination of the two values may also be specified if desired.

Figure 6.53 Tip tilt angle definition.

Figure 6.54 Hub tilt angle definition.

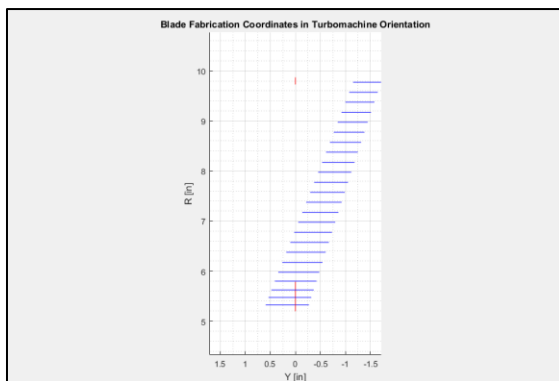


Figure 6.55 Linearly tilted axis resulting from 20° tip angle definition.

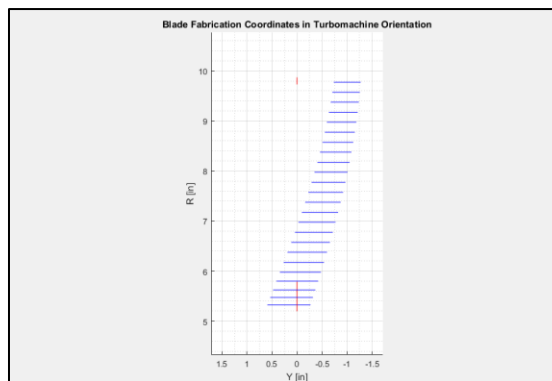


Figure 6.56 Curved axis resulting from 20° hub angle definition.

6.10.12. Material Density

The next input field allows the user to specify the material density (in lb/in^3) of a given rotor blade. If a positive nonzero value is entered into the field shown in Figure 6.57, the program will attempt to stack the blade geometry in a way such that the

resulting gas bending moments are balanced with the centrifugal forces associated with the blade's material density. This is performed by adjusting the tip location of the stacking axis accordingly (note that the hub location remains fixed). No adjustments are made if the *Neglect* option is selected from the dropdown list (default).

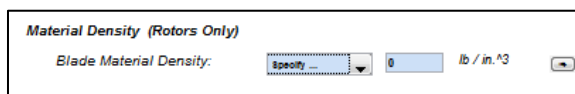


Figure 6.57 Rotor blade material density definition.

6.10.13. Incidence Angle Treatment

The *Incidence Angle Treatment* section enables the user to select the method that the program implements to calculate a blade's incidence angle distribution. The user may select one of four options shown in Figure 6.58.

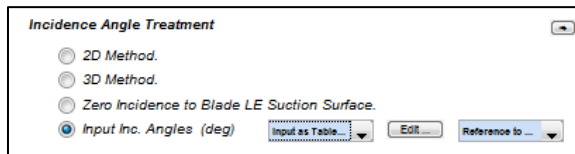


Figure 6.58 Incidence angle treatment options.

If either of the first two options shown in Figure 6.58 are selected, the program calculates the incidence angle distributions for all blade rows using empirical correlations. Blade metal angles are then determined using the flow angles from the Throughflow solution and the incidence angles that are predicted by the internal models. These correlations are derived from experimental work carried out for double circular arc and NACA 65-series airfoils. The *2D* option shown in Figure 6.58 is based on experimental data obtained for low-speed two-dimensional cascades, while the *3D* option correlates subsonic and transonic data obtained using a single-stage annular cascade test

installation. A complete description these correlations, as well as the methods and procedures used to derive them is given by Johnsen & Bullock (1965). Physical differences that may be observed between the two options are usually found to be minor as illustrated by Figure 6.59 and Figure 6.60.

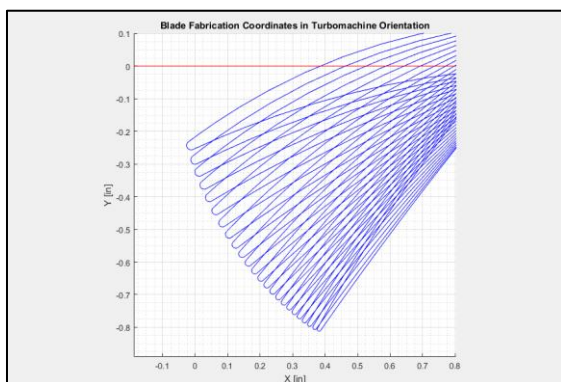


Figure 6.59 Rotor 1 LE geometry using 2D incidence treatment

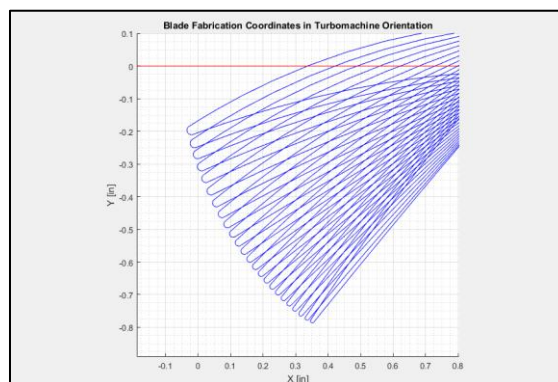


Figure 6.60 Rotor 1 LE geometry using 3D incidence treatment

The remaining options shown in Figure 6.58 enable the user to specify the incidence angles manually. The third option in the list, when selected, applies zero incidence with respect to the suction surface of the blade at the leading edge. The last option, *Input Inc. Angles*, allows the user to edit the incidence angle for each individual streamline manually. Custom angles may be specified by clicking the *Edit* button next to the dropdown list, and entering in the data in the corresponding table shown in Figure 6.61. The second dropdown menu associated with this option (to the right of the *Edit* button) refers to the reference location of the specified values. Angles may either be referenced to the leading edge centerline of the blade (default), or the leading suction surface of the blade.

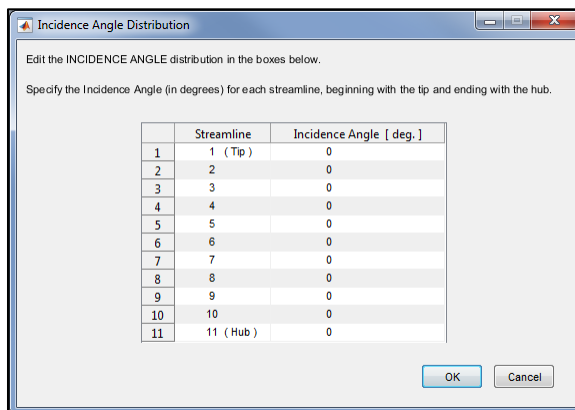


Figure 6.61 Manual incidence definition.

6.10.14. Deviation Angle Treatment

Similar to the incidence angle treatment options described in section 6.10.13, blade deviation angles may also be calculated by the program using empirical models. All such options are shown in Figure 6.62.

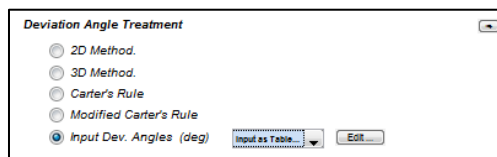


Figure 6.62 Deviation angle treatment options.

As illustrated by Figure 6.62, the two and three-dimensional correlation models outlined by Johnsen & Bullock (1965) are again available for predicting trailing edge flow deviation. Blade metal angles are once again determined using the flow angles from the Throughflow solution and the deviation angles that are predicted by the internal models. The user may additionally select Carter's rule, as well as a modified form of Carter's rule, for predicting flow deviation. The first option, *Carter's Rule*, refers to the two-dimensional model discussed in section 1.4.5, specifically equation 1.12. The *Modified* option indicates the use of Carter's rule with a modification for instances where

the front and rear segments of a blade element have different camber turning rates. Additional details regarding this model are given by Johnsen & Bullock (1965). A comparison between the deviation treatment using Carter's rule and the 3D option is shown in Figure 6.63 and Figure 6.64. The remaining option, *Input Dev. Angles*, enables the user to input custom deviation angles along the trailing edge of a given blade. This is done through a process similar to that discussed in 6.10.13.

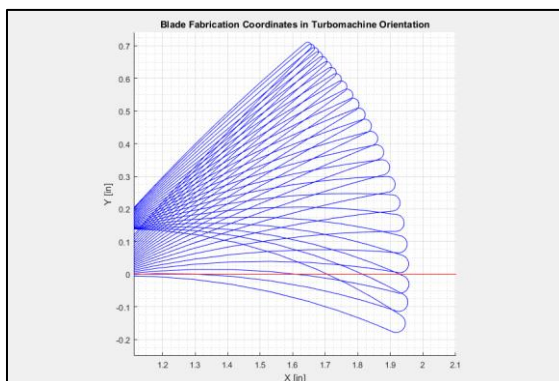


Figure 6.63 Rotor 1 TE geometry using Carter's rule.

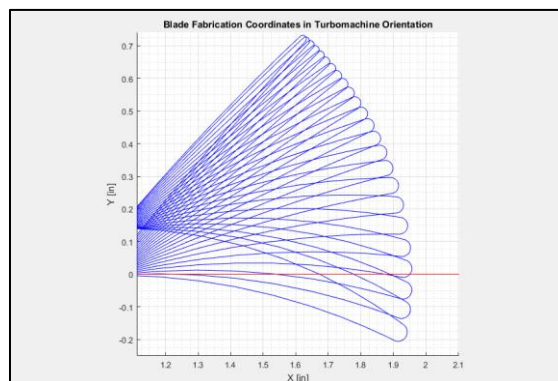


Figure 6.64 Rotor 1 TE geometry using 3D treatment.

6.10.15. Blade Element Shapes

The next input field enables the user to define the type of airfoil geometry that is to be used for blade design purposes. For clarification, all airfoil design references discussed herein refer to the nomenclature shown in Figure 6.65.

One of three options may be selected to define a given blade element shape. The first option, *Use Circular Arcs*, produces stacked airfoil geometry comprised of double-circular-arc elements. These shapes are applied to the pressure and suction surfaces of the airfoil, both forward and aft of the transition point displayed in Figure 6.65.

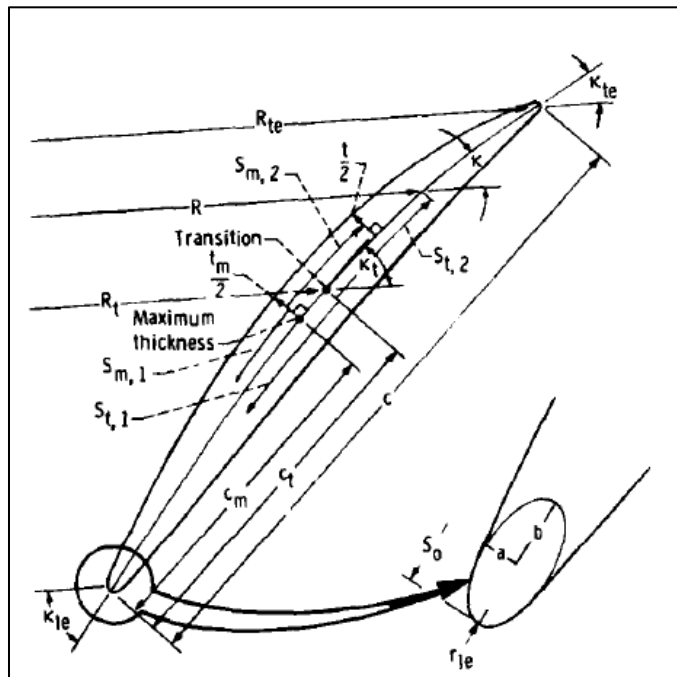


Figure 6.65 Airfoil reference and direction nomenclature (Crouse & Gorrell, 1981).

The second option, *Use Optimum Turning Rates*, is based on an empirical correlation to determine a more appropriate airfoil turning rate as the flow enters the transonic range. If selected, the turning rates of the front and rear blade segments (split at the transition point) will be calculated based on a function of inlet relative Mach number. Below a relative Mach number of 0.8, the program will apply circular-arc elements as previously explained. As the Mach number is increased, however, the ratio of the front segment turning rate to the rear segment turning rate $(dk/dS)_1/(dk/dS)_2$ is reduced. A limit of zero camber at the leading edge of the suction surface is attained as the flow approaches a relative Mach number of 1.6.



Figure 6.66 Blade element shape definition.

The remaining option, *Define Turning Rates*, allows the user to manually specify the turning rate ratio of the given blade segment. Custom values may be applied for each streamline by selecting the appropriate option from the dropdown list shown in Figure 6.66. The result displays the input window shown in Figure 6.67 where all values may be entered in tabular form.

Turning Rate Ratio Distribution

Edit the TURNING RATE RATIO distribution in the boxes below.

Specify the ratio of the Inlet Segment Turning Rate to the Outlet Segment Turning Rate (TR. Ratio = $(dk/ds)_1 / (dk/ds)_2$) for the blade element, beginning with the tip and ending with the hub.

	Streamline	Turning Rate Ratio	
1	1 (Tip)	0	
2	2	0	
3	3	0	
4	4	0	
5	5	0	
6	6	0	
7	7	0	
8	8	0	
9	9	0	
10	10	0	
11	11 (Hub)	0	

OK Cancel

Figure 6.67 Turning rate ratio definition.

6.10.16. Blade Segment Transition Point

The transition point, although briefly mentioned in section 6.10.15, is defined as the point which splits the forward and rear segments of a given blade element. This point is clearly marked in Figure 6.65. The user may control the location of this point by selecting one of the three options shown in Figure 6.68.

Blade Segment Transition Point

Set at Mid Chord.
 Set at PS Shock Impingement Point.
 Define Transition Point.

Input as Table... Edit...

Figure 6.68 Blade element transition point definition.

The first option, *Set at Mid Chord*, fixes the location of the transition point at the mid chord of the blade element. This is the default option. The second option, on the

other hand, positions the transition point on the suction surface of the blade at the normal shock impingement point from the leading edge of the adjacent blade. The last option enables the user to define the transition point location (as a fraction of chord length) for each streamline. Numerical values may be entered into the table shown in Figure 6.69. This table is displayed by selecting the *Edit* button located to the right of the dropdown list.

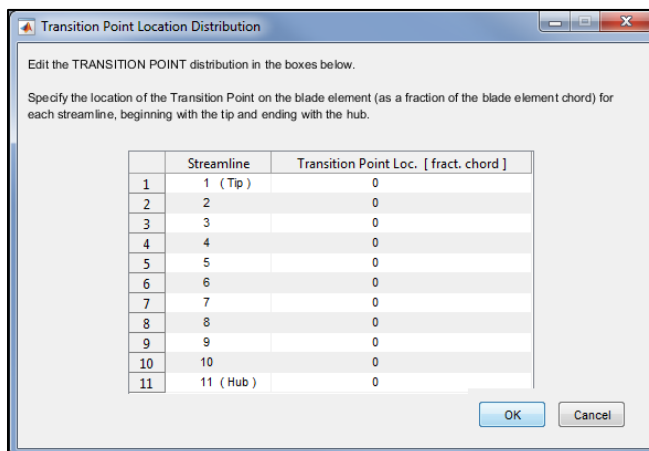


Figure 6.69 Transition point definition.

6.10.17. Maximum Thickness Point

The location of the maximum thickness point for a given blade element may also be assigned by selecting one of the two options shown in Figure 6.70. The physical location of this point with respect to the rest of the airfoil geometry is shown for reference in Figure 6.65.

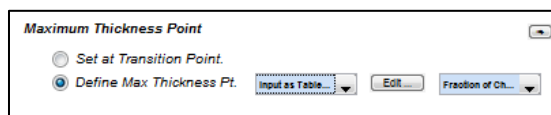


Figure 6.70 Maximum thickness point definition.

The first option (also the default), sets the location of the maximum thickness

point to coincide with the transition point discussed in 6.10.16. The second option, on the other hand, allows the user to define the maximum thickness location for each streamline along the span of the blade. This is done by clicking the *Edit* button shown in Figure 6.70. Values may be entered in the input window shown Figure 6.71. The dropdown list located to the right of the *Edit* button allows the user to reference the entered values either as the fraction of chord length behind the transition point (default), or as the fraction of chord from the leading edge of the blade.

Max Thickness Point Location Distribution

Edit the MAX THICKNESS POINT distribution in the boxes below.

Specify the location of the Maximum Thickness Point on the blade element (as a fraction of the blade element chord) for each streamline, beginning with the tip and ending with the hub.

	Streamline	Max Thickness Point Loc. [fract. chord]
1	1 (Tip)	0
2	2	0
3	3	0
4	4	0
5	5	0
6	6	0
7	7	0
8	8	0
9	9	0
10	10	0
11	11 (Hub)	0

OK Cancel

Figure 6.71 Max thickness point definition.

6.10.18. Basic Radial Geometry Parameters

The remaining input fields in the blade design tab refer to settings for controlling the physical geometry of the blade. These fields are split into two sections: Basic and Advanced geometry definition. The so-called *basic* fields are shown for reference in Figure 6.72. These fields are automatically populated by the program with default values, but may be updated by the user if desired. The *advanced* settings are discussed in the next section.

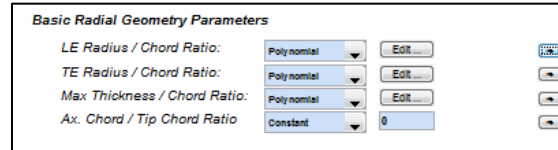


Figure 6.72 Basic geometry definition options.

With an exception of the turning rate, transition point, and maximum thickness location, blade geometry is defined using third-order polynomial functions with respect to non-dimensional passage height. The first two fields shown in Figure 6.72 refer to the radius-to-chord ratio at the leading and trailing edges of a given blade respectively. The function used to define each of these parameters is given as follows:

$$\frac{t}{c} = A + BR + CR^2 + DR^3 \quad (6.4)$$

In equation 6.4, R is the non-dimensional fraction of passage height given as:

$$R = \frac{r_t - r}{r_t - r_h} \quad (6.5)$$

In equation 6.5, r_t refers to the radius at the passage tip, and r_h refers to the radius at the hub. When defining the radius-to-chord ratio at the leading edge of a blade, the left side of equation 6.4 is interpreted as t_{LE} / c , and R refers to the passage height at the leading edge. For trailing edge definition, the left side of equation 6.4 is t_{TE} / c , and R is defined at the trailing edge. The coefficients A , B , C , and D in equation 6.4 may be specified by the user by clicking the *Edit* button located to the right of the corresponding dropdown menu shown in Figure 6.72. When selected, the input window shown in Figure 6.73 is displayed. The figure also shows the default coefficients applied for the leading edge polynomial. For the trailing edge, the default values become $A = 0.006$ and $B = 0.008$.

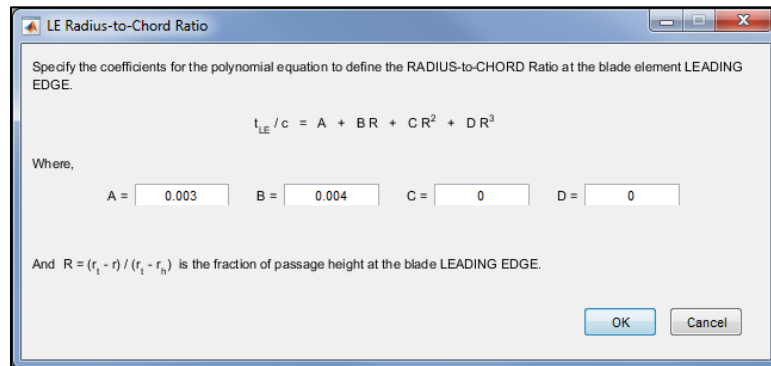


Figure 6.73 LE/TE radius-to-chord definition.

The maximum thickness-to-chord ratio of a given blade may also be defined by the user. This parameter is specified using the same third-order polynomial as the one defined by equation 6.4. In this case, however, the left side of the equation is interpreted as t_{max} / c , and the radius parameter, R , refers to the fraction of annulus height at the blade stacking line. The input window for the maximum thickness-to-chord ratio, along with its default coefficients, is shown in Figure 6.74.

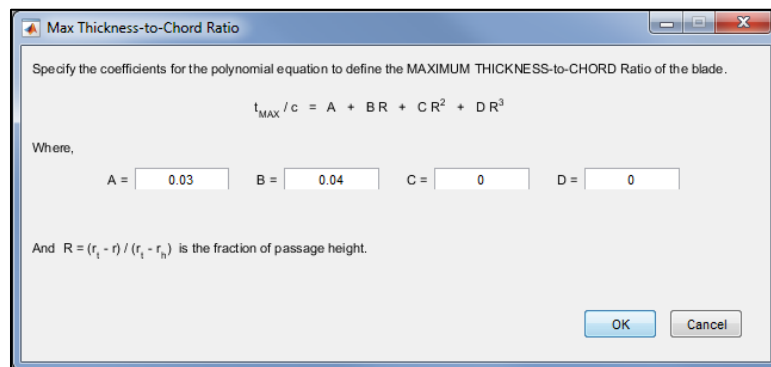


Figure 6.74 Max thickness-to-chord definition.

The remaining input field in the *basic* geometry definition section refers to the blade element axial chord-to-tip-chord ratio in the projected (meridional) plane. The polynomial function used to define this parameter is given as follows:

$$\frac{c}{c_{tip}} = 1 + AR + BR^2 + CR^3 \quad (6.6)$$

The radius parameter in equation 6.6, R , refers to the fraction of annulus height at the blade stacking axis. This variable is again modeled using the expression given in equation 6.5. The dropdown list corresponding to this field additionally provides the user with another option for defining the chord-to-tip-chord ratio of a given blade. The *Use Meanline* option enables the user to manually apply the axial chord distribution that was previously solved by the Meanline application. Selecting this option automatically populates the input fields shown in Figure 6.75 with curve-fit coefficients obtained from the Meanline solution (if available).

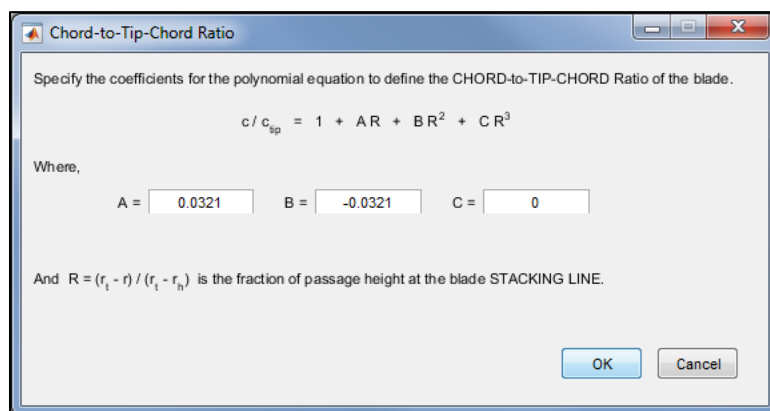


Figure 6.75 Axial chord-to-tip-chord ratio definition.

6.10.19. **Advanced Blade Definition Parameters**

The remaining input fields shown in Figure 6.76 provide the user with the ability to apply additional geometrical constraints to a given blade element. If desired, the centerline angle distribution, thickness distribution, and LE/TE eccentricity distributions may be specified using a combination of high-order polynomial functions. The application of these parameters in reference to a given airfoil profile can be observed in Figure 6.65.

Advanced Blade Definition Parameters

Toggle Advanced Options: Yes Normalize by...

FWD of Blade Segment Transition Point

Centerline Angle Distribution: Constant 1

Thickness Distribution: Constant 1

LE Eccentricity Distribution: Polynomial Edit...

AFT of Blade Segment Transition Point

Centerline Angle Distribution: Constant -1

Thickness Distribution: Constant -1

TE Eccentricity Distribution: Polynomial Edit...

Figure 6.76 Advanced geometry definition.

The advanced settings shown in Figure 6.76 are optional, and by default, the input fields are disabled. They may be enabled by selecting the appropriate option from the *Toggle Advanced Options* dropdown list. The menu to the right of the dropdown list enables the user to normalize all inputted values either to 1.0 (default), or by chord length.

The centerline angle distribution of a given blade element, both forward and aft of the transition point, is specified with the following polynomial function:

$$\kappa = \kappa_{tip} + AS + BS^2 + CS^3 + DS^4 \quad (6.7)$$

Unlike the basic geometry parameters discussed in section 6.10.18, coefficients A , B , C , and D are defined by another set of polynomial functions given by:

$$A = a_1 + a_2R + a_3R^2 + a_4R^3 \quad (6.8a)$$

$$B = b_1 + b_2R + b_3R^2 + b_4R^3 \quad (6.8b)$$

$$C = c_1 + c_2R + c_3R^2 + c_4R^3 \quad (6.8c)$$

$$D = d_1 + d_2R + d_3R^2 + d_4R^3 \quad (6.8d)$$

The radius parameters in equations 6.8a-6.8d are again defined by equation 6.5. If

editing the polynomial forward of the transition point, R refers to the passage height at the leading edge of the blade. If editing the rear segment of the blade, R is referenced to the trailing edge. All coefficients ($a_1\dots d_4$) may be edited by selecting the *Polynomial* option from the corresponding dropdown list shown in Figure 6.76. Numerical values may be entered into their respective fields through an input window similar to that shown in Figure 6.79. The effect of altering the centerline angle distribution is demonstrated by Figure 6.77 and Figure 6.78. These figures may be referenced to the default blade geometry shown in Figure 6.40.

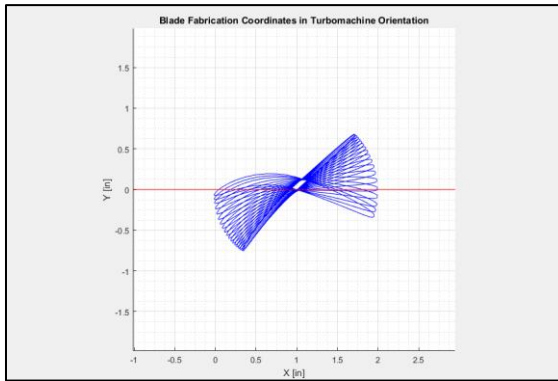


Figure 6.77 Rotor 1 geometry with $a_{I, FWD} = 20$ and $a_{I, AFT} = -1$.

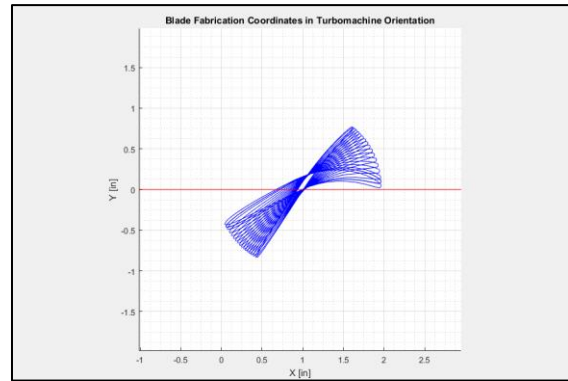


Figure 6.78 Rotor 1 geometry with $a_{I, FWD} = 1$ and $a_{I, AFT} = -20$.

The second set of input fields shown in Figure 6.76, labeled *Thickness Distribution*, allow the user to model the thickness distribution of a blade segment both forward and aft of the specified transition point. This is done in a similar manner as described for the centerline angle definition. The blade thickness distribution, both forward and aft of the transition point, is specified with the following polynomial function:

$$\frac{t}{2c} = \frac{t_m}{2c} + A \left(\sqrt{S_o - S} - \sqrt{S_o + \frac{S}{2\sqrt{S_o}}} \right) - BS^2 - CS^3 - DS^4 \quad (6.9)$$

In equation 6.9, coefficients, A , B , C , and D are defined by another set of polynomial functions identical to those defined by equations 6.8a-6.8d. The radius parameter, R , retains the same value as described by equation 6.5. All corresponding coefficients required to fully define the thickness polynomial may be edited by selecting the appropriate option from the dropdown list shown in Figure 6.76. The result of doing so displays the input window shown in Figure 6.79.

Figure 6.79 Thickness distribution definition.

The last geometrical parameter that the user may specify refers to the magnitude of eccentricity, e , at the leading and trailing edges of the blade. The polynomial functions used to define the ellipse ratio of semi-major to semi-minor axes are given by:

$$e = \frac{b}{a} - 1 = A + BR + CR^2 + DR^3 \quad (6.10)$$

In equation 6.10, the terms a and b refer to the lengths of the semi-minor and

semi-major axes of an ellipse respectively. Both quantities are illustrated for reference in Figure 6.65. The coefficients, A , B , C , and D may be edited by the user by selecting the appropriate option from the dropdown list shown in Figure 6.76. The effect of altering the eccentricity distribution at the leading edge of a blade is demonstrated by Figure 6.80 and Figure 6.81.

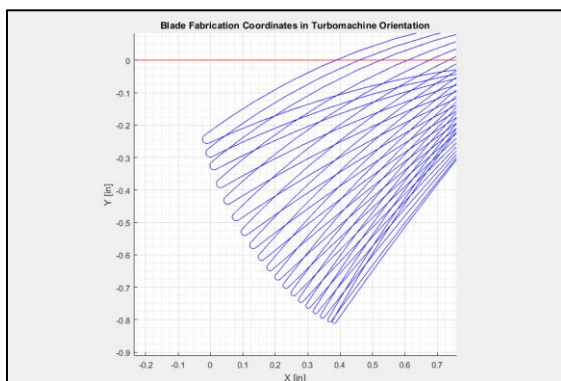


Figure 6.80 Rotor 1 default (circular) LE geometry ($e = 0$)

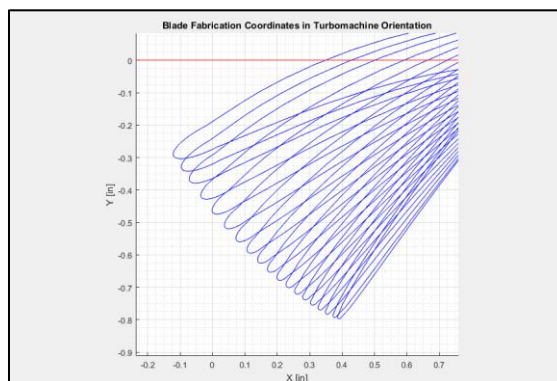


Figure 6.81 Rotor 1 LE geometry with $B_{FWD} = 2$ and $C_{FWD} = 0.5$.

6.11. Miscellaneous Input Tab

The *Miscellaneous* input tab provides the user with additional control over various Throughflow solver properties. These fields are shown in Figure 6.82 for reference. The first input field, *Output File Printout*, enables the user to control the density of information that is physically printed to the solution output file. The first checkbox is a flag for controlling the printout of small fabrication coordinates used for plotting the stacked blade geometry. When the checkbox is selected (default), the program will print very small coordinates as required. Otherwise, a 99.999 is printed instead. The next field in this field serves as a flag for controlling the printout of convergence information during the main program iteration loop. When selected, the program will print all convergence information to the solution output file. The result

produces a very dense output file and prolongs post-processing time. Under certain circumstances, however, this option may be beneficial for troubleshooting a simulation when convergence problems are experienced. By default, this field is left blank.

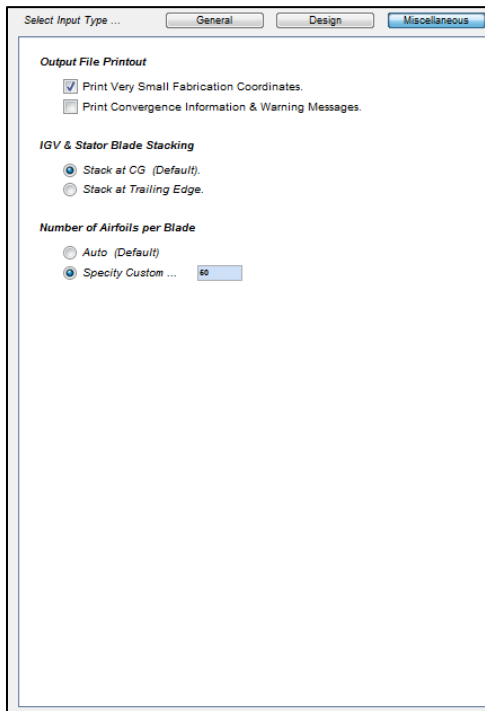


Figure 6.82 Miscellaneous input tab.

The next input field shown in Figure 6.82 serves as a flag for controlling the stacking method for inlet guide vanes and stators. If the first option is selected, the program stacks all stationary blades at their respective center of gravity (*CG*) locations. This is the default option, and the method used for all rotor blades. As an alternative, the second option positions the stacking locations of all stationary blades at their trailing edge locations.

The last input field shown in Figure 6.82 allows the user to specify the number of cross-section elements used to define the stacked blade fabrication coordinates. If the *Auto* option is selected (default), the program defines the number of airfoil cross-sections

based on the aspect ratios of the corresponding blades. If a *custom* number is specified, the program will evenly distribute the given number of elements across the span of the blade. It is important to note that this feature does not represent the streamline distribution of the compressor. The shapes of the resulting blade cross-sections are instead interpolated from the streamline solutions. Higher refinement of the blade shapes may be produced by increasing the number shown Figure 6.82. The result of doing so, however, increases the density of the solution output file, and may increase the time required to post-process the solution. The effect of altering the cross-section distribution is shown in Figure 6.83 and Figure 6.84.

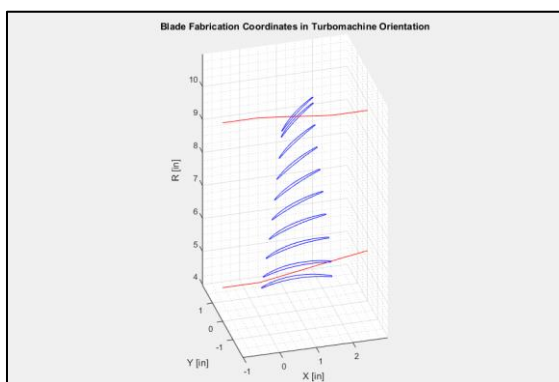


Figure 6.83 Rotor 1 stacking distribution (10 elements specified).

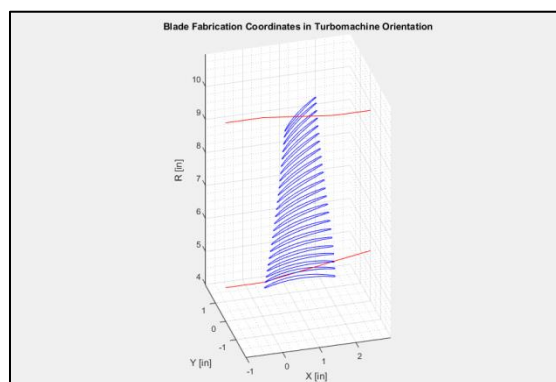


Figure 6.84 Rotor 1 stacking distribution (24 elements specified).

6.12. Post Processing

Many of the post-processing functions discussed in the Meanline application (section 5.11) are available to post-process the Throughflow solution. The quantity of information available, however, is significantly greater than that available for the Meanline simulation. Once a converged Throughflow solution is obtained, the outputted aerodynamic and geometric data is immediately post-processed and presented in the window located to the right of the user input pane. The three buttons located at the top of

the window again allow the user to toggle between one of three view modes: *Blade Geometry*, *Stage Plots*, and *Radial Plots*. Examples of all three are shown in Figure 6.85, Figure 6.86, and Figure 6.87 respectively. The sections below give a general description of all post-processing functions.

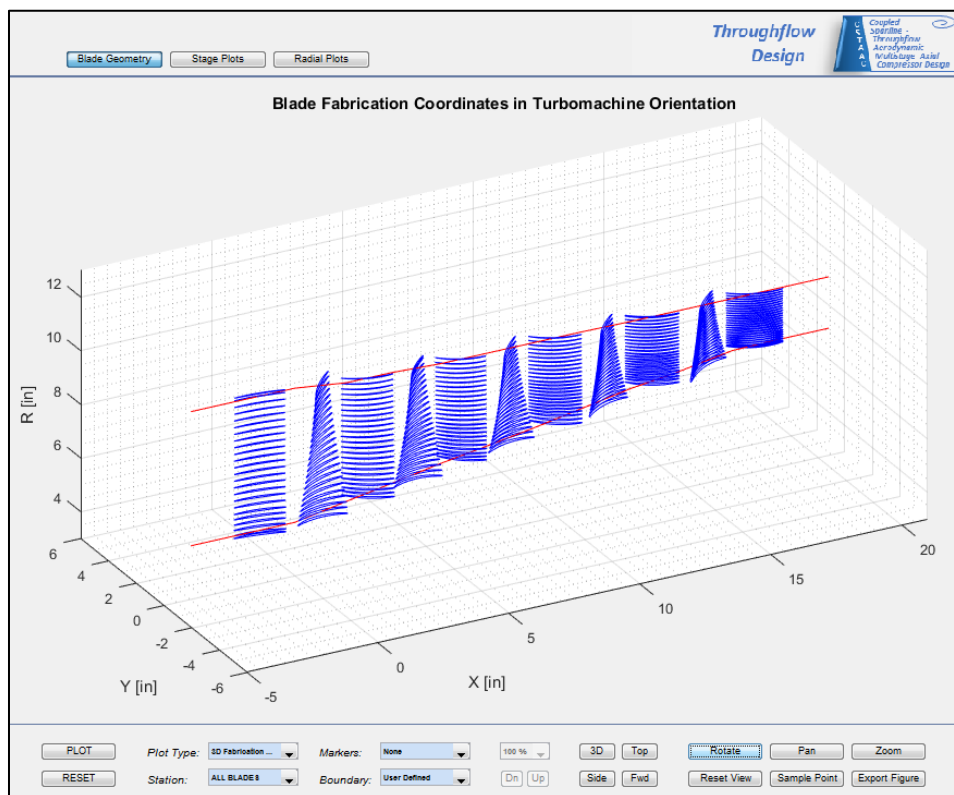


Figure 6.85 Blade geometry post-processing window (fabrication coords view).

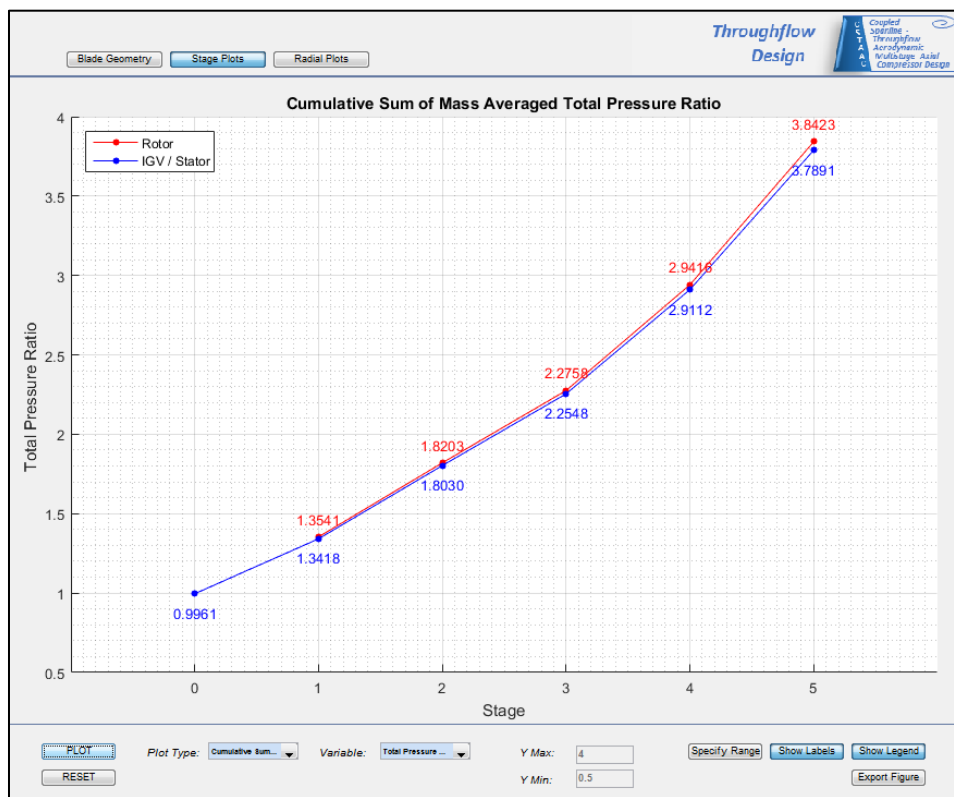


Figure 6.86 Stage plot post-processing window.

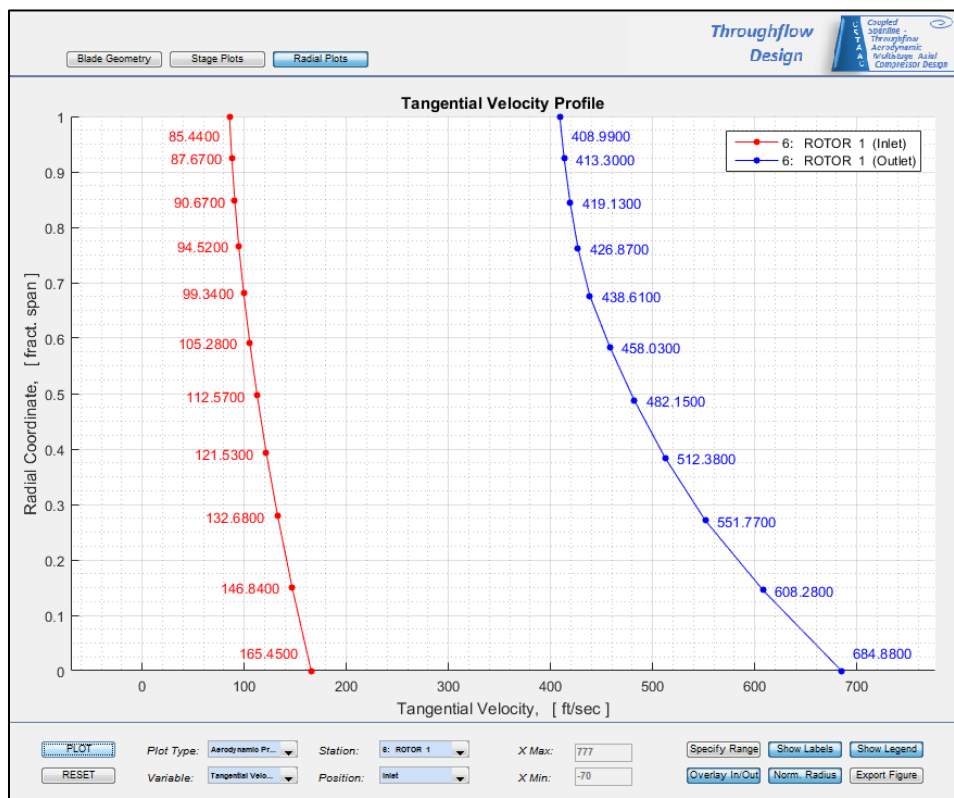


Figure 6.87 Radial plot post-processing window.

6.12.1. Blade Geometry Post-Processing Window

Similar to the features available for the Meanline application, the input fields located at the bottom of the post-processing window offer a substantial number of options to help the user visualize the geometry of the compressor. In addition to the stacked fabrication coordinates seen in Figure 6.85, the user may plot the meridional view of the compressor, as well as a top-down representation of individual airfoil elements. Examples of these views are shown in Figure 6.88 and Figure 6.89. They may be selected from the *Plot Type* dropdown list located in the upper left corner of the input window.

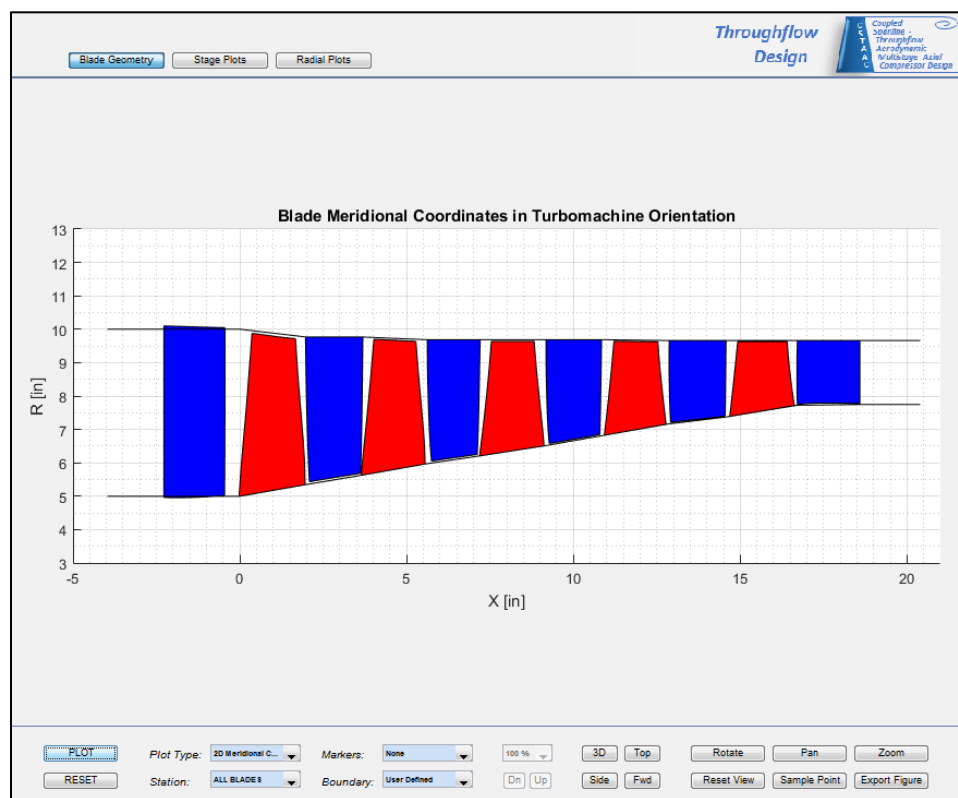


Figure 6.88 Blade geometry post-processing window (meridional view).

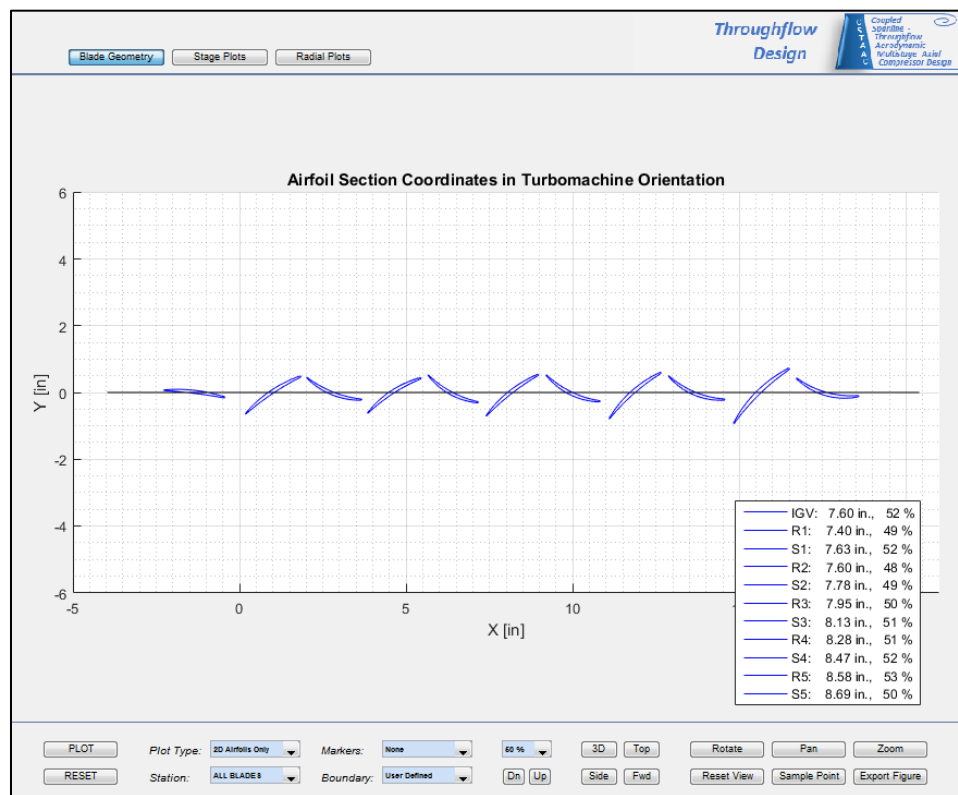


Figure 6.89 Blade geometry post-processing window (airfoil view).

The *Station* list located in the lower left corner of the input pane enables the user to display the full compressor geometry as demonstrated above, or to select an individual blade row station for closer inspection. The result produces enlarged views of the given blade row as illustrated in Figure 6.90 and Figure 6.91. Views such as these may be beneficial in tracking specific geometric changes made through successive iterations.

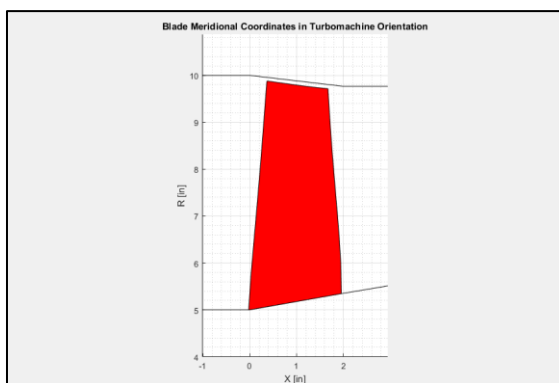


Figure 6.90 Meridional view of rotor 1.

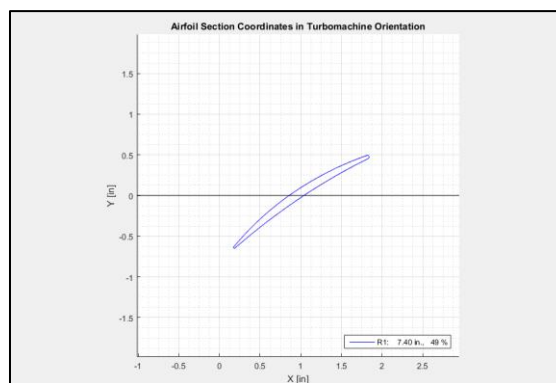


Figure 6.91 Airfoil view of rotor 1 (at 50% span).

When post-processing the compressor geometry in the *2D Airfoils Only* view, additional navigation controls become available to the user. This may be observed by comparing the input panes shown in Figure 6.88 and Figure 6.89. The fields located between the dropdown lists and the navigation button group allow the user to select the span location that is displayed in the window. The location, given as a percentage of the passage height, may be selected in 10 percent increments from the corresponding dropdown list. The two buttons directly below this field allow for rapid toggling between successive span locations.

The next dropdown list, labeled *Markers*, provides an additional means of visualizing the stations of a given compressor. One of three options may be selected. The first option, *Plot Stacking Lines*, provides the user with a visual representation of all blade stacking axes in the compressor. The stacking axis is defined at the mid chord location (distributed radially) for all blade elements. The next option, *Plot Free Stations*, displays the axial locations of the so-called *Free Stations* discussed in section 6.9. The option to display both or none of these features is available to the user as well. The application of these options is demonstrated in Figure 6.92.

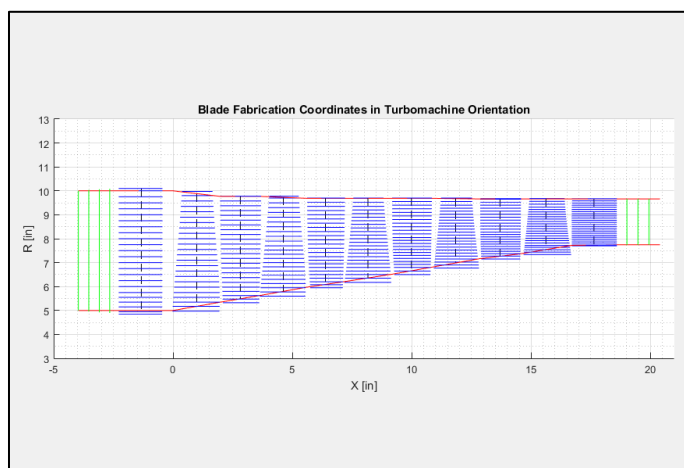


Figure 6.92 Compressor geometry with stacking axes and free stations shown.

The remaining dropdown list in the input pane provides the user with control over the type of annulus boundary that is displayed in the post-processing window. The first option, *User Defined*, displays the hub and tip boundary coordinates that are defined by the user (refer to section 6.7). Alternatively, the user may display a smoothed representation of the boundary coordinates that are automatically interpolated by the program. This is accomplished by selecting the *Smoothed* option from the dropdown list. A comparison between the two boundary types is shown in Figure 6.93 and Figure 6.94.

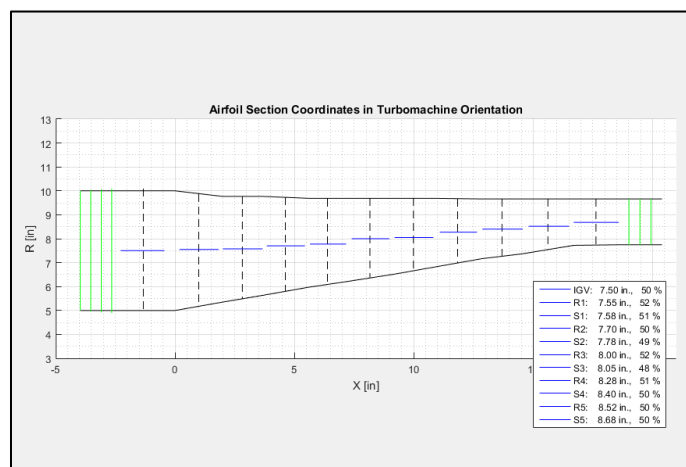


Figure 6.93 User-defined boundary with stacking axes and free stations shown for reference.

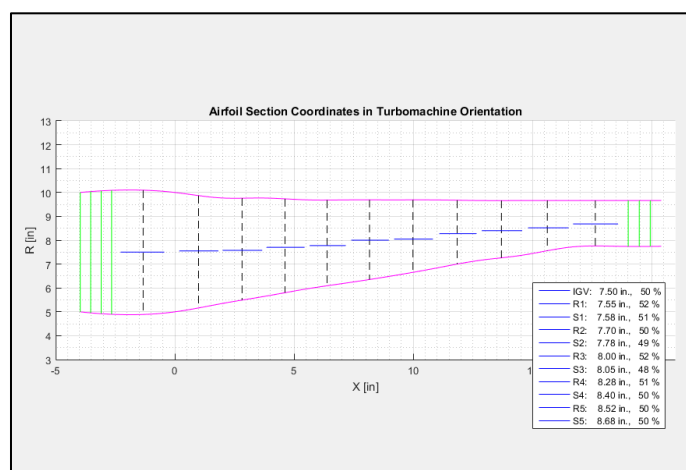


Figure 6.94 Smoothed boundary with stacking axes and free stations shown for reference.

The button group located to the right of the airfoil selection fields shown in Figure 6.89 provides additional navigation options for the user. The four options, *3D*, *Top*, *Side*, and *Fwd*, refer to the view angle setting of the figure shown in the post-processing window. Each of these four settings is demonstrated in Figure 6.95, Figure 6.96, Figure 6.97, and Figure 6.98 respectively.

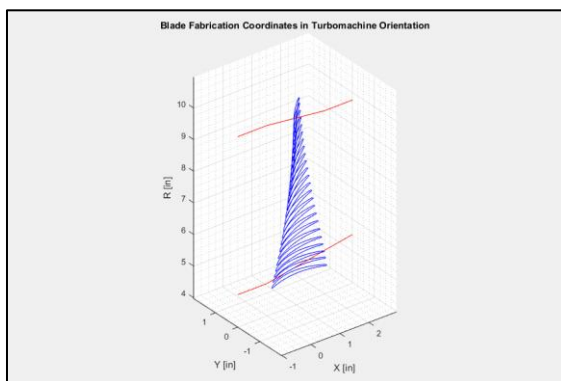


Figure 6.95 *3D* (isometric) view of rotor 1.

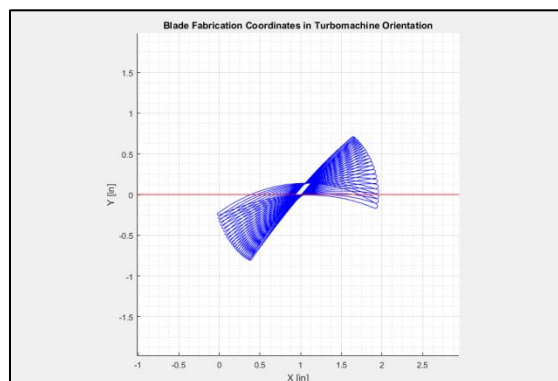


Figure 6.96 *Top* view of rotor 1.

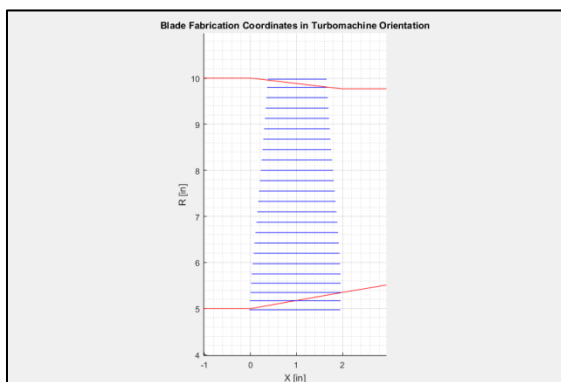


Figure 6.97 *Side* view of rotor 1.

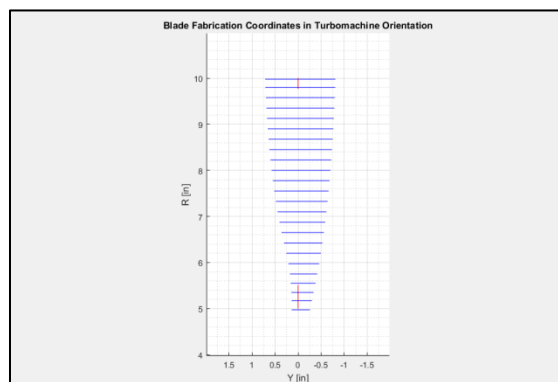


Figure 6.98 *Front* view of rotor 1.

The remaining button group located on the right side of the input pane shown in Figure 6.89 provides the user with additional post-processing controls related to view settings, coordinate sampling, and export controls. These options are identical to the ones discussed for the Meanline application. Refer to 5.11.1 for additional information regarding these features.

6.12.2. Stage Plot Post-Processing Window

Similar to the Meanline application, the user again has the ability to post-process stage-specific aerodynamic and geometric stage parameters. In this case, however, a larger selection of variables is provided to the user. The complete list of stage variables available to plot is provided in Appendix C.

Any of the stage parameters displayed in Appendix B may be displayed by selecting the appropriate option from the *Variable* dropdown list. When done in combination with the first *Plot Type* option, *Mass Averaged Stage Parameters*, the program plots the specified information for each blade row as shown in Figure 6.99. If, however, the second *Plot Type* option is selected, the program displays the cumulative sum of the specified parameters across all blade rows. This is demonstrated in Figure 6.100.

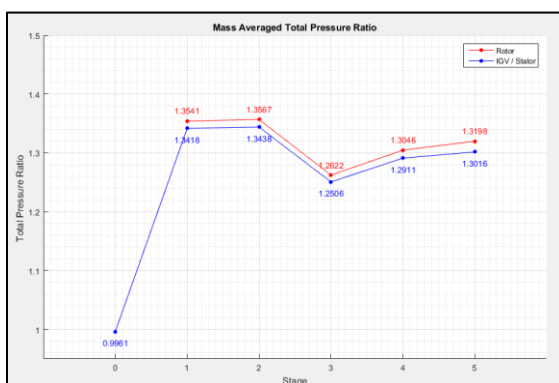


Figure 6.99 Mass averaged total pressure ratio across the compressor.



Figure 6.100 Cumulative sum of the mass averaged total pressure ratio across the compressor.

The remaining input selection fields shown Figure 6.86, namely the axis range, label visibility, legend visibility, and export controls, are identical to those described for the Meanline application. Refer to 5.11.2 for additional details.

6.12.3. **Radial Data Post-Processing Window**

The user input options shown at the bottom of the radial data post-processing window (Figure 6.87) are identical to those discussed for the Meanline application. Refer to section 5.11.3 for additional information regarding their functionality. The Thoughtflow application, however, offers a wider selection of variables available for plotting. The complete list of parameters is provided in Appendix D.

7. Conclusion

A computer program for simplifying the aerodynamic design of multistage axial compressors has been developed. This program, named C-STAAC, improves the efficiency of the Preliminary-to-Throughflow design sequence outlined in section 2.2 by conveniently combining the Meanline and Throughflow capabilities of two independent compressor codes to form one standalone design platform. The fully coupled interaction between the Meanline and Throughflow applications provides the user with the ability to produce stacked airfoil geometry from only a handful of initial input parameters. The user may iterate between the one- and two-dimensional solutions as required until a desired compressor configuration is achieved.

C-STAAC additionally offers a wide selection of pre- and post-processing capabilities that were not previously available with the independent design codes. The implementation of an easy-to-use graphical user interface greatly improves user productivity and design turnaround time, and ultimately provides the user with the resources required to design and post-process the aerodynamic solution of stacked blade geometry in a matter of minutes. An equivalent industry-standard process may take hours or even days to achieve the same task.

A complete overview of the functional capabilities of C-STAAC and its associated applications has been presented. Detailed descriptions of all input fields within the program have been documented, and the application of various input parameters have been demonstrated with illustrated examples. This documentation was included for the purpose of explaining the program in its entirety, but may substitute for a user manual if desired.

REFERENCES

- Anderson, J. D. (2013). *Modern Compressible Flow: With Historical Perspective* (Third ed.). McGraw-Hall Companies, Inc.
- Carter, A. (1955). *The Axial Compressor*. Gas Turbine Principles and Practice, 5.
- Crouse, J. E., & Gorrell, W. T. (1981). *Computer Program for Aerodynamic and Blading Design of Multistage Axial-Flow Compressors*. NASA-TP-1946. National Aeronautics and Space Administration Lewis Research Center.
- Cumpsty, N. A. (1989). *Compressor aerodynamics*. Longman Scientific & Technical.
- De Ruyck, J., & Hirsch, C. (1981). Investigations of an axial compressor end-wall boundary layer prediction method. *Journal of Engineering for Power*, 103(1), 20-33.
- Denton, J. D. (2010). Some Limitations of Turbomachinery CFD (GT2010-22540). *ASME Turbo Expo 2010: Power for Land, Sea, and Air. 7: Turbomachinery*, pp. 735-745. Glasgow: American Society of Mechanical Engineers.
- Denton, J. D., & Dawes, W. N. (1998). Computational fluid dynamics for turbomachinery design. *Proceedings of the Institution of Mechanical Engineers, Part C: Journal of Mechanical Engineering Science*, 213(2), 107-124.
- Dixon, S. L., & Hall, C. A. (2010). *Fluid Mechanics and Thermodynamics of Turbomachinery* (Sixth ed.). Elsevier Inc.
- Farokhi, S. (2014). *Aircraft Propulsion*. John Wiley & Sons, Inc.
- Gallimore, S. J. (1999). Axial flow compressor design. *Proceedings of the Institution of Mechanical Engineers, Part C: Journal of Mechanical Engineering Science*, 213(5), 437-449.
- Glassman, A. J., & Lavelle, T. M. (1995). *Enhanced capabilities and modified users manual for axial-flow compressor conceptual design code CSPAN*.
- Hill, P., & Peterson, C. (1992). *Mechanics and Thermodynamics of Propulsion* (Second ed.). Addison-Wesley Publishing Company, Inc.
- Hirsch, C., & Denton, J. D. (1981). *Propulsion and Energetics Panel Working Group 12 on Through Flow Calculations in Axial Turbomachines*. AGARD-AR-175. Advisory Group for Aerospace Research and Development Neuilly-Sur-Seine (France).

- Horlock, J. H. (1958). *Axial flow compressors: fluid mechanics and thermodynamics*. Butterworths scientific publications.
- Johnsen, I. A., & Bullock, R. O. (1965). *Aerodynamic Design of Axial Flow Compressors*. NASA SP-36.
- Lieblein, S., Schwenk, F. C., & Broderick, R. L. (1953). *Diffusion factor for estimating losses and limiting blade loadings in axial-flow-compressor blade elements* (No. NACA-RM-E53D01). Lewis Flight Propulsion Lab. National Advisory Committee for Aeronautics .
- Molinari, M., & Dawes, W. N. (2006). Review of evolution of compressor design process and future perspectives. *Proceedings of the Institution of Mechanical Engineers, Part C: Journal of Mechanical Engineering Science*, 220(6), 761-771.
- Novak, R. A. (1967). Streamline curvature computing procedures for fluid-flow problems. *Journal of Engineering for Power*, 89(4), 478-490.
- Oyama, A., Liou, M.-S., & Obayashi, S. (2004). Transonic Axial-Flow Blade Optimization: Evolutionary Algorithms/Three-Dimensional Navier–Stokes Solver. *Journal of Propulsion and Power*, 20(4), 612-619.
- Peng, W. W. (2008). *Fundamentals of Turbomachinery*. John Wiley & Sons, Inc.
- Petrovic, M. V., Dulikravich, G. S., & Martin, T. J. (2000). Optimization of multistage turbines using a through-flow code. *ASME Turbo Expo 2000: Power for Land, Sea, and Air* (pp. V001T03A086-V001T03A086). American Society of Mechanical Engineers.
- Pratt & Whitney. (n.d.). [Online Image]. Retrieved August 2016, from <http://www.purepowerengine.com/photos.htm>
- Saravanamuttoo, H., Rogers, G., & Cohen, H. (2001). *Gas Turbine Theory* (Fifth ed.). Pearson Education Limited.
- Siemens. (n.d.). [Online Image]. Retrieved August 2016, from <http://www.energy.siemens.com/hq/en/fossil-power-generation/gas-turbines/sgt-700.htm%20-%20content=Features%20and%20fields%20of%20application>
- Smith, L. H. (n.d.). The radial-equilibrium equation of turbomachinery. *Journal of Engineering for Power*, 88(1), 1-12.
- Tiwari, P., Stein, A., & Lin, Y. L. (2013). Dual-solution and choked flow treatment in a streamline curvature throughflow solver. *Journal of Turbomachinery*, 135(4).

Wu, C.-H. (1952). *A General Theory of Three-Dimensional Flow in Subsonic and Supersonic Turbomachines of Axial-, Radial-, and Mixed-Flow Types*. NACA TN-2604. Washington D.C: National Advisory Committee for Aeronautics.

A. Stage Variables Available for Plot - Meanline Application

Table A.1 Output variables solved by the program.

Parameter	Units
Mass Flow Rate	lb / sec
Cumulative Pressure Ratio (Mass averaged)	-
Cumulative Temperature Ratio (Mass averaged)	-
Cumulative Adiabatic Efficiency (Mass averaged)	fract.
Cumulative Polytropic Efficiency (Mass averaged)	fract.
Pressure Ratio (Mass averaged)	-
Temperature Ratio (Mass averaged)	-
Adiabatic Efficiency (Mass averaged)	fract.
Blade aspect ratio	-
Number of blades	-
Blade Actual Chord	in.

Table A.2 Input variables specified by the user.

Parameter	Units
Meridional Velocity Ratio	-
Polytropic Efficiency	fract.
Tip Blade Solidity	-
Blade Aspect Ratio	-
Hub/Tip Blockage Factor	fract.
Max Hub/Tip Ramp Angle	deg.
Max Diffusion Factor	-
Max Hub Turning Rate (rotors only)	deg.
Max Hub Inlet Mach Number (stators only)	-
Tip Radius Ratio	-
Coefficients B, C, D and E fir Equation 5.1	-

B. Radial Variables Available for Plot - Meanline Application

Table B.1 Variables for *Aerodynamic* plot type.

Parameter	Units
Meridional Velocity	ft/sec
Tangential Velocity	ft/sec
Absolute Velocity	ft/sec
Relative Velocity	ft/sec
Wheel Speed	ft/sec
Absolute Mach Number	-
Relative Mach Number	-
Absolute Flow Angle	deg.
Relative Flow Angle	deg.
Total Temperature	deg. R
Total Pressure	psi
Diffusion Factor	-
Shock Loss Coefficient	-
Total Loss Coefficient	-

Table B.2 Variables for *Geometric* plot type.

Parameter	Units
Axial Chord	in.
Actual Solidity	-
Stagger Angle	deg.
Incidence Angle	deg.
Deviation Angle	deg.
Camber Angle	deg.
Blade Inlet Angle	deg.
Blade Exit Angle	deg.

C. Stage Variables Available for Plot - Throughflow Application

Table C.1 Mass averaged stage variables.

Parameter	Units
Flow Coefficient	-
Head Coefficient	-
Ideal Head Coefficient	-
Total Pressure Ratio	-
Total Temperature Ratio	-
Adiabatic Efficiency	fract.
Polytropic Efficiency	fract.
Blade Aspect Ratio	-
Axial Shaft Thrust	lbs
Gas Bending Moment (Axial Component)	ft-lbs
Gas Bending Moment (Tangential Component)	ft-lbs
Torque	ft-lbs
Power	hp

Table C.2 Cumulative sums of mass averaged stage variables.

Parameter	Units
Mass Flow	lbs/sec
Total Pressure	psia
Total Temperature	deg. R
Total Pressure Ratio	-
Total Temperature Ratio	-
Head Coefficient	-
Ideal Head Coefficient	-
Adiabatic Efficiency	fract.
Polytropic Efficiency	fract.
Axial Shaft Thrust	lbs
Torque	ft-lbs
Power	hp
Energy Addition Fractio	fract. of total

D. Radial Variables Available for Plot - Throughflow Application

Table D.1 Aerodynamic variables for *Free* stations.

Parameter	Units
Axial Velocity	ft/sec
Meridional Velocity	ft/sec
Tangential (Swirl) Velocity	ft/sec
Absolute Velocity	ft/sec
Absolute Mach Number	-
Absolute Flow Angle	deg.
Axial Coordinate	in.
Total Pressure	psia.
Total Temperature	deg. R
Static Pressure	psia.
Static Temperature	deg. R
Streamline Slope	deg.
Streamline Curvature	1/in.

Table D.2 Aerodynamic variables for *Rotor Inlet* stations.

Parameter	Units
Axial Velocity	ft/sec
Meridional Velocity	ft/sec
Tangential (Swirl) Velocity	ft/sec
Absolute Velocity	ft/sec
Relative Tangential Velocity	ft/sec
Relative Velocity	ft/sec
Wheel Speed	ft/sec
Absolute Mach Number	-
Relative Mach Number	-
Absolute Flow Angle	deg.
Relative Flow Angle	deg.
Flow Coefficient	-
Axial Coordinate	in.
Total Pressure	psia.
Total Temperature	deg. R
Static Pressure	psia.
Static Temperature	deg. R
Streamline Slope	deg.
Streamline Curvature	1/in.

Table D.3 Aerodynamic variables for *Rotor Outlet* stations.

Parameter	Units
Axial Velocity	ft/sec
Meridional Velocity	ft/sec
Tangential (Swirl) Velocity	ft/sec
Absolute Velocity	ft/sec
Relative Tangential Velocity	ft/sec
Relative Velocity	ft/sec
Wheel Speed	ft/sec
Absolute Mach Number	-
Relative Mach Number	-
Absolute Flow Angle	deg.
Relative Flow Angle	deg.
Flow Coefficient	-
Head Coefficient	-
Ideal Head Coefficient	-
Adiabatic Efficiency	fract.
Diffusion Factor	-
Loss Coefficient	-
Shock Loss Coefficient	-
Degree of Reaction	-
Aerodynamic Chord	in.
Solidity	-
Pressure Ratio	-
Temperature Ratio	-
Total Pressure	psia.
Total Temperature	deg. R
Static Pressure	psia.
Static Temperature	deg. R
Streamline Slope	deg.
Streamline Curvature	1/in.
Radial Location of Blade Force Component	in.
Local Blade Force (Axial Component)	lbs/in.
Local Blade Force (Radial Component)	lbs/in.

Table D.4 Aerodynamic variables for *Stator Inlet* stations.

Parameter	Units
Axial Velocity	ft/sec
Meridional Velocity	ft/sec
Tangential (Swirl) Velocity	ft/sec
Absolute Velocity	ft/sec
Absolute Mach Number	-
Absolute Flow Angle	deg.
Relative Flow Angle	deg.
Flow Coefficient	-
Axial Coordinate	in.
Total Pressure	psia.
Total Temperature	deg. R
Static Pressure	psia.
Static Temperature	deg. R
Streamline Slope	deg.
Streamline Curvature	1/in.

Table D.5 Aerodynamic variables for *Stator Outlet* stations.

Parameter	Units
Axial Velocity	ft/sec
Meridional Velocity	ft/sec
Tangential (Swirl) Velocity	ft/sec
Absolute Velocity	ft/sec
Absolute Mach Number	-
Absolute Flow Angle	deg.
Flow Coefficient	-
Head Coefficient	-
Ideal Head Coefficient	-
Stage Adiabatic Efficiency	fract.
Diffusion Factor	-
Loss Coefficient	-
Shock Loss Coefficient	-
Degree of Reaction	-
Axial Coordinate	in.
Aerodynamic Chord	in.
Solidity	-
Pressure Ratio	-
Stage Pressure Ratio	-
Total Pressure	psia.
Total Temperature	deg. R
Static Pressure	psia.
Static Temperature	deg. R
Streamline Slope	deg.
Streamline Curvature	1/in.
Radial Location of Blade Force Component	in.
Local Blade Force (Axial Component)	lbs/in.
Local Blade Force (Radial Component)	lbs/in.

Table D.6 Geometric variables for *Rotor* and *Stator Inlet* stations.

Parameter	Units
Radius-to-tip-radius Ratio	-
Percent Span	pcent. span
Radius-to-Chord Ratio	-
Max Thickness-to-Chord Ratio	-
Max Thickness Point Location-to-Chord Ratio	-
Transition Point Location-to-Chord Ratio	-
Segment Inlet-to-Exit Turning Rate-to-Chord Ratio	-
Layout Cone Angle	deg.
Incidence Angle	deg.
Incidence Angle (Relative to Suction Surface)	deg.
Inlet Blade (metal) Angle	deg.
Inlet Blade Angle (on Layout Cone)	deg.
Transition Point Blade Angle (on Layout Cone)	deg.
Blade Set Angle (on Layout Cone)	deg.
FWD Segment Camber Angle (Relative to Suction Surface) (on Layout Cone)	deg.
Mach Number at Shock Location (on Layout Cone)	-
Shock Location (as Fraction of Suction Surface) (on Layout Cone)	fract. of s.s.
Cov. Channel (as Fraction of Suction Surface) (on Layout Cone)	fract. of s.s.
Minimum Choke Area Margin (on Layout Cone)	-
Min. Choke Point Location in Cov. Channel (on Layout Cone)	-
Edge Circle Center $r.d0/dr$	-

Table D.7 Geometric variables for *Rotor* and *Stator Outlet* stations.

Parameter	Units
Radius-to-tip-radius Ratio	-
Percent Span	pcent. span
Radius-to-Chord Ratio	-
Deviation Angle	deg.
Outlet Blade (metal) Angle	deg.
Outlet Blade Angle (on Layout Cone)	deg.
Max Camber Point Location-to-Chord Ratio (on Layout Cone)	-
Edge Circle Center $r.d0/dr$	-